Structural Analysis of the *Helicobacter pylori* Toxin VacA

By

Tasia Marie Pyburn

Dissertation

Submitted to the Faculty of the

Graduate School of Vanderbilt University

in partial fulfillment of the requirements

for the degree of

DOCTOR OF PHILOSOPHY

In

Cell and Developmental Biology

May 2017

Nashville, Tennessee

Approved:

James R, Goldenring, M.D., Ph.D.

Timothy L. Cover, M.D.

Matthew J. Tyska, Ph.D.

Ethan Lee, M.D., Ph.D.

Melanie D. Ohi, Ph.D.

To my family – my lucky stars

ACKNOWLEDGEMENTS

First and foremost, I want to thank my advisor, Dr. Melanie Ohi. Thank you for allowing me to join your lab and work on a project I felt very passionate about. Your guidance and trust in me has allowed me to grow as a scientist. Thank you for letting me pop into your office to chat and helping whenever a problem arose. Your mentorship has elevated my abilities as a scientist and thank you for letting me attend workshops and conferences which only propelled my training to a new level. And thank you for allowing me to work on other areas to develop professionally as well. Thank you for the wonderful graduate experience.

Thank you to all lab members, past and present. Melissa and Yoshi, you both got me started with electron microscopy and I thank you for your time and patience. Scott and Elad, our conversations have been extremely helpful in this journey to understand all the new cryo-EM programs and problems. Thank you for letting me hang out in your new office downstairs while writing and for the random conversations that we've had. Thank you, Nora, for being the best rotation student and now labmate! VacA discussions over the past couple of years have given great insight into our beloved toxin and helped me to become the best VacA scientist possible.

Thank you to the Cover lab for being a wonderful collaborator. Thank you Christian and Anne and for providing me with purified protein. Thank you, Arwen, for all of our conversations over the years and giving me the opportunity to work with you on your project. Thank you, Tim, for being a wonderful committee member and collaborator, and allowing me to pursue a high-resolution structure of VacA.

Thank you to my committee - Dr. James Goldenring, Dr. Timothy Cover, Dr. Matthew Tyska, and Dr. Ethan Lee. Thank you for being part of my committee

and allowing me to share my work with you. Your constructive criticisms and advice over the years have made me a better scientist and elevated my work to be the best possible.

Thank you to the Puck Ohi and Kathy Gould labs. It has been incredibly helpful to receive 'outside of the lab' input on my project. Your input has also allowed me to present my work as clearly and effectively and it has been great to work with everyone over the years.

I want to give a huge thank you to Dr. Tina Iverson. You took a chance on me right out of college when I knew nothing about structural biology and taught me all I know about crystallography. In your lab, I developed a love and appreciation for structural biology. Your support and belief in me is invaluable and one of the main reasons I chose to pursue graduate school. Thank you.

Thank you to all of my friends. I have met a lot of people while at Vanderbilt and each person has had an impact on me. Tara, Katie W., and Katie N., our girls' lunches were always what I needed. Kendra, I loved working with you on the adhesin project in Tina's lab and am so grateful for your friendship. To you ladies and all my friends, I love you all!

To my rock, Greg, thank you for everything that you have done for me since we met. Your support and encouragement and been amazing and I'm so lucky to have you in my life. And to my family – you are amazing. Thank you for supporting my decision to attend graduate school and for your help and guidance throughout this journey. You are the best family I could ever ask for and I am so grateful for each one of you. Thank you for listening to me when I talk science, making me laugh, and helping me to relieve stress by hanging out, climbing, and playing with the pups. To my dad, you have taught me so much and are one of the

coolest people I know. And to my mother, you are my best friend. Thank you both for always being there for me. I love you all!

Thank you to the administrative staff in the Cell and Developmental Biology department. You are all wonderful and kind and patient. Thank you to the Center for Structural Biology. I feel very fortunate to have been part of the CSB for almost twelve years and it is a wonderful and collaborative group of scientists.

This work was supported by NIH F31AI112324 to Tasia M. Pyburn; AI039657, CA116087, AI118932 and the Department of Veterans Affairs to Dr. Timothy Cover; RO1AI039657, AI118932 and the Vanderbilt Center for Structural Biology to Dr. Melanie Ohi.

LIST OF TABLES

LIST OF FIGURES

TABLE OF CONTENTS

ABBREVIATIONS

RCT	Random Conical Tilt
AFM	Atomic Force Microscopy
TEM	Transmission Electron Microscopy
ePC	L-α-phosphatidylcholine from egg
DOPC	1,2-dioleoyl-*sn*-glycero-3-phosphocholine
DOPS	1,2-dioleoyl-*sn*-glycero-3-phospho-L-serine
SM	Egg Sphingomyelin
CHOL	Ovine Cholesterol
LUV	Large Unilamellar Vesicle
HEPES	4-(2-hydroxyethyl)-1-piperazineethanesulfonic acid)
RPTP	Receptor Protein Tyrosine Phosphatase
LRP-1	Lipoprotein Receptor-Related Protein-1
EGFR	Epidermal Growth Factor Receptor
MALT	Mucosa-Associated Lymphoid Tissue
PPI	Proton Pump Inhibitor
CagA	Cytotoxin-Associated Antigen A
VacA	Vacuolating Cytotoxin A
T4SS	Type 4 Secretion System
T5SS	Type 5 Secretion System
LPS	Lipopolysaccharide
CDC	Centers for Disease Control and Prevention
PFTs	Pore Forming Toxins
T4P	Type 4 Pili
CDCs	Cholesterol Dependent Cytoloysin

BabA	Blood-Antigen Binding Protein
SabA	Sialic Acid Binding Protein
NAP	Neutrophil-Activating Protein
GPI-AP	Glycosylphosphatidyl Inositol Anchored Protein
GEEC	GPI-AP Enriched Early Endosomal Compartments
MDR	Multidrug Resistant
CRE	Carbapenem Resistant *Enterobacteriaceae*
CHAPS	(3-[(3-Cholamidopropyl)dimethylammonio]-1-propanesulfonate hydrate
OG	n-Octyl-β-D-Glucopyranoside
DM	n-Decyl-β-D-Maltopyranoside
SUV	Small Unilamellar Vesicles
BSA	Bovine Serum Albumin
KCl	Potassium chloride
DED	Direct Electron Detector
RT	Room Temperature
HBS	HEPES Buffered Saline
CV	Column Volume
DMPC	1,2-dimyristoyl-*sn*-glycero-3-phosphocholine
MWCO	Molecular Weight Cut Off
$MgCl_2$	Magnesium chloride
GPI	Glycosylphosphatidylinositols

CHAPTER I

INTRODUCTION

Bacterial Pathogens and their Role in Disease.

Bacterial pathogens pose a serious worldwide health risk. If left untreated, infection can be fatal. Unfortunately, antibiotic resistance is increasing, leading to the dire need to develop improved, pathogen specific therapeutics. Even commensal bacteria, those that typically are not harmful to humans, can lead to devastating disease in immunocompromised or unhealthy individuals.

Gram-positive Bacteria. Gram-positive bacteria are characterized by their thick peptidoglycan wall and lack of outer membrane, which leads to the ability to retain crystal violet staining (Fig. 1-1A). There are several well-known gram-positive pathogens whose infection can lead to disease including the *Staphylococcal, Streptococcal, Clostridial,* and *Enterococcal* species. For example, *Streptococcus pneumoniae* is the leading cause of bacterial pneumonia and currently poses a serious threat due to increasing antibiotic resistance (Eurosurveillance editorial, 2015; Gauthier et al., 2007). Another bacterium, *Clostridium difficile* is the most common hospital acquired infection in the United States and is considered by the Center for Disease Control and Prevention (CDC) to be an urgent threat (Miller et al., 2011). An infection by this bacterium leads to severe diarrhea and can be fatal in weakened immune systems.

Gram-negative Bacteria. Gram negative bacteria are characterized by their thin peptidoglycan layer and outer membrane which contains a layer of

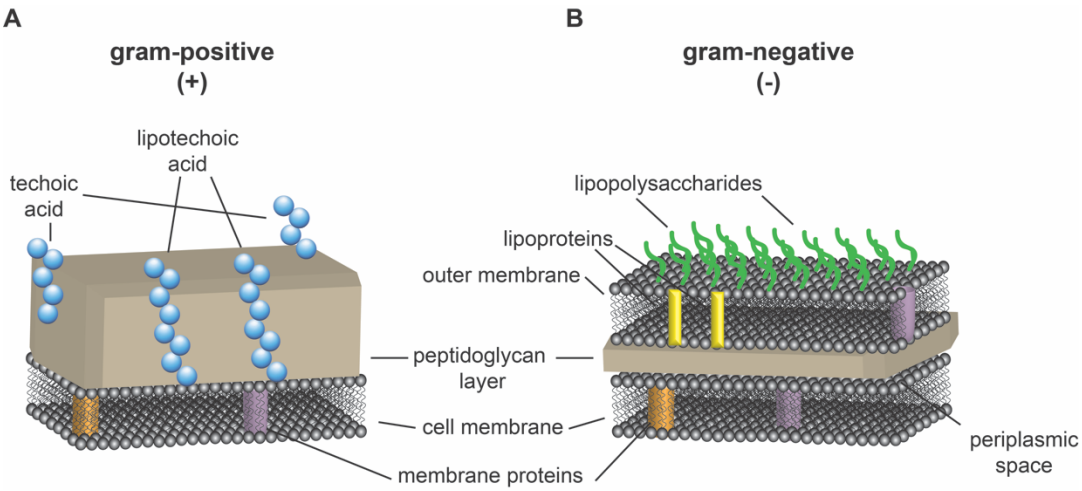

Figure 1-1: Gram-positive and Gram-negative bacteria. A) Gram-positive bacteria are characterized by a thick peptidoglycan layer. B) Gram-negative bacteria are characterized by a thin peptidoglycan layer and outer membrane with LPS.

lipopolysaccharide (LPS) (Fig. 1-1B). LPS can bind to TLRs, which can then provoke an immune response, leading to damage of the host cell. Several gram-negative species have become multidrug resistant (MDR) and some have even become carbapenem resistant (carbapenem resistant enterobacteriaceae; CRE). Carbapenems are antibiotics typically used to fight against infection of MDR bacteria as a final effort to eradicate infection. One of the most common gram-negative pathogens is *Escherichia coli.* *E. coli* is commensal in healthy individuals, but can cause a multitude of different infections, including urinary tract infections and diarrhea. Both *E. coli* and *Salmonella enterica* are involved in food poisoning, and according to the World Health Organization (WHO), these gram-negative species are responsible for over 120,000 deaths each year (Havelaar et al., 2015). Another common environmental pathogen, *Pseudomonas aeruginosa,* is widespread throughout the environment but can be fatal when found in the bloodstream of immunocompromised individuals (Aloush et al., 2006; Driscoll et al., 2007). A gram-negative bacterium of importance to this work is *Helicobacter pylori* whose colonization in the human stomach can lead to various degrees of disease.

Bacterial Pathogens Use Pili to Colonize the Host. In order for many bacteria to be pathogenic they must bind and invade the host cell. One external feature of bacteria are pilins and/or fimbriae (smaller forms of pili). Hundreds of pilins come together in order to form pili, which are hair-like protrusions that extrude from the bacteria. These pili contain adhesins at the tips which interact with host cell surface receptors, allowing for binding of bacteria to host (Fig 1-2A) (Soto and Hultgren, 1999). Pili are found both in gram-negative and, more recently, gram-positive bacteria

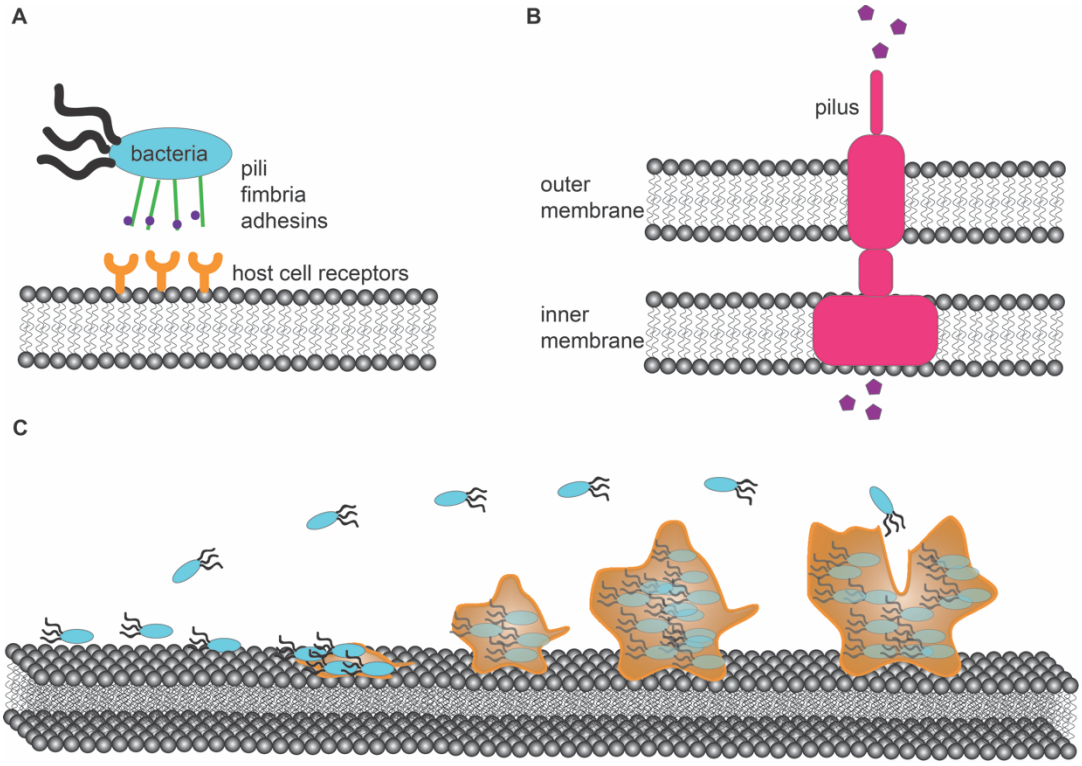

Figure 1-2: Bacterial attachment and invasion of host cells. A) Bacterial adhesion to host cell receptors can be achieved with pili containing adhesins at the tips and fimbriae (a smaller yet similar appendage to pili). B) Bacteria utilize secretion systems in order to invade host cells by secreting effector proteins. C) Bacteria can create microcolonies on the host cell surface leading to biofilm formation.

(Mandlik et al., 2008; Proft and Baker, 2009; Ton-That and Schneewind, 2004). Individual pilins are also prominent components of secretion systems (Fig 1-2B). There are different types of pili in gram-negative bacteria, including type I pili, pyelonephritis-associated pili (P Pili) and type IV pili (T4P) which are the most common type of pili found in several bacterial species. T4P are responsible for a multitude of functions including motility, secretion, DNA uptake, and biofilm formation (Giltner et al., 2012; O'Toole and Kolter, 1998). T4P also give the bacterium a method to attach to the host cell and propel it to the next host cell, a novel mechanism that lacks the use of flagella (Giltner et al., 2012; O'Toole and Kolter, 1998). Type I pili and P pili are only expressed in the outer membrane and utilize the chaperone-usher pathway where they can bind to specific carbohydrate receptors on the host cell (Proft and Baker, 2009). Both pili types are found throughout *Enterobacteriaceae* species. For example, uropathogenic *E. coli* have Type I pili responsible for adherence to the bladder and P pili containing factors that bind to the kidney epithelium (Wiles et al., 2008). The actions of these pili lead to the development of infections including urinary tract infections (Capitani et al., 2006; Connell et al., 1996; Proft and Baker, 2009; Sauer et al., 2004). The pili of *Streptococcal* species are involved in the development of meningitis, sepsis, and pneumonia (Parks et al., 2015)

Pili can also form structures within secretion systems. Bacterial secretion systems allow for the transport of different proteins and molecules for invasion of the host cell. (Fig. 1-2B). There are currently eight known secretion systems. One of the best characterized T4SS is that of *Agrobacterium tumefaciens*. The component VirB5 of this pilus has been suggested to be localized to the tips of the pilus to allow for adhesion to the host cell (Aly and Baron, 2007).

There are many adhesin factors responsible for host binding. One of the best characterized adhesins is located at the distal tip of Type I fimbria of uropathogenic *E. coli,* FimH. FimH binds to mannose receptors of urinary epithelial cells in a catch-bond mechanism (Sauer et al., 2016; Thomas et al., 2002; Zhou et al., 2001). The binding of FimH to the host urinary epithelial cells is part of the virulence of *E. coli* in the development of urinary tract infections. Another example of a bacterial pilus playing a large role in virulence are the T4P of *Neisseria meningitidis* (Berry and Pelicic, 2015). This bacterium is typically located in the nasopharynx, however, it can enter the bloodstream where it becomes pathogenic leading to the development of septicemia (Pathan et al., 2003). In more severe cases, the bacteria can cross the blood brain barrier, leading to the development of meningitis (Pathan et al., 2003). It has been determined that two adhesins found on the T4P are responsible for bacterial binding to the endothelial cells (Bernard et al., 2014), further demonstrating the importance of adhesins as virulence factors.

Since pili are a major factor in bacterial binding to the host cell through different adhesin molecules, they can also play a role in biofilm formation. Biofilms are described as microcolonies of bacteria that can exist in the host environment (Fig. 1-2C). Due to the ability of bacteria to form these large colonies, they are resistant to treatment. A common biofilm is dental plaque, created by commensal gram-positive bacteria, such as the *Streptococcal* and *Actinomyecetal* species (Marsh, 2004). For example, biofilm formation by *Pseudomonas aeruginosa*, a gram-negative opportunistic pathogen, can lead to pneumonia and other hospital acquired infections, that can be fatal if left untreated (Stryjewski and Patel, 2003).

Pore-Forming Toxins.

Pore-forming toxins (PFTs) are the most common bacterial toxin and have become increasingly important drug targets due to their utilization by many

bacteria as virulence factors. Not only do these toxins pose serious health risks (i.e. listeriolysin O and alpha hemolysin) but they have also been used as biological weapons, as in the case of anthrax toxin (Inglesby et al., 2002; Schwartz, 2009). These toxins create pores within membranes, which can alter membrane permeability. In order to achieve this, first, the toxin binds as a monomer to the membrane via a lipid or protein receptor. Next, the toxin can take one of two paths. On the first path, the several monomers will oligomerize on the membrane creating a pre-pore state followed by membrane insertion to create the pore (Fig. 1-3A). On the second path, the monomers will insert into the membrane followed by oligomerization to create a pore (Fig. 1-3B). Once the pore is created, the toxin can cause an influx or efflux of ions, small molecules, and/or larger molecules such as proteins. PFTs are characterized by the type of pore it creates, either alpha helical or beta barrel.

Alpha helical pore-forming toxins. There are three major families of bacterial α-PFTs: colicins, actinoporins, and cytolysin A (ClyA) (Table 1). These toxins have proven to be more difficult to study using structural methods in the past twenty years. However, these studies have provided great insight into how these toxins come together to create pores and cause host damage. Colicin PFTs are found in *E. coli* and are toxic to other bacterial species (Lakey et al., 1994). These toxins are targeted to receptors on the host outer membrane where they create a voltage dependent pore within the inner membrane of the host cell (Lakey et al., 1991; Ridley et al., 2010). X-ray crystallographic studies have revealed that colicin A is comprised of alpha helices that bundle together in three domains that take the shape of an ‘umbrella’ (Parker et al., 1992; Parker et al., 1990). The channel forming domain contains ten helices that upon contact with the

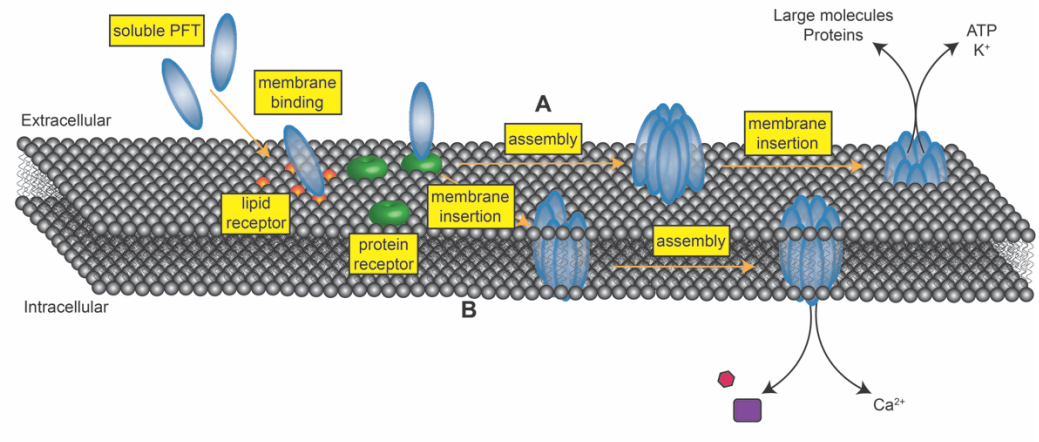

Figure 1-3: Pore formation by PFTs. PFTs first bind to the host cell receptors as soluble monomers. A) PFTs can oligomerize on the surface creating a pre-pore intermediate, followed by membrane insertion and pore formation. B) Following monomer binding, the monomers can insert in to the membrane and then oligomerize to create the pore. Adapted from Peraro, *et al (Dal Peraro and van der Goot, 2016).*

PFT	Family	Organism
Colicin E1	Colicins	*E. coli*
Colicin Ia	Colicins	*E. coli*
Colicin A	Colicins	*E. coli*
Colicin N	Colicins	*E. coli*
Equinatoxin II	Actinoporins	*A. equina*
Sticholysin II	Actinoporins	*S. helianthus*
Fragaceatoxin C	Actinoporins	*A. fragacea*
Cytolysin A	ClyA	*E.coli, S. enterica, S. flexneri*
Non-hemolytic tripartite enterotoxin	ClyA	*B. cereus*
Hemolysin BL	ClyA	*B. cereus*

Table 1-1: α-PFTs and their respective organisms. Adapted from Peraro, *et al* (Dal Peraro and van der Goot, 2016).

membrane, insert to create the pore (Fig. 1-4A) (Ghosh et al., 1994; Wiener et al., 1997).

For actinoporins, there are several crystal structures determined of soluble monomers. Two recent structural studies by X-ray crystallography and cryo-EM with large unilamellar vesicles (LUVs) revealed that fragaceatoxin C (FraC), a haemolytic protein toxin of sea anemones, undergoes four major steps to create a pore (Morante et al., 2016; Tanaka et al., 2015). First, the soluble monomer binds to membrane followed by dimer formation. Then, four dimers come together to create a pre-pore intermediate on the membrane surface prior to membrane insertion and pore completion (Fig. 1-4B) (Morante et al., 2016; Tanaka et al., 2015). Previous structural studies of FraC suggested that the toxin is capable of forming both octameric and nonameric pores (Mechaly et al., 2011). However, both of the recent structural studies strongly suggest that the octameric pore is dominant (Tanaka et al., 2015). Interestingly, the crystallographic studies indicated that the pore contains openings that may serve to release toxic molecules found in sea anemone venom (Tanaka et al., 2015).

The last family of alpha helical PFTs is the ClyA family. In this family is Cytolysin A (also known as hemolysin E or Hlye), and toxins from *Shigella flexineri,* and *Salmonella enterica* all of which are causes of food poisoning in humans. The first crystal structure of ClyA revealed an elongated protein with a four helix bundle at the shaft of one end and a characteristic beta-tongue at the opposing end proposed to interact with membrane (Wallace et al., 2000). More recently, a crystal structure was determined of the ClyA pore in the presence of detergent (Mueller et al., 2009) where the authors determined that ClyA transitions from a four to a three helix bundle in order to transition to a dodecameric pore (Mueller et al., 2009). In the proposed mechanism, the β-tongue interacts with the

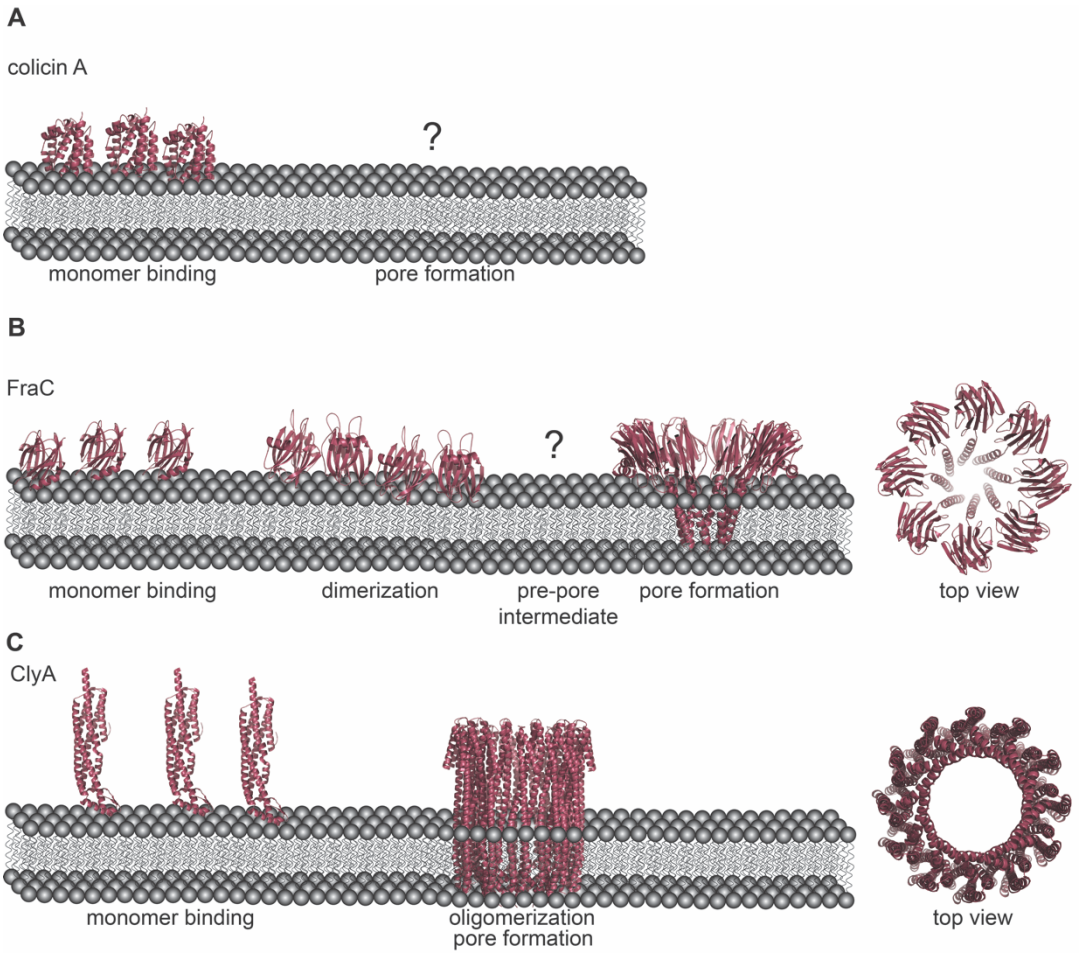

Figure 1-4: Structure and proposed mechanisms for α-PFTs. A) The structure of a colicin A monomer has been determined. To date, there is no structural information on the pore-formed state. (PDBID: 1COL) B) Recently, a mechanism for pore formation by FraC has been elucidated. Following monomer binding to the host, FraC dimerizes on the surface and then creates a pre-pore intermediate (structure not known) followed by membrane insertion. (PDBIDs: 3W9P, 4TSL, 4TSY) C) The mechanism for pore formation by ClyA has been reported where after monomer binding, oligomerization and pore formation are likely concomitant. (PDBIDs: 1QOY, 2WCD) Adapted from Peraro, *et al* (Dal Peraro and van der Goot, 2016).

membrane to enable protomer insertion followed by oligomerization, creating the active pore (Fig. 1-4C). Each of these examples represent well characterized and proposed mechanisms of pore formation based on structural analysis.

Beta barrel pore-forming toxins. β-PFTs are more common and found throughout both gram-negative and gram-positive bacteria. The largest families of β-PFTs are aerolysins, haemolysins, and cholesterol dependent cytolysins (CDCs) (Table 1-2). The first crystal structure determined of a β-PFT was that of the *Aeromonas* spp proaerolysin (Parker et al., 1994). Proaerolysin is plays a major role in bacterial pathogenesis and can lead to wound infections or gastroenteritis (Parker et al., 1994). While several crystal structures have been determined for toxin monomers, only recently there have been structural observations of an aerolysin pore (Degiacomi et al., 2013). Using a combination of X-ray crystallography, cryo-EM and computational modelling, Degiacomi and colleagues determined that aerolysin creates a heptameric pore, which had previously been suggested using 2D crystallography (Degiacomi et al., 2013; Wilmsen et al., 1992). However, in 2016, two structures of aerolysin pores were determined by cryo-EM, aerolysin of *Aeromonas hydrophilia* and lysenin of *Eisenia fetida* (Bokori-Brown et al., 2016; Iacovache et al., 2016). Both structures propose mechanisms in which oligomerization occurs on the membrane prior to insertion (Fig. 1-5A).

The haemolysin family of β-PFTs are well characterized. The first structure determined for haemolysin PFT was in 1996 of the *S. aureus* α-hemolysin heptameric pore (Song et al., 1996). Since then, crystal structures have been determined of several haemolysin toxins (De and Olson, 2011; Huyet et al., 2013; Olson and Gouaux, 2005; Olson et al., 1999; Savva et al., 2013; Yamashita et al., 2014; Yamashita et al., 2011). For example, *Clostridium perfringens*, which is one

PFT	Family	*Organism*
α-haemolysin	Haemolysin	*S. aureus*
γ-haemolysin	Haemolysin	*S. aureus*
Leukocidins	Haemolysin	*S. aureus*
Necrotic enteritis toxin	Haemolysin	*C. perfringens*
δ-toxin	Haemolysin	*C. perfringens*
***V. cholera* cytolysin**	Haemolysin	*V. cholerae*
***V. vulnificus* haemolysin**	Haemolysin	*V. vulnificus*
Aerolysin	Aerolysin	*Aeromonas* spp.
α-toxin	Aerolysin	*Clostridium* spp.
Hydralysin	Aerolysin	*Cnidaria* spp.
ε-toxin	Aerolysin	*C. perfringens*
Enterotoxin	Aerolysin	*C. perfringens*
Hemolytic lectin	Aerolysin	*L. sulphureus*
Kysenin	Aerolysin	*E. fetida*
Perfringolysin O	CDCs	*C. perfringens*
Suilysin	CDCs	*S. suis*
Intermedilysin	CDCs	*S. intermedius*
Listeriolysin O	CDCs	*S. monocytogenes*
Lectinolysin O	CDCs	*S. mitis*
Anthrolysin O	CDCs	*B. anthracis*
Streptolysin O	CDCs	*P. luminescens*

Table 1-2: β-PFTs and their respective organisms. Adapted from Peraro, *et al* (Dal Peraro and van der Goot, 2016).

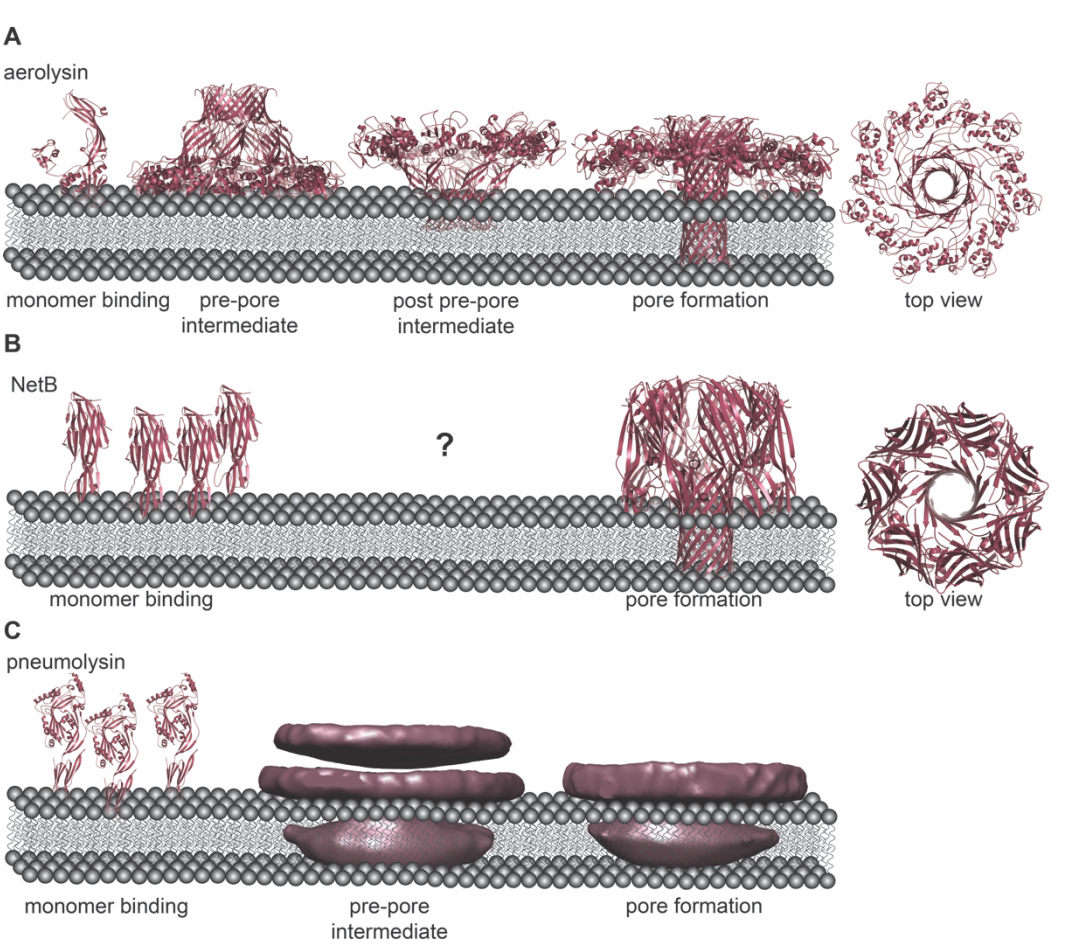

Figure 1-5: Structure and proposed mechanisms for β-PFTs. A) The mechanism for pore formation by aerolysin has been reported where after monomer binding, oligomerization occurs on the surface creating a pre-pore intermediate. A structure of a post pre-pore (or quasipore) state has been determined followed by pore formation. (PDBIDs: 1PRE, 5JZH, 5JZT, 5JZW) B) The NetB monomer crystal structure has been determined. Following monomer binding to the host is membrane insertion. No intermediate structure has been determined. (PDBIDs: 4H56, 41ON) C) Pneumolysin binds as a monomer then creates a pre-pore intermediate followed by membrane insertion and pore formation. (PDBID: 5AOD; EMDBID: 1106, 1107, 1108) Adapted from Peraro, *et al* (Dal Peraro and van der Goot, 2016).

of the top five leading causes of food borne illnesses in the United States, expresses two β-PFTs whose high-resolution structures have been determined (Huyet et al., 2013; Savva et al., 2013). The heptameric pore crystal structure of Necrotic enteritis toxin B-like, or NetB (responsible for necrotic enteritis in poultry), was determined and revealed a similar domain architecture to α-hemolysin as well as an overall similar 3D structure (Fig. 1-5B) (Savva et al., 2013).

The CDC family of β-PFTs is more prevalent in gram-positive bacteria. These PFTs are thiol activated and use cholesterol as the receptor on host cells. Examples include listeriolysin O (LLO; from *Listeria monocytogenes*, a leading cause of listeriosis), perfringolysin O (PFO; from *Clostridium perfringens*, a leading cause of food borne illness), pneumolysin (of *Streptococcus pneumoniae*, which causes pneumonia) and streptolysin O (SLO; from *Streptococcus pyogenes,* a cause of skin infection). Although each of these toxins leads to a different disease, their mode of action is similar where domain 4 of an inactive monomer binds to a cholesterol-rich membrane, followed by oligomerization of 30-50 monomers, with a final step of membrane insertion creating the active pore, inducing lysis of the target cell (Tweten, 2005). While there have been several crystal structures determined of the monomeric form of CDCs, high resolution structural information has been difficult to obtain of these toxins in the pore-formed state. One of the best characterized of the CDCs is PFO. Initial x-ray crystallographic data determined that PFO is composed predominantly of β-sheets comprised of 4 domains (Rossjohn et al., 1997). Domain 4 was postulated to be responsible for host cell binding. Subsequently, structures determined of CDCs have verified this role for domain 4 and revealed that domain 3 spans the membrane (Feil et al., 2014; Koster et al., 2014; Lawrence et al., 2015; Marshall et al., 2015). There have been

low resolution cryo-EM studies of pre-pore and pore-formed CDCs. For example, cryo-EM analysis of pneumolysin revealed both a pre-pore and pore state where the pore diameter measured at ~300 Å (Fig. 1-5C) (Tilley et al., 2005).

Given the role that each of these PFTs plays in virulence and disease progression, continuation of structural studies is imperative. With the improvements in structural techniques, technology and the advancements made with cryo-EM, hopefully the future will bring more structures of the pore-formed states of toxins that have eluded scientific research.

Helicobacter pylori

Helicobacter pylori is a gram-negative spiral shaped bacterium that infects and colonizes the human stomach. Typically, the acidic pH of the stomach makes it an inhospitable environment for bacterial growth and colonization. However, *H. pylori* has two major characteristics that allow the bacteria to colonize. First, *H. pylori* synthesizes the enzyme urease, which hydrolyzes urea in order to generate ammonia (NH_3) and carbamate, followed by further decomposition into one more NH_3 ion and carbonic acid. The release of ammonia creates a buffer for the bacteria to temporarily survive in the acidic environment of the stomach lumen (Atherton, 2006; Mobley, 1996; Montecucco and Rappuoli, 2001). Second, the bacteria are capable of colonizing the human gastric mucus layer, a feat that no other bacteria can accomplish. The urease also alters the viscosity of the gastric mucus. With this altered viscosity as a result of urease activity, *H. pylori* makes use of its flagella as well as its spiral shape to travel through the mucus layer in a 'corkscrew'-like mechanism toward the neutral pH of the stomach mucosa (Fig. 1-6) (Atherton, 2006; Salama et al., 2013).

Disease Progression and Epidemiology. H. pylori is thought to be transmitted by contaminated food and water and orally through families, most likely

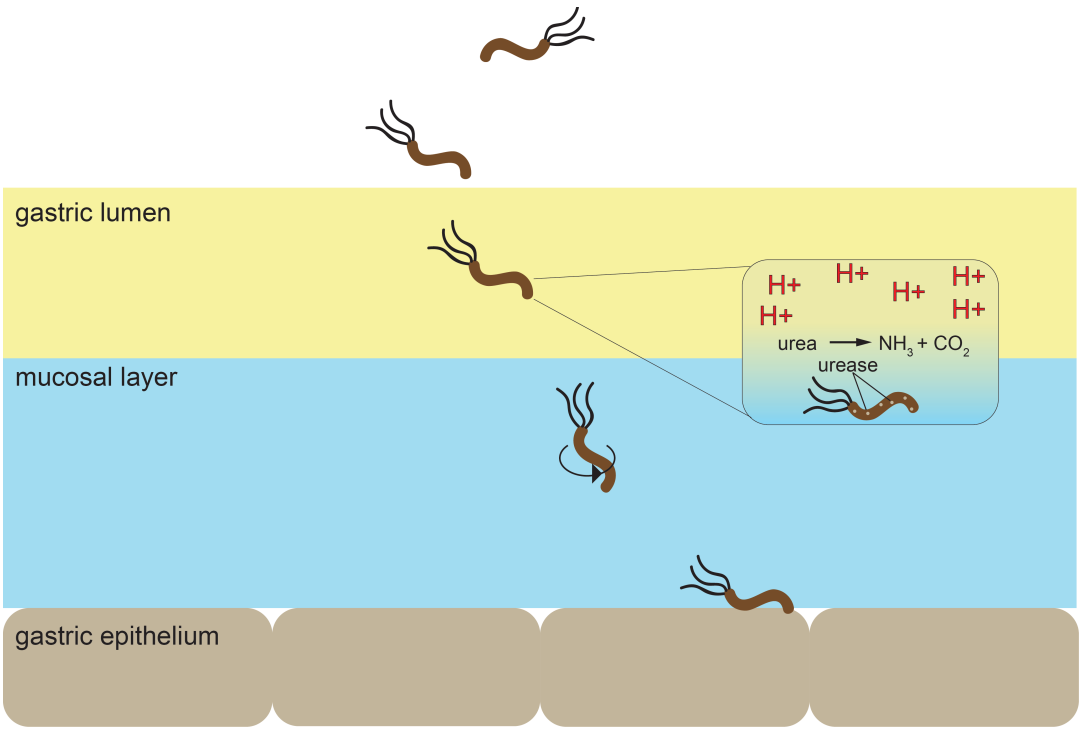

Figure 1-6: *H. pylori* movement through mucosal layer to reach gastric epithelium. *H. pylori* utilizes its spiral shape and flagella in order to traverse the thick mucosal layer. In order to combat the acidity of the environment, the bacteria produce urease which catalyzes the conversion of urea to ammonia and carbon dioxide.

during childhood (Brown, 2000; Bui et al., 2016). Its persistent colonization in the stomach leads to the development of chronic gastritis, and in some cases peptic ulcer disease, mucosa-associated lymphoid tissue (MALT) lymphoma or gastric adenocarcinoma (Atherton and Blaser, 2009; Cover and Blaser, 2009; Marshall et al., 1984; Suerbaum and Michetti, 2002; Uemura et al., 2001). Due to the involvement of *H. pylori* in the development of these cancers, the World Health Organization classified the bacteria as a type I carcinogen in 1994 (Anonymous, 1994). Gastric cancer is the second leading cause of cancer-related deaths in the world, and it is more prevalent in developing countries, where infection can be as high as 90% of the population (Leja et al., 2016). Currently, the bacteria infect approximately 50% of the world's population (Amieva and El-Omar, 2008; Atherton, 2006; Nomura et al., 1991; Parsonnet et al., 1991a; Parsonnet et al., 1991b; Suerbaum and Michetti, 2002).

Adhesin Molecules. There are several adhesin proteins of *H. pylori* that aid in bacterial to attachment to host cells and each adhesin serves a different role. The best characterized adhesins are blood-antigen binding protein (BabA) and sialic acid binding protein (SabA). Recent x-ray crystallographic analysis has determined the binding site of BabA to lewis B antigens, a great step in understanding how the bacteria adheres to host gastric epithelium through blood antigens (Hage et al., 2015). BabA exhibits striking similarities in overall 3D structure when compared to SabA. Structural and functional analysis will be required to fully understand how these adhesins function in different strains of *H. pylori* and their role in the development of disease.

Increasing Antibiotic Resistance. Traditionally a triple therapy consisting of a proton pump inhibitor (PPI) and two antibiotics (such as clarithromycin, metronidazole, or amoxicillin) has been given to patients in order to eradicate the

infection. However, there has been increasing resistance to clarithromycin and metronidazole, leading to necessity for different therapeutics, such as the use of bismuth (Urgesi et al., 2012). While other therapies are becoming more widely utilized, the antibiotic resistance threat poses a need for development of a more specific drug target. Structural studies of the virulence factors of *H. pylori* will grow increasing useful toward this goal.

Virulence Factors. *H. pylori* secretes two major virulence factors – cytotoxin-associated antigen A (CagA) and vacuolating cytotoxin A (VacA; detailed in the next section). VacA is secreted by nearly all strains of *H. pylori*; however, CagA is not found in all strains of the bacteria but its presence is associated with a higher risk of developing *H. pylori* associated diseases (Blaser et al., 1995; Covacci et al., 1993; Crabtree et al., 1991; Gwack et al., 2006). It has been suggested that patients with gastric cancer are two times more likely to have a *cagA* positive strain of *H. pylori* than a *cagA* negative strain (Blaser et al., 1995; Gwack et al., 2006).

The *cag* pathogenicity island is 40kb segment that encodes for *cagA* and components for the type 4 secretion system (T4SS) of *H. pylori* (Censini et al., 1996). CagA is the last encoded gene and is an effector protein that is injected into the host cell by a T4SS and is the only known effector protein of the bacteria (Akopyants et al., 1998; Censini et al., 1996). Once inside the host cell, CagA can elicit several cellular effects, both in its phosphorylated and unphosphorylated state. If left unphosphorylated, for example, CagA can cause disruption of tight junctions and adherens junctions, cell proliferation and differentiation, cell scattering, and inflammatory response induction (Amieva et al., 2003; Bagnoli et al., 2005; Brandt et al., 2005; Chang et al., 2006; Franco et al., 2005; Lee et al., 2010; Mimuro et al., 2002; Murata-Kamiya et al., 2007; Oliveira et al., 2009). CagA

is phosphorylated at a Glu-Pro-Ile-Tyr-Ala (EPIYA) motif located at its C-terminus and this phosphorylation event can result in activation of signaling pathways, leading to changes in cell motility and shape (Brandt et al., 2007; Higashi et al., 2002; Suzuki et al., 2005; Tammer et al., 2007). Recently, the core membrane spanning components of the T4SS of *H. pylori* were visualized using negative stain single particle EM (Frick-Cheng et al., 2016). The data revealed that the core complex is a ring-like structure with 14 spoke-like densities, suggesting a 14-fold symmetry, connected to an inner ring. The side view of the complex revealed a stalk-like structure representing the membrane spanning region. Using mutational analysis with negative stain electron microscopy, the authors were able to localize the different components of the complex. Further high resolution structural analysis will be required to better understand the mechanism of CagA secretion and the structure of the corresponding secretion system.

Vacuolating Cytotoxin A

Vacuolating cytotoxin A, VacA, is a pore-forming exotoxin secreted by *H. pylori*. Known for its ability to induce the formation of large vacuoles when applied to cells, the *vacA* gene encodes a 139kDa preprotoxin that is secreted by the autotransporter pathway (type Va secretion pathway) (Fig. 1-7A). The VacA preprotoxin contains a signal sequence, passenger domain, and an autotransporter domain (Fig. 1-7B). In this pathway, the C-terminus inserts into the membrane forming a β-barrel pore. Then a linker region within the autotransporter domain moves through the pore followed by folding of the passenger domain once it has passed through the pore. The final step is proteolysis yielding the mature toxin. Once VacA has undergone cleavage at the N- and C-terminus, an 88kDa mature toxin emerges (Fig 1-7C). The mature toxin contains two distinct domains,

an N-terminal p33 domain and a C-terminal p55 domain (de Bernard et al., 1998; Torres et al., 2004).

There are currently three known polymorphic regions within VacA that are associated with different degrees of virulence of the bacteria (Fig. 1-7C). The signal region, or s region, is located at the N-terminus of the mature toxin. Noted s1 and s2, the differences between them are the result of differential cleavage of the N-terminus after secretion (McClain et al., 2001b). The s2 form contains a twelve amino acid hydrophilic extension and is associated with a lower risk of disease and inability to induce vacuolation within cells (Letley and Atherton, 2000; McClain et al., 2001b). The intermediate region, or i region, is located at the C-terminus of the p33 domain, near the linkage between both domains, and are designated i1, i2, and i3 (Rhead et al., 2007). This region has been reported to be involved in the ability of VacA to vacuolate cells as well as the ability of VacA to bind different cell types(Gonzalez-Rivera et al., 2012; Rhead et al., 2007). It has been suggested that this region is the best marker for the development of disease (Rhead et al., 2007). The middle region, or m region, is located within the center of the p55 domain and the major sequence difference between m1 and m2 is an additional 23 amino acids between residues G475 and I476 of m1 (Atherton et al., 1995; Cover et al., 1994). The polymorphism in this region is associated differences in cell tropism (Pagliaccia et al., 1998). VacA s1/i1/m1 is the most common allele and vacuolates cells efficiently and is associated with a higher risk of disease while VacA s2/i2/m2 is incapable of vacuolating cells efficiently and is associated with a lower risk of disease (Cover and Blanke, 2005).

*VacA domain architecture***.** As previously mentioned, VacA is composed of two domains, p33 and p55 (Fig. 1-7C). Each domain is responsible for different VacA effects, but both domains are required for cell vacuolation and host cell

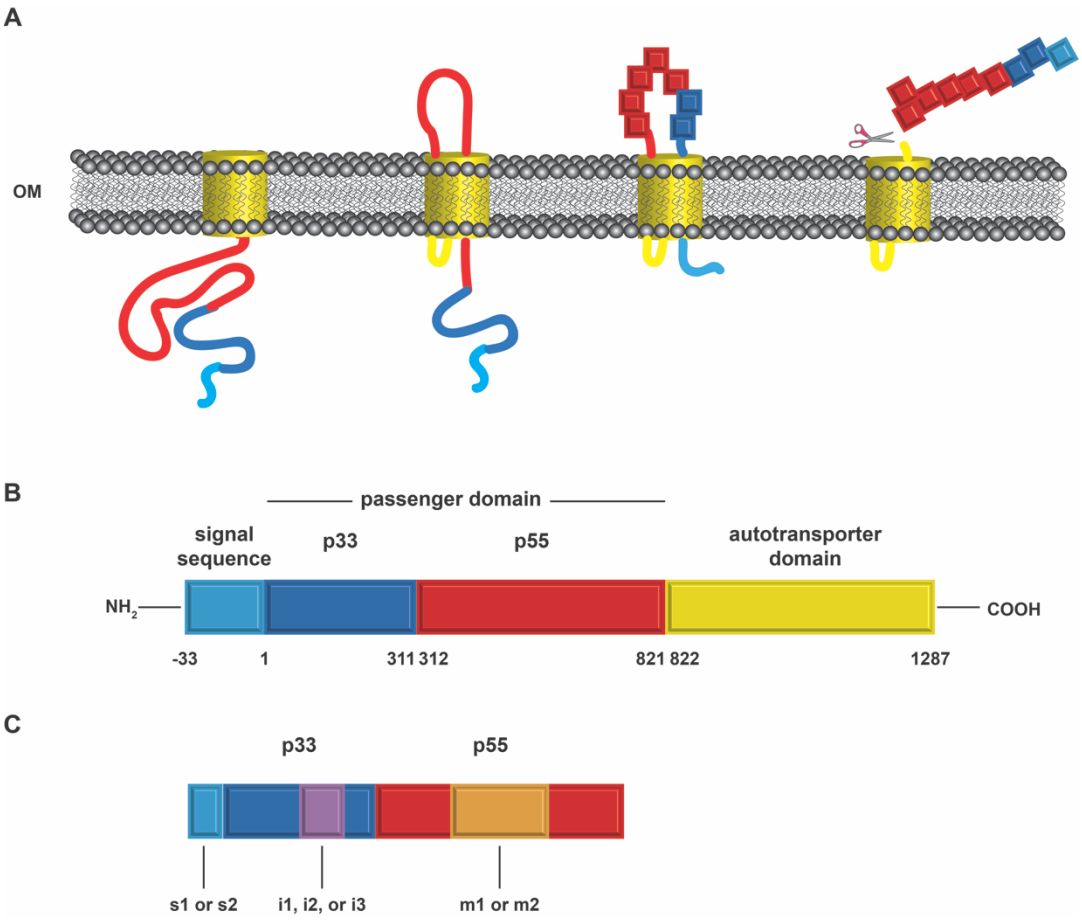

Figure 1-7: VacA secretion and polymorphic regions related to virulence. A) VacA is secreted via the type Va secretion system (or autotransporter pathway) where first the autotransporter domain creates a β-barrel pore through which the signal peptide extends. Then the passenger domain is threaded through and properly folded once in the outer membrane. The signal peptide is then cleaved. B) The VacA preprotoxin is composed of a signal sequence, passenger domain and autotransporter domain. C) VacA contains three regions of polymorphism, the signal (s) region, intermediate (i) region, and the middle (m) region. Differences in these regions are related to differences in virulence. Adapted from Desvaux, *et. al.* (Desvaux et al., 2004).

binding (Cover and Blanke, 2005; Domanska et al., 2010; El-Bez et al., 2005; Gonzalez-Rivera et al., 2010; McClain et al., 2003; Torres et al., 2005). The p33 domain is also responsible for VacA pore formation (McClain et al., 2003). It contains a stretch of 32 uncharged residues that are responsible for insertion into membrane (Cover and Blanke, 2005; Nguyen et al., 2001). Within these 32 residues are three tandem repeats of a known membrane insertion motif, GXXXG, which were first discovered in human glycophorin A (GpA) as dimerization motifs (Furthmayr and Marchesi, 1976; Lemmon et al., 1992; McClain et al., 2003; Russ and Engelman, 2000; Teese and Langosch, 2015). In fact, deletion of these motifs abolishes the ability of VacA to create an active pore and induce vacuolation (McClain et al., 2001a; McClain et al., 2003). Studies have shown using planar lipid bilayers in combination with electrophysiology that VacA forms an anionic channel within the membrane, with a preference for channeling chloride ions (Czajkowsky et al., 1999; Czajkowsky et al., 2005; Iwamoto et al., 1999; Szabo et al., 1999; Tombola et al., 1999a; Tombola et al., 1999b).

The p55 domain is responsible for VacA binding to receptors on host cells. There have been numerous reported receptors for VacA. VacA has been shown to be targeted to lipid raft and a major component of lipid rafts, the sphingolipid sphingomyelin, has recently been shown to be a VacA receptor (Geisse et al., 2004; Gupta et al., 2008; Kuo and Wang, 2003; Nakayama et al., 2006; Patel et al., 2002; Schraw et al., 2002). Other receptors reported for VacA include receptor protein tyrosine phosphatases (RPTP) α and β, low density lipoprotein receptor-related protein-1 (LRP-1), epidermal growth factor receptor (EGFR), heparan sulfate, CD18, glycosphingolipids, and phospholipids (Foegeding et al., 2016; Kuo and Wang, 2003; Ricci et al., 2000; Seto et al., 1998; Utt et al., 2001; Yahiro et al.,

1999; Yahiro et al., 2012; Yahiro et al., 2003). This wide range of receptors for VacA lends to the toxin's ability to trigger a multitude of cellular effects.

Cellular Effects of VacA. VacA is internalized into cells via clathrin independent, actin dependent and Cdc42 dependent pinocytosis (Gauthier et al., 2007; Gauthier et al., 2005; Gauthier et al., 2004; Sewald et al., 2011). Once internalized, it is known that VacA is found in glycosylphosphatidyl inositol anchored protein (GPI-AP) enriched early endosomal compartments (GEECs) (Gauthier et al., 2007). Followed by detection in early endosomes, VacA is found late endosomes where vacuolation occurs (Gauthier et al., 2007; Sewald et al., 2011).

As previously mentioned, VacA is named for its ability to induce large vacuoles when applied to cells. Vacuolation is the result of anion channel formation in endosomes, allowing for the influx of chloride ions upon activation of V-type ATPases, to which VacA has been shown to colocalize (Genisset et al., 2007; Morbiato et al., 2001). This leads to the accumulation of weak bases, leading to osmotic swelling (Fig. 1-8A). The Rab7 GTPase is required for this late endosomal swelling (Papini et al., 1998a). A mutant lacking the membrane spanning GXXXG motifs, VacA ∆6-27, not only lacks the ability to vacuolate cells but also exhibits a dominant negative effect when mixed with VacA s1/i1/m1 (Chambers et al., 2013; Vinion-Dubiel et al., 1999).

VacA intoxication also leads to alterations in mitochondrial function resulting in cell death. Intriguingly, it has been demonstrated that VacA p33 colocalizes with mitochondria by targeting the inner mitochondrial membrane (IMM), leading to apoptosis (Fig. 1-8B) (Domanska et al., 2010; Galmiche et al., 2000). Later studies reported that purified VacA interacts with mitochondria leading to the depolarization of mitochondrial membrane potential, followed by the release

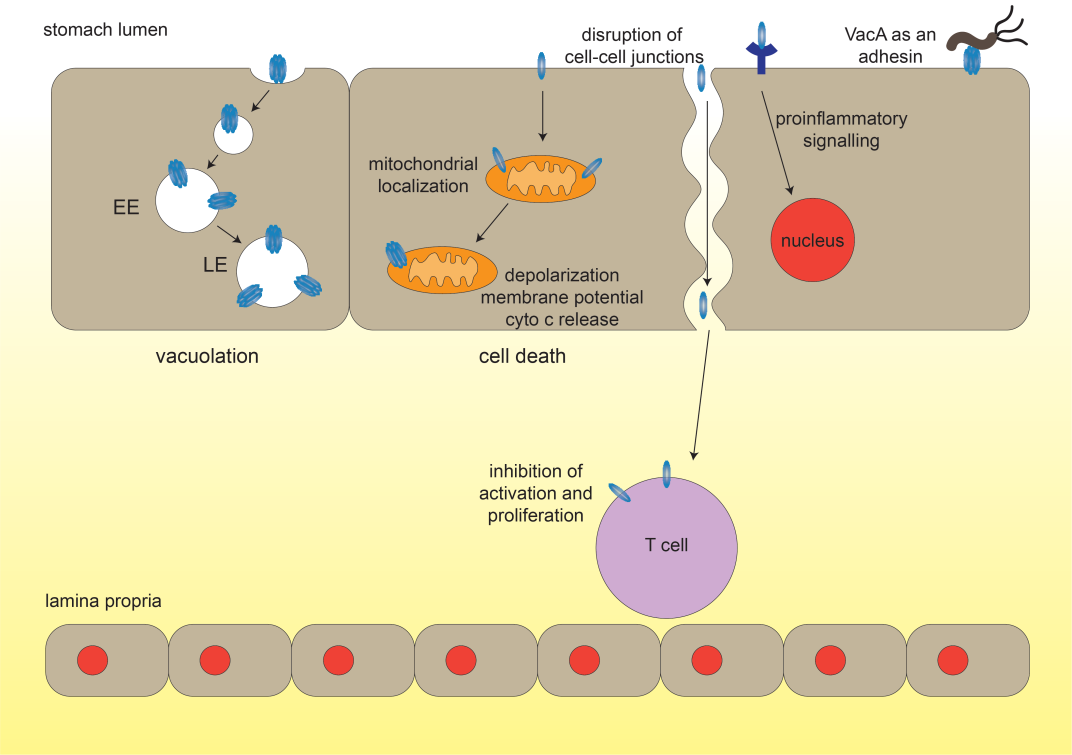

Figure 1-8: VacA causes multiple cellular effects. When VacA is applied to cells, it induces different cellular effects. These effects include vacuolation (A), mitochondrial dysfunction (B) and membrane permeability, proinflammatory signaling (C), and T cell inhibition (D). Adapted from Palframan, *et al.* (Palframan et al., 2012).

of cytochrome c into the cytosol, and thus, cell death (Calore et al., 2010a; Gebert et al., 2003; Jain et al., 2011; Nakayama et al., 2004; Radin et al., 2011; Sewald et al., 2008b; Sundrud et al., 2004; Terebiznik et al., 2009; Willhite and Blanke, 2004; Willhite et al., 2003; Yamasaki et al., 2006). In contrast to the idea that VacA directly interacts with mitochondria, Yamasaki, *et. al.* reported that VacA continues inducing vacuolation and does not interact directly with mitochondria or induce cytochrome c release; however, VacA does increase activity of pro-apoptotic factors Bax and Bak (Yamasaki et al., 2006). Therefore, the mechanism of action that VacA takes in order to induce apoptosis is not well understood. An endosomal-mitochondrial juxtaposition has been proposed; however, this has not been previously observed inside the cell and no other evidence of this fusion exists (Calore et al., 2010b).

Not only does VacA induce membrane depolarization in mitochondria, but the toxin also alters membrane permeability in epithelial cells, allowing for the efflux of molecules other than chloride ions (Amieva et al., 2003; Debellis et al., 2001; Papini et al., 1998a; Pelicic et al., 1999; Tombola et al., 2001). This could potentially be beneficial for the bacteria in order to continue colonization within the stomach. VacA can also bind and induce proinflammatory signalling (Fig. 1-8C) (Palframan et al., 2012).

H. pylori vacA+ bacteria as well as purified VacA application to gastric epithelial cells (AGS cells) has been shown to induce autophagy (Greenfield and Jones, 2013; Raju et al., 2012; Terebiznik et al., 2009; Yahiro et al., 2012). One study determined that VacA induced autophagy is dependent on channel formation by VacA, as mutants unable to oligomerize and the s2/m2 form of VacA was unable to induce autophagy (Terebiznik et al., 2009).

Previous studies have shown that the interaction of VacA with T lymphocytes (T cells) hinders the IL-2 signaling pathway (Fig. 1-8D) (Boncristiano et al., 2003; Gebert et al., 2003; Sundrud et al., 2004). More recently, a T cell receptor for m1-VacA has been identified, CD18, which is an integrin subunit found on T cells (Sewald et al., 2008b). The interaction between these two proteins suggests a potential immunomodulatory role for VacA.

Overall Structure of VacA. Although VacA is secreted as an 88kDa monomer, it is capable of forming large oligomeric complexes at neutral pH, including single-layer hexamers and heptamers and double-layered dodecamers and tetradecamers (Adrian et al., 2002; Chambers et al., 2013; Lanzavecchia et al., 1998; Lupetti et al., 1996). Upon acid-activation of the toxin, which is required for cellular internalization, the oligomers are dissociated into monomers (Cover et al., 1997; McClain et al., 2000; Yahiro et al., 1999). Due to the heterogeneity of VacA, structural determination efforts have been hindered. In 2004, a crystal structure of the majority of the p55 domain was determined to 2.4 Å resolution (Fig. 1-9A) (Gangwer et al., 2007). The crystal structure revealed that the p55 domain, residues 355-811, consists of a right handed β-helix with a globular domain at the C-terminus. Unfortunately, efforts to crystallize the full length monomer has been difficult due to the flexibility of the p33 domain. An important result of the study was that the authors were able to place the crystal structure into a previously determined oligomer structure and demonstrate that the p55 domain is localized to the arms of the oligomer (Gangwer et al., 2007; Ivie et al., 2010). Gonzalez-Rivera reported a 4.5 Å crystal structure of a non-oligomerizing form of VacA, Δ346-347, a mutant that contains a two amino acid deletion at the N-terminus of the p55 domain, near the junction of p33 and p55 (Fig. 1-9B)

(Gonzalez-Rivera et al., 2016). Negative stain analysis shows that this mutant at neutral pH resembles acid-activated monomeric VacA (Chambers et al., 2013; Gonzalez-Rivera et al., 2016; Pyburn et al., 2016). While the authors were able to determine that the β-helix continued into the p33 domain, the N-terminus remained unresolved leading to the hypothesis that the pore-forming region of p33 is disordered until in contact with membrane.

There have been multiple deep etch microscopy studies performed two decades ago that gave the first glimpses into VacA oligomer structure. A first look at VacA oligomers using deep etch transmission electron microscopy (TEM), revealed that VacA forms 'flower-like' structures mainly consisting of hexamers and heptamers (Adrian et al., 2002; Cover et al., 1997; Lanzavecchia et al., 1998; Lupetti et al., 1996). Cover, *et. al.* showed that VacA oligomers also extend to 12-mers and that acid dissociated VacA can re-anneal to form the large oligomeric complexes when the pH is raised back to neutral (Cover et al., 1997). Later studies using cryo-negative staining revealed that VacA not only creates hexamers and heptamers, but also octamers, nonamers, as well as double-layered oligomers (Fig. 1-9C) (El-Bez et al., 2005). Computational modeling was then performed to generate ~19 Å structures of the oligomers, the highest resolution of an oligomer at the time. One major observation of this study was that in order to form the double-layered oligomers, two single-layers undergo different degrees of rotation in relation to one another, leading to different forms of double-layers (El-Bez et al., 2005). Unfortunately, despite the efforts and improved technology, the central region was unresolvable, continuing the lack of information regarding the p33 pore-forming domain.

VacA membrane interactions. The transition of VacA from a secreted soluble protein to a membrane inserted protein has been difficult to study

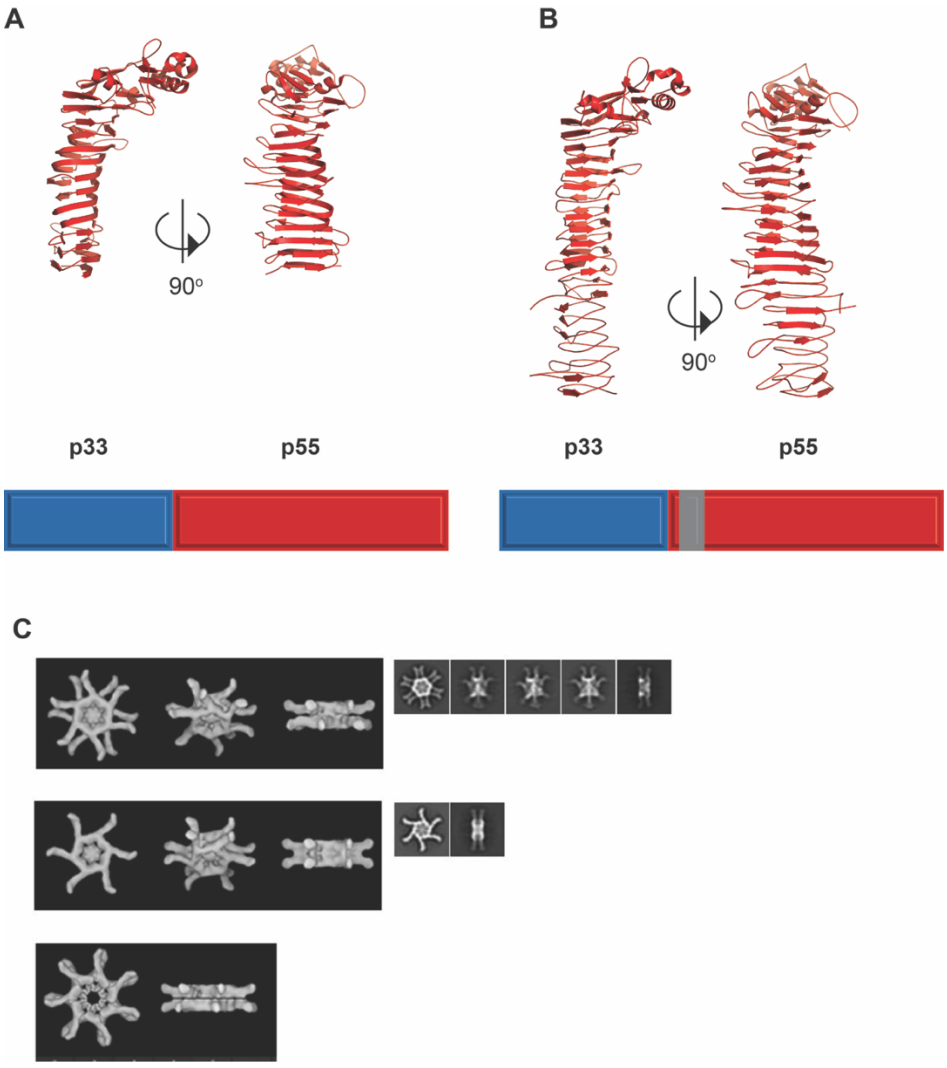

Figure 1-9: Known structural information of VacA. A) Crystal structure of p55 revealed a β-helix with a globular domain at the C-terminus (PDBID: 2QV3). B) Crystal structure of VacA Δ346-347 showed that the β-helix extends into the p33 domain (Gonzalez-Rivera et al., 2016). C) Previously reported cryo-negative EM structures determined using computational methods (El-Bez et al., 2005).

structurally. There have been multiple efforts to determine how VacA interacts with membranes. A major question has been, what oligomeric form is the physiologically relevant form that creates pores within membranes.

Atomic force microscopy of VacA bound to supported lipid bilayers as a two-dimensional crystal array first suggested that VacA bound to lipid bilayers as a single-layered oligomer forming a hexameric chloride channel (Czajkowsky et al., 1999; Iwamoto et al., 1999; Tombola et al., 1999a). However, later studies indicated VacA bound as a double-layered oligomer (Adrian et al., 2002). Therefore, due to the lack of resolution it could not be definitively determined whether these oligomers were single- or double-layered and no information on the p33 domain could be gleaned.

Since VacA has been shown to be an anion specific chloride channel, it has been hypothesized that it creates an alpha helical pore. In 2004, Bowie and colleagues generated a structural model of the VacA pore (Kim et al., 2004). The model used a known anion channel structure, the mechanosensitive channel of small conductance, or MscS from *Escherichia coli* (Kim et al., 2004). MscS is an alpha helical chloride channel which contains GXXXG motifs (Bass et al., 2002). Using the structure prediction procedure in the Monte Carlo package, they determined that both structures had similar residues lining the pore. In MscS the anion selective residue is proposed to be Arg-88, a positively charged residue located at the top of the pore. Correspondingly, based off the structure predictions, Lys-33 of VacA was proposed to be the anion selective residue (Kim et al., 2004). Although this model for the VacA pore shares striking similarities to that of a known chloride channel, there is still a lack of experimental evidence of the VacA pore.

Research Objective.

VacA is a secreted PFT that transitions from a soluble protein to a membrane inserted anion channel to induce multiple cellular effects. This toxin does not exhibit and sequence homology to any other toxin of known structure. While it is known that the p55 domain of VacA is comprised of a β-helix and a C-terminal globular domain, the structure of the p33 domain remains unknown. VacA also, under neutral conditions, is capable of forming multiple large oligomeric complexes. As with the soluble structure of the p33 domain, there is a lack of structural knowledge on what the pore of VacA looks like. Work detailed in Chapter III shows optimal conditions for VacA s1/i1/m1 insertion into membrane as a single-layer hexamer, data that can be utilized towards the determination of a high-resolution structure of a VacA pore.

The work presented here details the highest resolution of a VacA oligomer to date at 10 Å resolution. Chapter I will detail negative stain random conical tilt (RCT) EM structures at ~15 Å resolution of different VacA oligomers. Chapter II investigates the physiological relevant oligomeric form of VacA in order to begin understanding pore formation by the toxin. Recent advancements in electron microscopy, namely the advent of the direct electron detector (DED), as well as improvements in data processing, has allowed for the determination by cryo-EM of a 10Å structure of a VacA dodecamer, detailed in Chapter IV.

CHAPTER II

STRUCTURAL ANALYSIS OF THE OLIGOMERIC STATES OF *HELICOBACTER PYLORI* VacA TOXIN

Introduction

Helicobacter pylori is a Gram-negative bacterium that colonizes the human stomach (Atherton and Blaser, 2009; Cover and Blaser, 2009; Marshall et al., 1984) and can lead to the development of peptic ulcer disease, gastric adenocarcinoma, or gastric lymphoma (Amieva and El-Omar, 2008; Atherton, 2006; Suerbaum and Michetti, 2002). Gastric cancer is the second leading cause of cancer-related deaths worldwide, and *H. pylori* is classified as a type 1 carcinogen by the World Health Organization (Fuchs and Mayer, 1995).

The major secreted exotoxin of *H. pylori* is known as VacA, named for its ability to induce vacuolation in the cytoplasm of mammalian cells (Boquet and Ricci, 2012; Cover and Blanke, 2005; Fischer et al., 2004; Montecucco and de Bernard, 2003; Rassow and Meinecke, 2012). Additionally VacA causes a slew of cellular responses that include depolarization of membrane, mitochondrial dysfunction, autophagy, cell death, activation of mitogen-activated protein kinases, and inhibition of T cells (Calore et al., 2010a; Domanska et al., 2010; Galmiche et al., 2000; Gebert et al., 2003; Jain et al., 2011; Nakayama et al., 2004; Radin et al., 2011; Sewald et al., 2008b; Sundrud et al., 2004; Szabo et al., 1999; Terebiznik et al., 2009; Willhite and Blanke, 2004). The mechanisms by which these alterations occur are not fully understood, but many require VacA intoxication (Calore et al., 2010b; Gauthier et al., 2007; Willhite and Blanke, 2004). VacA forms anion-selective channels in planar lipid bilayers and in the plasma

membranes of cells, and it is hypothesized that VacA can also form channels in endosomal and mitochondrial membranes (Cover and Blanke, 2005; Czajkowsky et al., 1999; Iwamoto et al., 1999; Tombola et al., 1999b).

VacA, secreted as an 88-kDa toxin, consists of two domains, designated p33 and p55. The p33 domain is postulated to form the anion-selective channel, and both the p33 and p55 domains mediate VacA binding to host cells (Cover and Blanke, 2005; Domanska et al., 2010; El-Bez et al., 2005; Gonzalez-Rivera et al., 2010; McClain et al., 2003; Torres et al., 2005). A 2.4 Å 3D structure of the p55 domain was determined by X-ray crystallography, but there is no structural information on the p33 domain (Gangwer et al., 2007).

VacA assembles into a heterogeneous assortment of oligomeric "snowflake"-structures, which have been visualized by several approaches (Adrian et al., 2002; Czajkowsky et al., 1999; El-Bez et al., 2005; Gonzalez-Rivera et al., 2010; Lanzavecchia et al., 1998; Lupetti et al., 1996; Reyrat et al., 1999). Mutant VacA proteins that fail to oligomerize lack toxin activity (Genisset et al., 2006; Ivie et al., 2008; Vinion-Dubiel et al., 1999). The snowflake structures likely represent water-soluble forms of the anion-selective membrane channels formed by VacA. The highest resolution structures of VacA oligomers thus far (~19 Å) were obtained by cryo-negative stain EM (El-Bez et al., 2005). In this previous structural analysis, it was not possible to obtain tilt pair images, and therefore the 3D models relied on a number of modeling techniques to generate structures from the heterogeneous images of VacA oligomers (El-Bez et al., 2005). Analysis of the X-ray crystallographic structure of p55 together with EM images of the oligomers has led to a model of VacA oligomer organization in which the p33 domain occupies the inner core of the "snowflakes" and the p55 domain extends outward from the central core (Gangwer et al., 2007). However, the cryo-negative stain EM

structure contained no details about p33 organization and did not allow an analysis of how VacA monomers interact to form oligomers.

Sequence variations within VacA influence cytotoxicity and are associated with distinct pathological responses (Atherton et al., 1995; Rhead et al., 2007). Three polymorphic regions have been identified: an N-terminal region that is differentially cleaved during toxin export to form either an s1 or s2 variant, an intermediate region (i1 or i2) located at the C-terminus of the p33 domain, and a middle region (m1 or m2) in the p55 domain that affects receptor binding (Atherton et al., 1995; Gangwer et al., 2010; Pagliaccia et al., 1998; Rhead et al., 2007). Type s1m1 and s1m2 VacA variants are considered fully active, although the s1m2 variant binds to a narrower range of cells (Letley et al., 2003; Pagliaccia et al., 1998). Type s2 VacA variants contain a twelve-residue hydrophilic N-terminal extension, do not vacuolate cells, and form membrane channels less efficiently than s1 variants, moreover, s2 forms of VacA are associated with a very low risk of symptomatic gastric disease (Atherton et al., 1995; Letley and Atherton, 2000; Letley et al., 2003; McClain et al., 2001b). The mechanism by which these additional residues disrupt VacA activity is not well understood.

Analysis of experimentally constructed VacA mutant proteins has identified specific VacA domains and/or residues required for pore formation and oligomerization. However, the limited structural understanding of how VacA oligomerizes, coupled with the lack of structural information on p33, has made it difficult to elucidate the exact roles of these domains or residues in VacA function. One mutant, VacAΔ6-27, lacks three hydrophobic GXXXG motifs posited to be important for pore formation and exhibits a dominant negative phenotype when mixed with equal molar ratios of acid activated wild-type (WT) VacA (McClain et al., 2003; Vinion-Dubiel et al., 1999). Although this mutant has previously been

structurally characterized, the low resolution and lack of structural detail in the central p33 region of the 3D maps made it difficult to mechanistically explain how the Δ6-27 mutation disrupts function, and the structural consequences of VacAΔ6-27 interaction with WT VacA were not explored (El-Bez et al., 2005). Another mutant, containing a deletion between the p33/p55 domains of VacA, retains cell-vacuolating activity, and was reported to assemble into predominantly six-sided oligomeric structures instead of seven-sided oligomers (Burroni et al., 1998; Tombola et al., 2001).

VacA does not exhibit homology to other known bacterial toxins; therefore, there is considerable interest in elucidating the structure of this protein and understanding the mechanism of membrane pore formation. Although the toxicity of VacA lies in its ability to form channels, a high-resolution 3D structure of oligomeric VacA has yet to be determined, creating a large gap in our understanding of this toxin and its role in *H. pylori* pathogenesis. In this study, we report the determination of ~15 Å 3D reconstructions of six oligomeric forms of VacA. These structures provide the first details of p33 organization in the central pore and allow us to generate a structure-based model for how VacA oligomerizes. We have also used EM analysis to characterize VacA variants and mutants that differ from WT VacA in activity or oligomeric structure, providing structural insights into the mechanism by which a dominant negative mutant inhibits the activity of WT VacA, and the mechanisms by which VacA oligomerizes and forms membrane channels.

Results and Discussion

Visualization of VacA oligomers by negative stain electron microscopy. WT VacA was purified from *H. pylori* culture supernatant and, as expected, acid-activated preparations caused vacuolation of epithelial cells (data not shown). Negative stain EM analysis of purified WT VacA revealed "snowflake"-like particles (Fig. 2-1A), corresponding to morphologies observed in other studies (Adrian et al., 2002; Cover et al., 1997; Czajkowsky et al., 1999; El-Bez et al., 2005; Lanzavecchia et al., 1998; Lupetti et al., 1996). In contrast to the random orientation of VacA in previously described cryo-negative stain images, VacA oligomers absorbed in a preferred "*en face*" orientation on the grids (El-Bez et al., 2005). If the specimen adsorbs on the carbon film in one or a few preferred orientations, the specimen must be tilted in the electron microscope to obtain the additional views required for 3D reconstruction. Using this technique, referred to as the random conical tilt (RCT) approach, the 3D volume is calculated by back-projection algorithms (Radermacher et al., 1987). Since in this technique the same specimen area is imaged twice, once at a high tilt angle and then again untilted, the orientation parameters are uniquely defined and the resulting 3D reconstruction is very reliable. This approach is especially useful when examining samples, such as VacA, that exist in more than one structural state since we are able to classify the distinct conformations using the untilted images then use the tilted images to determine the structure. Image pairs of grids containing negatively stained VacA were recorded at tilt angles of 55˚ and 0˚. A total of 14,573 pairs of particles were selected, and images of the untilted specimens were classified into 20 class averages (Fig. 2-2A). These class averages showed that while essentially all VacA particles adsorbed to the carbon grid in the same orientation, the oligomer adopts multiple conformations. As seen previously, the classes revealed VacA

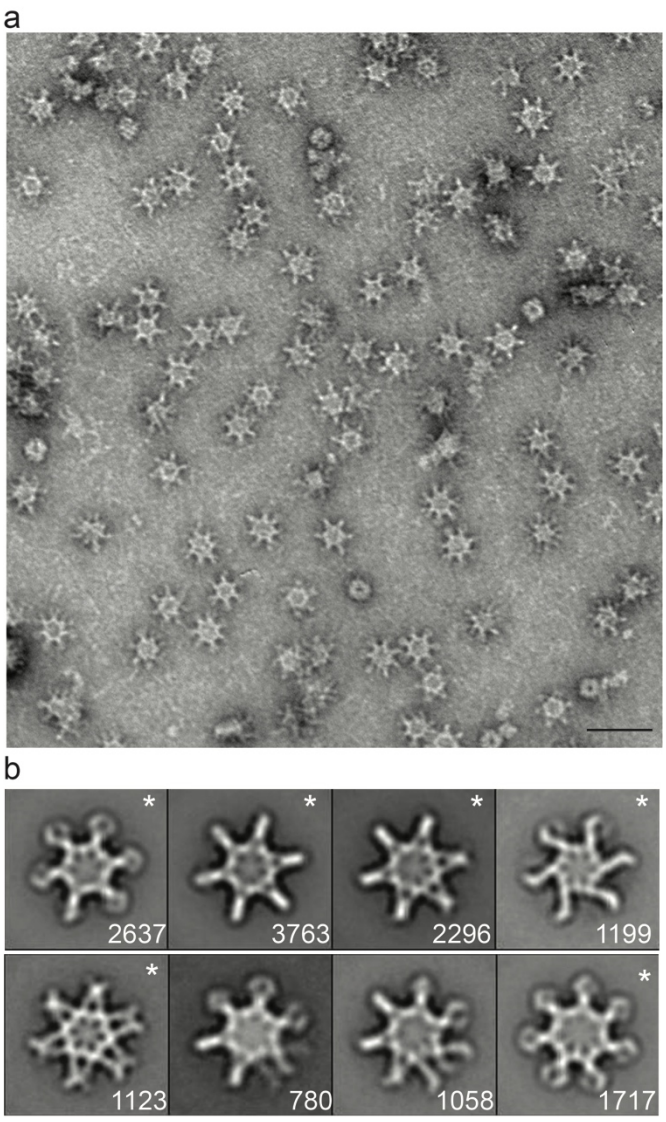

Figure 2-1. Characterization of negatively stained VacA oligomers. (A) Raw image of VacA particles in negative stain. Scale bar, 50 nm. (B) VacA class averages obtained by reference-based alignment and classification. "*" marks classes that yielded 3D structures (see Fig. 2-3). Numbers of particles included in each class is shown in bottom right corner. Side length of panels, 420 Å.

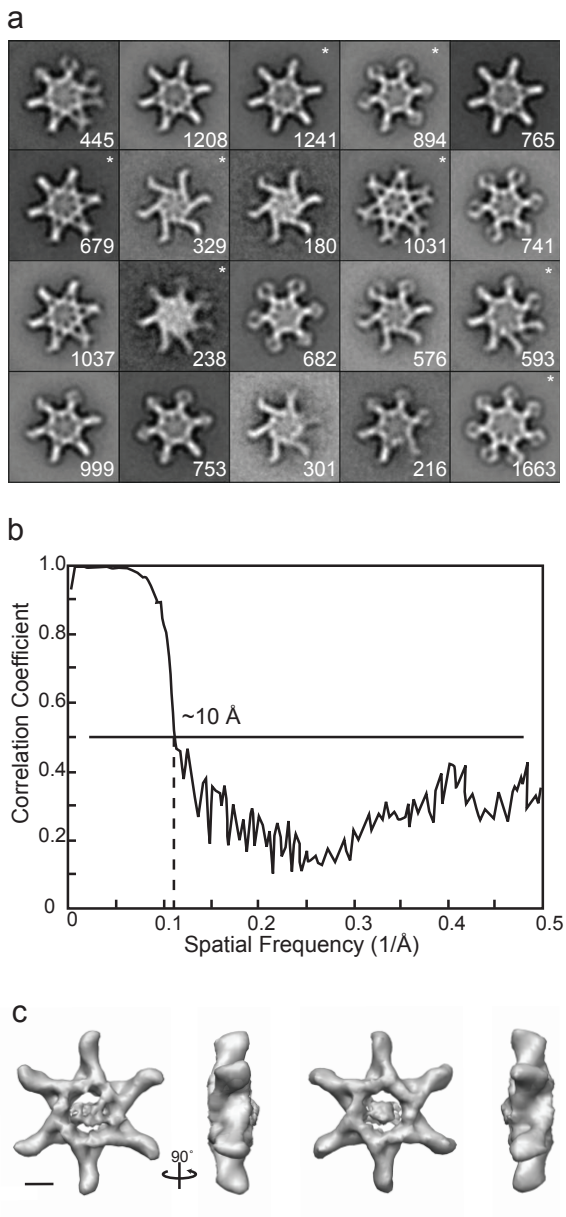

Figure 2-2. Analysis of VacA oligomers in negative stain. (A) Twenty class averages obtained by multi-reference alignment and classification of 14,573 VacA particle images in negative stain. Number of particles in each projection average is shown in the lower right corner of each average. The eight averages for reference based alignment (See Fig. 2-1B) are marked with a "*" in the upper left corner. Side length of panels, 420 Å. (B) Fourier shell correlation (FSC) was used to estimate the resolution of the density map of a VacA dodecamer. Using the FSC = 0.5 criterion, the map has a resolution of ~10 Å. (C) Structure of VacA oligomer shown in Figure 2-4 with no applied symmetry. Structure is rotated along vertical-axis by 90˚. Scale bar, 5 nm.

oligomers that contained six chiral arms (Fig. 2-2A, panel 7 and 8) and oligomers that contained six or seven arms arranged in an achiral fashion (El-Bez et al., 2005). In contrast to previous cryo-negative stain studies, we did not observe particles with eight or nine arms. Furthermore, all the averages, even the chiral forms, had a visible “spoke”-like density in the center of the oligomers (Adrian et al., 2002; El-Bez et al., 2005). From the 20 classes, we selected seven that represent distinct conformations and one less well-resolved VacA class (Fig. 2-2A, marked with “*”). These were used as references for a cycle of reference-based alignment (Fig. 2-1B). The results of the reference-based alignment revealed six well-resolved classes (Fig. 2-1B, marked with a “*”) and two classes that contained particles with disordered arms. Five of the well-resolved classes contained either six or seven achiral arms (Fig. 2-1B, panel 1, 2, 3, 5, and 8), while one class showed an oligomer with six chiral arms (Fig. 2-1B, panel 4). As seen in the reference-free alignment, all the reference-based classes had visible central densities that appear structurally organized.

To more carefully analyze the structural organization of the VacA oligomers, images from the tilted specimens corresponding to each of the eight classes were used to calculate 3D reconstructions using RCT (Fig. 2-3) (Radermacher, 1994). The 3D structures with six- or seven-fold applied symmetry are shown in Figure 2-3, while the same structures without applied symmetry are shown in Figure 2-4. Of the eight 3D reconstructions, only tilted particles associated with the six well-resolved class averages (Fig. 2-1B, marked with a “*”) led to well-defined 3D structures. Structures calculated from particles found in two of the classes looked very similar (Fig. 2-3B and C) and could easily be aligned. To further improve the reconstruction of a VacA oligomer, the tilted images plus 10% of the highest correlated zero degree images from these two classes were

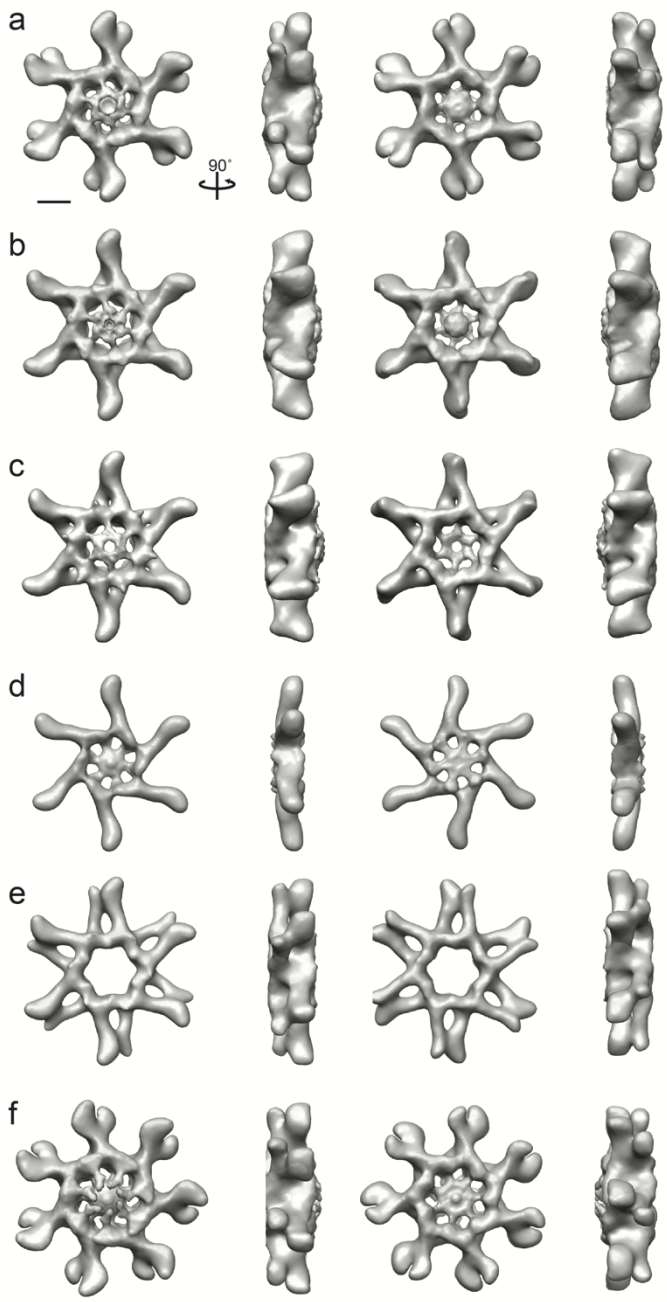

Figure 2-3. 3D reconstruction of negatively stained VacA oligomers using random conical tilt approach. (A-F) VacA organizes into a number oligomeric conformations that include both hexamers, dodecamers, and tetradecamers. These structures have applied symmetry. Structures are rotated along vertical-axis by 90˚. Scale bar, 5 nm.

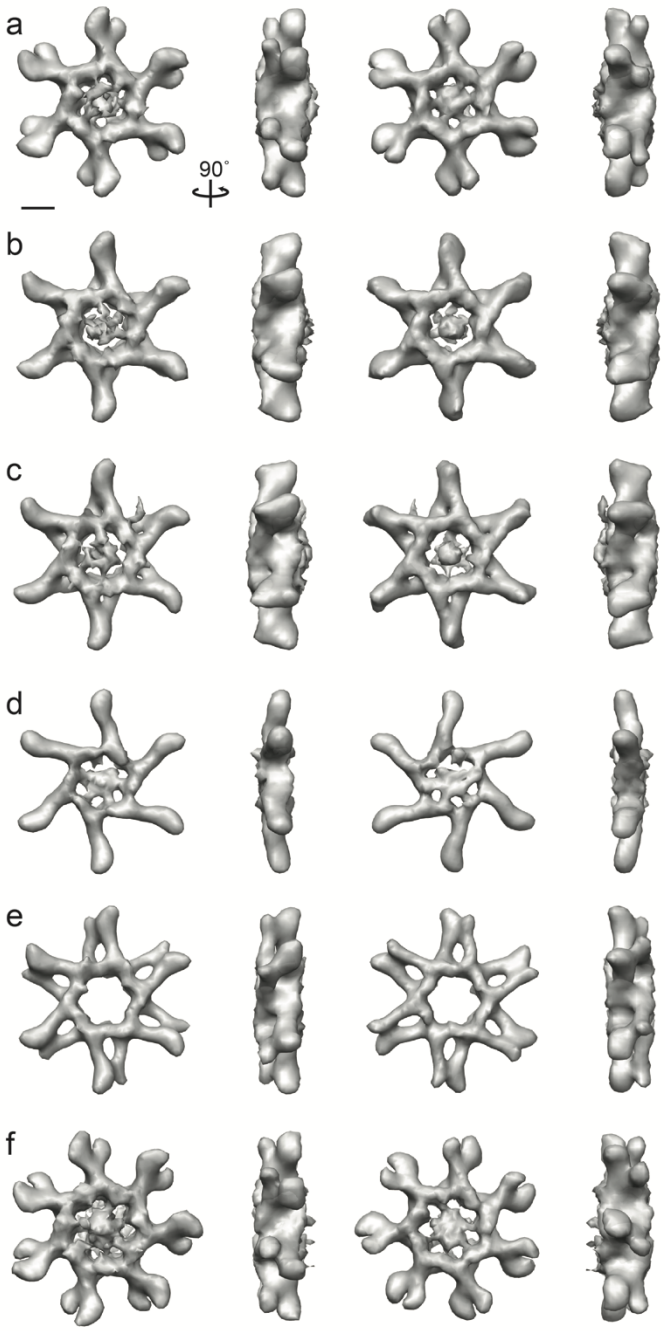

Figure 2-4. 3D reconstruction of negatively stained VacA oligomers without applied symmetry. (A-F) Structures of VacA oligomers shown in Figure 2-3 with no applied symmetry. Structures are rotated along vertical-axis by 90˚. Scale bar, 5 nm.

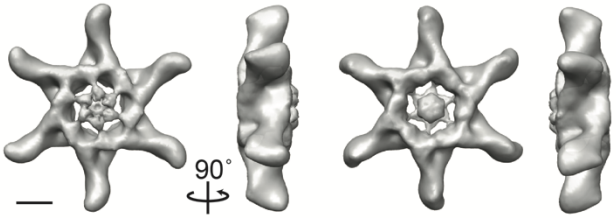

Figure 2-5. ~15 Å 3D reconstruction of VacA dodecamer. The structure contains two prominent features: extended straight “arms” with a slight kink at the distal end and a central “spoke-like” density composed of two distinct globular domains separated by a thinner connecting density. Structure rotated around vertical axis by 90˚. Scale bar, 5 nm.

combined and used to calculate a 3D reconstruction either with or without applied 6-fold symmetry (Fig. 2-5 and 2-2C).

From the presented structures, it is clear that VacA monomers can oligomerize into achiral double layer structures containing either six or seven arms (Fig. 2-3A, B, C, E, and F and 2-5) or into a chiral hexameric structure (Fig. 2-3D). Our statistics show that approximately 8% of the oligomers represent hexamers, 79% represent dodecamers, and 11% represent tetradecamers (Table 2-1). Interestingly, VacA heptamers, although seen previously under negative stain, cryo-negative stain and vitrified ice conditions (data not shown), were not observed in our analysis, even when we expanded the number of classes to 60 (data not shown) (El-Bez et al., 2005; Gonzalez-Rivera et al., 2010). One possible explanation stems from our observation that the preferred conformation of VacA oligomers in solution shifts over time towards hexameric, dodecameric, and tetradecameric forms (data not shown). The structures, regardless of oligomeric type, contain two prominent features: extended straight arms with a slight kink at the distal end and central “spoke”-like densities. The arms clearly represent the VacA p55 domain, leaving the central region to represent the p33 domain (Gangwer et al., 2007). The double-layer VacA oligomers contain a well-resolved central region on one side of the structure (Fig. 2-3A, B, C, and F and 2-5), although there is central density present on both sides when no symmetry is applied (Fig. 2-4). Additionally, some of the oligomers appear to contain a “plug” that occludes the central hole (Fig. 2-3 and 2-4). It is possible that the less ordered face is the one that makes contact with the carbon grid and that the presence of a plug either represents unorganized central density or stain accumulation. The exception to this observation is the structure of one VacA dodecamer, which does not contain any well-resolved central density at the molecular weight threshold

VacA	hexamers	dodecamers	heptamers	tetradecamers	disordered	6-fold	7-fold	ratio*
Wild-type	8%	79%	-----	11%	2%	87%	11%	7.9
∆6-27	8%	59%	-----	18%	15%	67%	18%	3.7
s2m1	17%	58%	8%	11%	6%	75%	17%	4.4
∆301-328	4%	84%	-----	5%	7%	88%	5%	17.6

Ratio* = %6-fold/%7-fold; "-----" = not found; "disordered" refers to averages that are difficult to determine whether they represent hexamers, dodecamers, or tetradecamers.

Table 2-1: Comparison of VacA oligomers formed by variants and mutants

corresponding to its calculated mass (1,056 kDa), regardless whether or not symmetry is applied (Fig. 2-3E and 2-4E). The six-sided oligomers have a diameter of 290 Å. The extended arms are ~95 Å long, while the central region has a diameter of 100 Å (Fig. 2-3A-E and 2-5). The central regions for all the oligomers, with the exception of the dodecamer shown in Figure 2-3E, contain two domains separated by a thinner connecting density (Fig. 2-5 and 2-6A and 2-6C). The innermost, central domain has dimensions of ~15 x 15 x15 Å, while the domain positioned that extends seamlessly from the arm has dimensions of ~30 x 25 x 20 Å (Fig. 2-3 and 2-5). The tetradecamer is slightly larger than the six-sided oligomers, with an overall diameter of 310 Å and a central region with a diameter of 120 Å (Fig. 2-3F); however, the size of the arms and central densities are similar to those in the hexameric and dodecameric oligomers.

VacA structure and oligomerization. To gain insight into how VacA oligomerizes, we placed the 2.4 Å crystal structure of the VacA p55 domain into the 3D density maps of the VacA oligomers using the program Chimera (Fig. 2-6A and C and 2-7) (Gangwer et al., 2007; Pettersen et al., 2004). As is common for negative stained specimens, VacA oligomers were slightly flattened, causing the tips of the peripheral arms to appear to be touching, a feature that is less pronounced in side views of VacA particles in vitrified ice ((El-Bez et al., 2005) and data not shown). Although the flattening in the z-axis limits our ability to map inter-p55 interactions in double-layered oligomers to specific loops rather than to specific amino acids, the distortion was fairly minor since even in the double-layered VacA oligomers, the p55 structure unambiguously fits into the EM maps. Placing the p55 crystal structure into the VacA oligomers (Fig. 2-6 and 2-7) clearly shows that the extended arms represent the p55 domain and the central densities represent the p33 domain along with regions of p55 that have not been crystallized

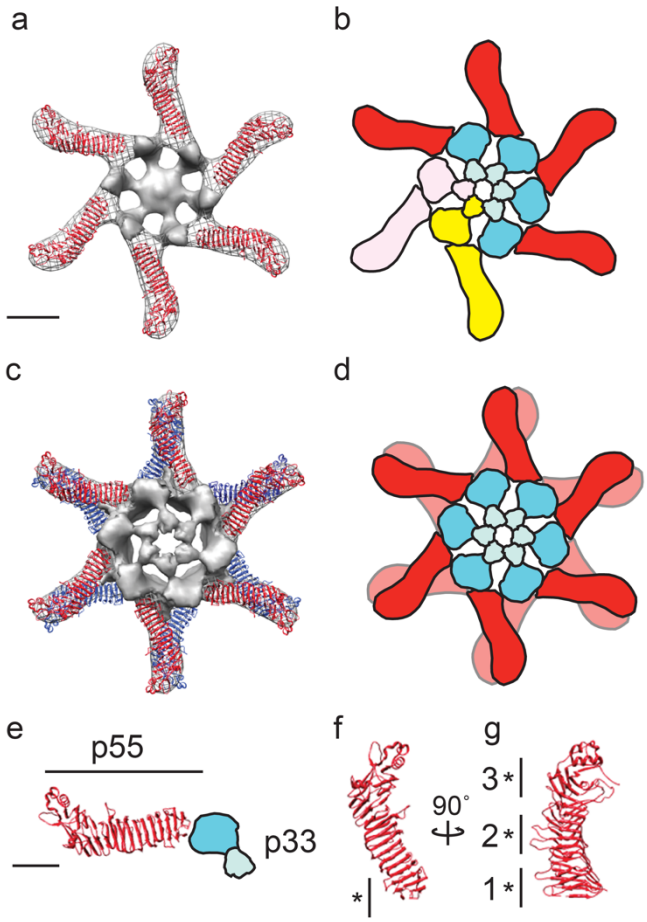

Figure 2-6. Structural model of the VacA oligomerization process. (A) The 2.4 Å crystal structure of p55 (PDBID: 2QV3) fits into the straight "arms" of the EM map of a VacA hexamer. Subtracting the density of the p55 crystal structure from the EM map highlights p33 (gray, central density and spokes) (B) p88 oligomerizes into hexamers supported by inter-molecular interactions between the N-terminal portions of p33 in adjacent protomers, as well as contacts between p33 and an adjacent p55 arm. Blue domains, p33; red domain, p55. Two p88 protomers are colored pink and yellow to show p88 protomers interaction. (C) The 2.4 Å crystal structure of p55 fits into the straight "arms" of the EM map of a VacA dodecamer. For ease of viewing model, the p33 density of only the well-organized side is shown. (D) Cartoon of dodecamer formation. Colors the same as in B. (A-D) Scale bar, 5 nm. (E) The C-terminal p55 domain forms a straight arm with a kink at the end, while the N-terminal p33 domain consists of two globular densities connected by a thinner density (blue domains). (F and G) 2.4 Å p55 crystal structure rotated 90˚ on vertical axis. "*" marks regions of p55 involved in (F) hexamer interactions (residues 442-448) and (G) dodecamer and tetradecamer interactions. "1": residues 395-404 and 421-435; "2": residues 519-530 and 547-559; and "3": residues 645-654 and 687-692 (F-G) Scale bar, 2.5 nm.

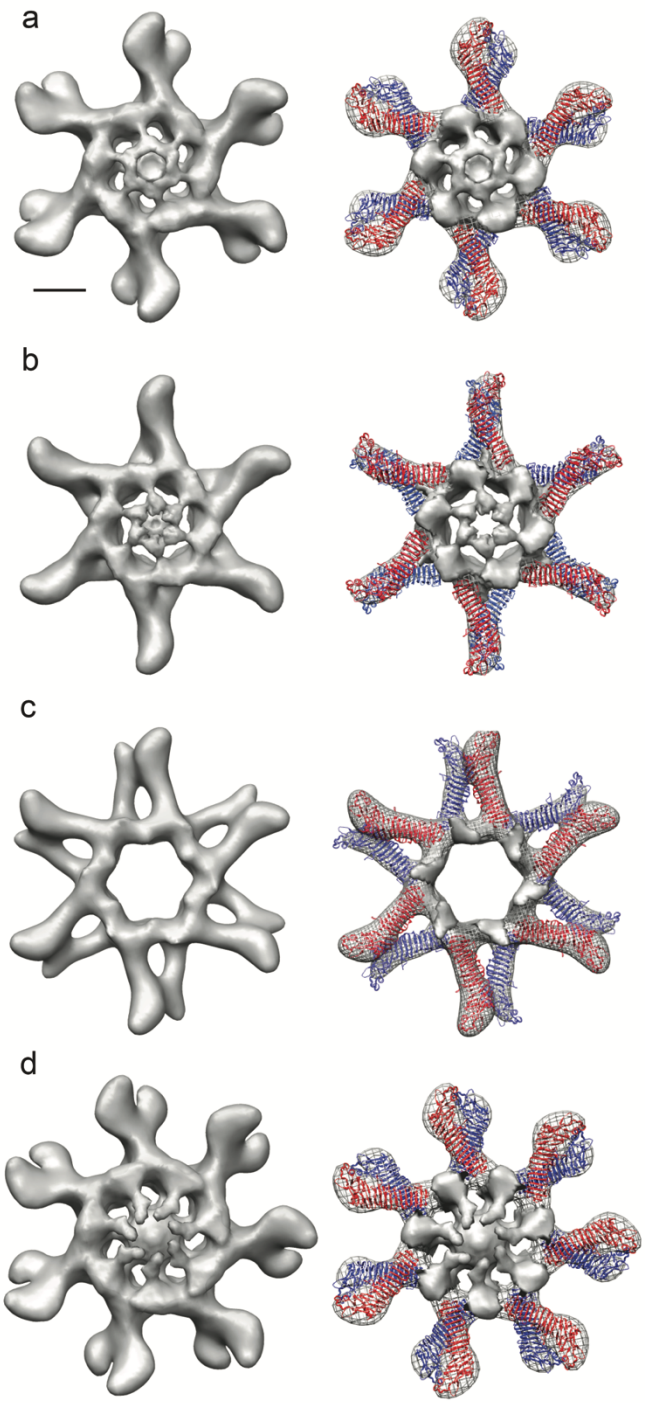

Figure 2-7. Generating pseudo-atomic models of VacA oligomers. (A-D) The 2.4 Å crystal structure of p55 [1] unambiguously fits into the straight "arms" of EM maps of VacA dodecamers and the tetradecamer. Subtracting the density of the p55 crystal structure from the EM maps highlights the p33 portion of each oligomer (gray, central density and spokes). Scale bar, 5 nm.

(residues 312-354) (Fig. 2-6E). As previously predicted, the portion of p33 contiguous to the p55 domain likely adopts an extended α-helix fold since there is no clear demarcation in the density map at the p55-p33 intra-molecular interface (Fig. 2-6A, C, and E) (El-Bez et al., 2005).

The model of hexameric VacA (Fig. 2-6A) shows that oligomerization depends on inter-molecular interactions between the N-terminal portions of p33 in adjacent protomers, as well as contacts between p33 of one protomer and an adjacent p55 arm of another protomer (Fig. 2-6B, see p88 pink and yellow protomers). The interactions between the arms can be mapped to a region spanning residues 442-448 of p55 (Fig. 2-6F) and a region of p33 contiguous with the p55 β-helix in an adjacent arm. The lack of a high-resolution structure of the VacA N-terminus precludes mapping this interaction to specific residues; however, we speculate that this region likely includes residues 346 and 347, which are important in VacA oligomerization (Ivie et al., 2008).

VacA forms double layers through interactions mediated by the many loop regions extending from the p55 α-helix (Fig. 2-6C, D, and G). These loops can be grouped into three major blocks (Fig. 2-6G) and each oligomeric type uses a different block to support double layer formation (Fig. 2-6C and D, Fig. 2-7). Although this allows for numerous VacA double layer conformations, the different interactions, with the exception of one conformation (Fig. 2-7C), do not have any distinct effect on the arrangement of the central p33 domains. This suggests structural flexibility within p88 protomers, likely found at regions around the p33-p55 interface and within the short region connecting the two lobes of the p33 domain (Fig. 2-6E). The dodecamer lacking a well-defined central density uses regions in the C-terminus of p55 to support double layer formation (Fig. 2-7C).

Perhaps the angle the arms must adopt in this oligomer exceeds the inherent flexibility found in p88 disrupting ordered N-terminal p33 interactions. From the structural analysis of the numerous VacA oligomer conformations, we propose a model where soluble VacA first oligomerizes into hexamers or heptamers and then these single layers interact to form double layer structures via structural motifs along the arm domains.

Structural characterization of VacA mutants and variants. A number of VacA variants and mutants have been shown to differ from WT toxin in activity and/or oligomeric structural features. For example, both VacA∆6-27 and a VacA s2m1 chimera lack cell-vacuolating activity; VacA∆301-328 retains vacuolating activity (data not shown) but a similar mutant preferentially formed particles with increased 6-fold symmetry rather than 7-fold symmetry (Burroni et al., 1998; McClain et al., 2001b; Vinion-Dubiel et al., 1999). To gain a better mechanistic understanding for why certain VacA mutants and/or variants are more active than others, we examined VacA∆6-27, VacA s2m1, and VacA∆301-328 by negative stain EM and particles from the untilted images were subjected to alignment and classification (Fig. 2-8 and 2-9). The classes were compared to WT VacA classes using difference mapping. In cases where significant differences were detected, 3D structures were determined. In addition, we calculated the number of hexameric, heptameric, dodecameric, and tetradecameric forms for these variants and/or mutants (Table 2-1). In general, WT, ∆6-27, s2m1, and ∆301-328 VacA all formed oligomers with 6-fold symmetry more frequently than 7-fold symmetry and more double layer oligomers than single layer oligomers (Table 2-1). Consistent with a previous report, the ∆301-328 mutation leads to an increased proportion of oligomers with 6-fold symmetry, but what was not previously appreciated is that these oligomers also contain 50% fewer single layer oligomers when compared to

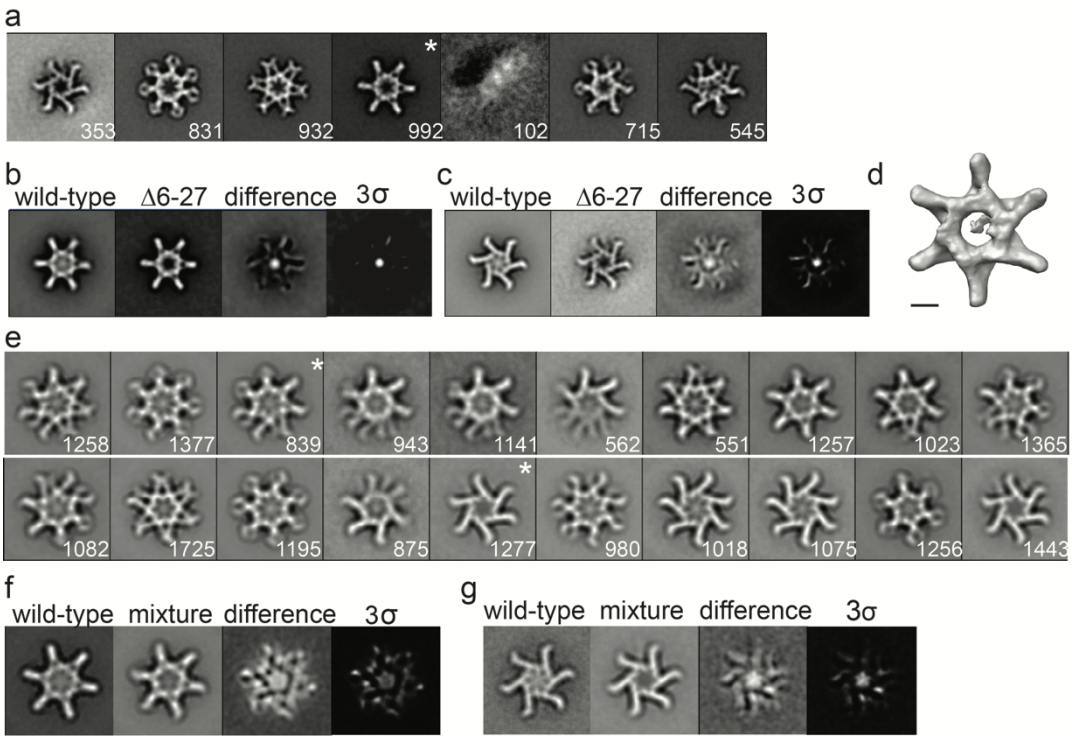

Figure 2-8. Characterization of VacAΔ6-27. (A) VacAΔ6-27 class averages obtained by reference-based alignment and classification. "*", class shown as a 3D volume in panel D. (B and C) Difference mapping between WT and similar VacAΔ6-27 class averages. Final panel shown at 3**?** threshold. (A-C) Side length of panels, 573 Å. (D) 3D structure of VacAΔ6-27 corresponding to the "*" average in A. Structure has no applied symmetry. Scale bar, 5 nm. (E) Class averages of VacA oligomers generated by mixing WT VacA and VacAΔ6-27. "*", classes used in difference mapping shown in panel F and G. (F and G) Difference mapping between WT VacA and mixture of WT:VacAΔ6-27 oligomers. Final panel shown at 3**?** threshold. (E-G) Side length of panels, 420 Å. Numbers of particles included in each class, bottom right corner.

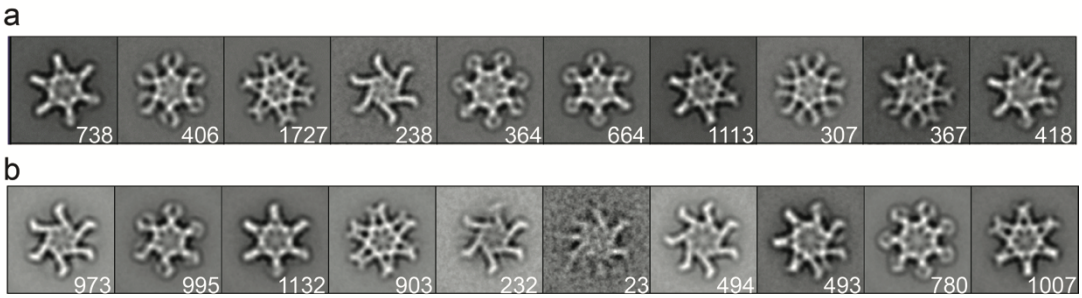

Figure 2-9. Reference-based alignment of VacAΔ301-328 and VacA s2m1. (A) VacAΔ301-328 class averages obtained by reference-based alignment and classification. (B) VacA s2m1 class averages obtained by reference-based alignment and classification. Side length of panels, 420 Å. Numbers of particles included in each class, bottom right corner.

WT VacA (Burroni et al., 1998). Interestingly, s2m1, a VacA variant lacking cell-vacuolating activity, forms single layer oligomers approximately three-times more often than WT VacA (Table 2-1, 24% vs. 8%) and six-times more frequently than VacA∆301-328 (Table 2-1, 24% vs. 4%). These analyses suggest that whether VacA forms single or double layer oligomers in solution is not a key determinant of VacA activity.

As seen previously, VacA∆6-27 double layer oligomers clearly lack density in the p33 region (Fig. 2-8A, B, C, and D) (El-Bez et al., 2005). We now show that the central density is absent in both single and double layer oligomers (Fig. 2-8B and C). To carefully examine the structural consequences of the ∆6-27 mutation, we determined the 3D structure of VacA∆6-27 using the RCT approach, with one representative structure shown in Figure 2-8D (Radermacher, 1994). For all calculated structures, the central region of each oligomer was no longer structurally organized. We propose a model in which deletion of residues 6-27 leads to the disruption of important interactions between the N-termini of p33 domains in the oligomers, causing the N-terminal globular domains of p33 to no longer adopt an organized central core in any oligomeric form.

VacA∆6-27 can inhibit WT VacA activity in a dominant negative manner, but the mechanism is not completely understood (Vinion-Dubiel et al., 1999). It has been proposed that this inhibitory activity arises from interaction of VacA∆6-27 with WT VacA and formation of mixed oligomers with defective activity (McClain et al., 2001b; Torres et al., 2006; Vinion-Dubiel et al., 1999). To determine whether VacA oligomers that contain a mixture of WT and VacA∆6-27 p88 subunits have a structurally organized central density, we mixed WT VacA and VacA∆6-27 in a 1:1 molar ratio, acidified the preparation to pH 3.5 to promote oligomer disassembly, and then neutralized the pH to promote oligomer formation (Vinion-Dubiel et al.,

1999). These oligomers were analyzed by negative stain EM. A total of 22,242 particles were selected, and images were classified into 20 class averages (Fig. 2-8E). Although these classes show that oligomers containing mixtures of WT and Δ6-27 VacA do seem to have central density, difference maps generated between a common hexamer and dodecamer class (Fig. 2-8F and G) show that the central density is not as well organized as that found in WT oligomers. This finding provides evidence supporting a model in which the 6-27 deletion disrupts important N-terminal p33 interactions required for organizing the central core, and supports a model in which the dominant negative mutant acts through the formation of mixed oligomers with defects in channel formation (Vinion-Dubiel et al., 1999). To ensure that these changes in the central organization are specific and not simply the result of a general change of structural conformation due to the deletion of residues, we also compared WT VacA averages with averages of VacAΔ301-328 and found no statistical differences (Fig. 2-9A and data not shown).

To determine whether the lack of an organized central core is a common feature found in variants and mutants of VacA that have defects in pore formation, we compared WT VacA averages with averages of VacA s2m1 and found no statistical differences (Fig. 2-9B and data not shown). This was especially surprising considering that s2m1 VacA contains 12 extra residues at its N-terminus, which we expected would disrupt the central core in a manner similar to what was observed with the VacAΔ6-27 mutant (Letley and Atherton, 2000; Letley et al., 2003; McClain et al., 2001b). The presence of an intact central core in s2m1 oligomers is notable because many wild-type *H. pylori* strains produce s2 forms of VacA (Atherton et al., 1995). These data suggest that, unlike VacAΔ6-27, the lack of vacuolating activity exhibited by VacA s2m1 does not arise from a disorganized p33 region, at least in solution. It is possible that the N-terminal extensions may

interfere with important hydrophobic interactions between p33 and lipids that are required for pore-formation in the context of a membrane environment.

In summary, we have analyzed how soluble VacA forms single and double layer oligomers and have provided the most detailed structural model of VacA to date. Our analysis of different VacA mutants and variants provides further insight into VacA structure-function relationships and the mechanism by which a dominant negative mutant exhibits inhibitory activity. There have been three published examples of VacA oligomers associated with supported lipid bilayers; however, the low resolution of these studies have made it difficult to conclude which oligomeric type of VacA associates with lipids (Adrian et al., 2002; Czajkowsky et al., 1999; Geisse et al., 2004). It is tempting to speculate that VacA hexamers (Fig. 2-3D) represent the conformation that associates with lipids and forms pores, while the dodecamers and tetradecamers (Fig. 2-3A, B, C, and F) represent interactions between hydrophobic regions of p88 that would normally interact with the lipid membrane if present. In future studies, it will be important to analyze the structure of VacA oligomers at a higher level of resolution, of VacA oligomers associated with lipids, and to investigate structural changes in VacA that are required for the formation of membrane channels.

Material and Methods

Purification of VacA. H. pylori strain 60190 [expressing WT VacA] and strains expressing either VacAΔ6-27 or VacA s2m1 proteins have been described previously (McClain et al., 2001b; Vinion-Dubiel et al., 1999). An *H. pylori* strain expressing a VacAΔ301-328 mutant was constructed using previously described methodology (Gonzalez-Rivera et al., 2012). Strains were grown in broth culture and VacA was isolated in oligomeric form as previously (Cover et al., 1997; Vinion-

Dubiel et al., 1999). VacA was further purified using Matrex affinity gel and gel-filtration chromatography as described (Adrian et al., 2002). Mixed WT VacA:VacAΔ6-27 oligomers were generated by mixing equal molar ratios of WT VacA and VacAΔ6-27 at neutral pH. The pH was acidified to 3.5 to promote oligomer disassembly and the tube lightly vortexed (Vinion-Dubiel et al., 1999). The pH of the mixture of was neutralized so that the mixed oligomers could form.

Specimen preparation and electron microscopy. Uranyl formate (0.7% w/v) was used for conventional negative staining as described (Ohi et al., 2004). For further details see Supplemental Data. Images of WT VacA, VacA Δ301-328, VacA s2m1, and WT: VacAΔ6-27 were taken using a F20 electron microscope (FEI) equipped with a field emission gun at an acceleration voltage of 200 kV under low-dose conditions at a magnification of 62,000X using a defocus value of –1.5 μm and recorded on a 4k x 4k Gatan CCD camera. Images were converted to mrc format, and binned by a factor of 2 resulting in final images with 3.5 Å/pixel. Images of WT VacA (used for difference mapping with VacAΔ6-27 particles) and VacAΔ6-27 were recorded using a Tecnai T12 electron microscope (FEI) equipped with a LaB_6 filament and operated at an acceleration voltage of 120 kV. Images were taken under low-dose conditions at a magnification of 67,000X using a defocus value of –1.5 μm. Images were recorded on DITABIS digital imaging plates (Pforzheim, Germany). The plates were scanned on a DITABIS micron scanner (Pforzheim, Germany), converted to mixed raster content (mrc) format, and binned by a factor of 2 yielding final images with 4.48 Å/pixel. All binned MRC files were converted to SPIDER format using EM2EM. Image analysis for all VacA samples was carried out with SPIDER and the associated display program WEB (Frank et al., 1996).

Classification and random conical tilt reconstruction of negatively stained WT, variant and mutant VacA particles. Micrograph tilt pairs of WT and ∆6-27 VacA were recorded at 55˚ and 0˚. Images for VacA s2m1, and VacAΔ301-328 and the mixture of VacA:VacA∆6-27 particles were collected at 0˚. Particle pairs (14,573 for WT VacA and 4,470 for VacA∆6-27 and particles for s2m1, VacAΔ301-328, and VacA:VacA∆6-27 (7,032 for VacA s2m1, 6,342 for VacAΔ301-328 and 22,242 for VacA:VacA∆6-27 were selected interactively using WEB. VacA particles were windowed into 120 x 120 pixel images (3.5 Å/pixel for WT, VacA s2m1, VacAΔ301-328 and the VacA:VacA∆6-27 mixture; 4.48Å/pixel for VacA∆6-27). The untilted images were rotationally and translationally aligned and subjected to 10 cycles of multi-reference alignment and K-means classification. Particles of WT VacA were grouped into 20 classes (Fig. 2-2A). The references used for the first multi-reference alignment were randomly chosen from the raw images. From the class averages eight representative projections were chosen and used as references for another cycle of reference based alignment (Fig. 2-2A marked with '*'). Particles of VacA∆6-27 were grouped into 10 classes (Fig. 2-10A) and from these class averages seven representative projections were chosen and used as references for another cycle of reference based alignment (Fig. 2-10A marked with a '*'). Particles of VacA s2m1 and VacAΔ301-328 were grouped into 60 classes (Fig. 2-10B and C) and from these class averages 10 representative projections were chosen and used as references for another cycle of reference based alignment (Fig. 2-10B and C marked with a '*'). Particles of VacA:VacA∆6-27 were grouped into 20 classes (Fig. 2-8E). Difference images were calculated using both Diffmap.exe and Spider (Frank et al., 1996). Results were similar using either program.

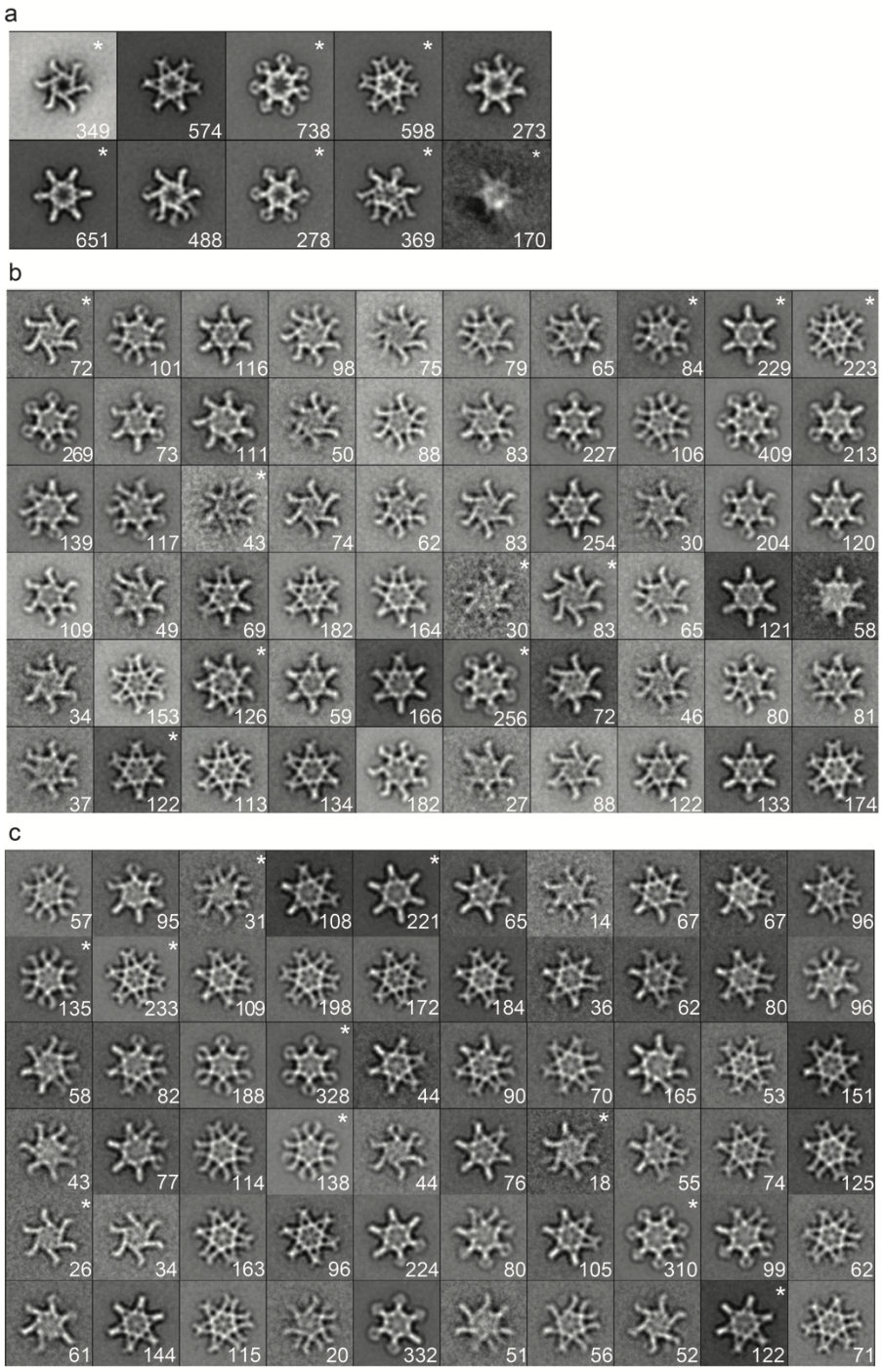

Figure 2-10. Analysis of VacA variants in negative stain. (A-C) Class averages obtained by multi-reference alignment and classification of 4,470 VacAΔ6-27 (A), 7,032 VacA s2m1 (B), and 6,342 VacAΔ301-328 (C) particle images in negative stain. Number of particles in each projection average is shown in the lower right corner of each average. Averages used for reference based alignments (See Figs. 2-8A and 2-9A and B respectively) are marked with a "*" in the upper left corner. Side length of panels, 573 Å (A) and 420 Å (B and C).

The tilted images corresponding to each of the WT and VacAΔ6-27 classes generated from reference-based alignment were used to calculate initial 3D reconstructions by back-projection using the in-plane rotation angles determined by rotational alignment and the pre-selected tilt angle of 55˚ implemented in the processing package SPIDER (Frank et al., 1996). The density maps were improved by back-projection and angular refinement in SPIDER. 10% of the particles selected from the images of the untilted specimens in each class were included in the data set and angular refinement was repeated. During the angular refinement process either 6- or 7-fold symmetry was applied to the final reconstructions as determined by the number of "arms" in each oligomeric form. Structures with no applied symmetry are shown in Figure 2-4. For further details about structural methods used in this analysis refer to Cheng *et al* (Cheng et al., 2006).

For WT VacA, two of the WT structures were very similar (Fig. 2-3B and C) and, therefore the 6,059 particles associated with these structures were combined and a new structure was calculated using angular refinement (Fig. 2-5). The FSC curve corresponds to normalized cross-correlation coefficients of Fourier shells from even and odd particles within the dataset. Using a FSC = 0.5 criteria the resolution is ~10 Å (Fig. 2-2B); however, the lack of any secondary structural details in our map suggests that the resolution more likely falls closer to 15 Å. This resolution corresponds to the appearance of the crystal structure of VacA p55 when filtered to 15 Å resolution (data not shown) (Gangwer et al., 2007). For display purposes structures were filtered in chimera using the "Hide Dust" command to diminish 'salt and pepper' noise from the maps by removing single voxels that were unconnected to the main volume of the 3D density (Pettersen et al., 2004). Contouring thresholds were chosen to match the molecular weight for

each VacA oligomer. Surface rendering of the structure was performed with the program Chimera (Pettersen et al., 2004).

CHAPTER III

STRUCTURAL ORGANIZATION OF MEMBRANE-INSERTED HEXAMERS FORMED BY *HELICOBACTER PYLORI* VacA TOXIN

Introduction

Helicobacter pylori is a Gram-negative bacterium that colonizes the human stomach and causes gastric inflammation, leading to the development of peptic ulceration and gastric cancer in a subset of infected individuals (Atherton and Blaser, 2009; Cover and Blaser, 2009; Marshall et al., 1984; Suerbaum and Michetti, 2002). *H. pylori* infects about 50% of humans (more than 3 billion people), with a prevalence as high as 90% in some developing nations (Amieva and El-Omar, 2008; Atherton, 2006; Nomura et al., 1991; Parsonnet et al., 1991a; Suerbaum and Michetti, 2002). Gastric cancer is the third leading cause of cancer-related deaths worldwide (de Martel et al., 2012; Fuchs and Mayer, 1995). *H. pylori*-associated gastric adenocarcinoma is a rare example of a human cancer attributed to a specific bacterial infection, a connection that led the World Health Organization to classify *H. pylori* as a type 1 carcinogen (Anonymous, 1994).

One of the major virulence factors secreted by *H. pylori* is the pore-forming exotoxin VacA (vacuolating cytotoxin A), named for its ability to induce the formation of large vacuoles in eukaryotic cells (Cover and Blanke, 2005). VacA causes multiple cellular effects that include cell vacuolation, depolarization of membrane potential, mitochondrial dysfunction, autophagy, cell death, activation of mitogen-activated protein kinases, and inhibition of T cell activities (Calore et al., 2010b; Cover and Blanke, 2005; Domanska et al., 2010; Galmiche et al., 2000; Gebert et al., 2003; Jain et al., 2011; Nakayama et al., 2004; Radin et al., 2011;

Sundrud et al., 2004; Szabo et al., 1999; Terebiznik et al., 2009; Willhite and Blanke, 2004). Most VacA-induced cellular alterations require oligomerization of the toxin, insertion into the lipid bilayer to form a membrane channel, and internalization into the cell (Calore et al., 2010a; Czajkowsky et al., 1999; Gauthier et al., 2007; Genisset et al., 2006; Ivie et al., 2008; Iwamoto et al., 1999; Szabo et al., 1999; Tombola et al., 1999b; Vinion-Dubiel et al., 1999; Willhite and Blanke, 2004). The molecular mechanisms underlying each of these steps and the order in which they occur are not understood.

VacA does not exhibit sequence relatedness to any other known bacterial toxins. Secreted as an 88 kDa protein, VacA contains an N-terminal p33 domain and a C-terminal p55 domain. Three polymorphic regions have been identified: an N-terminal region (s1 or s2), an intermediate region (i1 or i2) located within the p33 domain, and a p55 mid-region (m1 or m2) (Atherton et al., 1995; Gangwer et al., 2010; Pagliaccia et al., 1998; Rhead et al., 2007). Sequence variations at the N-terminus (s1 or s2) and within the p55 mid-region (m1 or m2) are associated with differences in the ability of VacA to form pores or differences in the binding of VacA to cells, respectively (Atherton et al., 1995; Ji et al., 2000; Letley and Atherton, 2000; McClain et al., 2001b; Pagliaccia et al., 1998; Sewald et al., 2008b; Wang et al., 2001). Sequence variation in the p33 intermediate-region and p55 mid-region may modulate differences in cellular tropism (Gonzalez-Rivera et al., 2012; Ji et al., 2000; Pagliaccia et al., 1998; Rhead et al., 2007; Wang et al., 2001). The *vacA* genotype of a strain is strongly associated with the risk of peptic ulceration and gastric cancer, and the various forms of VacA differ in activity *in vitro*. Specifically, humans infected with *H. pylori* strains containing *vacA* s1/i1/m1 alleles have an increased risk of developing gastric cancer compared to individuals who are infected with *H. pylori* strains containing *vacA* s2/i2/m2 alleles (Atherton et

al., 1995; Cover, 2016; Figueiredo et al., 2002; Memon et al., 2014; Rhead et al., 2007).

VacA forms anion-selective channels in planar lipid bilayers, an activity that correlates with the predicted formation of VacA channels in the plasma membrane, endosomal membranes, and mitochondrial membranes of host cells (Campello et al., 2002; Czajkowsky et al., 1999; Debellis et al., 2001; Galmiche et al., 2000; Iwamoto et al., 1999; Papini et al., 1998a; Papini et al., 1998b; Szabo et al., 1999; Tombola et al., 1999a; Tombola et al., 1999b; Willhite and Blanke, 2004; Willhite et al., 2003). Single channel analyses have provided evidence predicting that VacA pores are composed of six subunits and that they mimic the action of endogenous anion-selective channels (Czajkowsky et al., 1999; Domanska et al., 2010; Iwamoto et al., 1999; Tombola et al., 1999a). Deep-etch electron microscopy (EM) and atomic force microscopy (AFM) have been utilized to visualize VacA bound to mica-supported lipid bilayers, but these studies were not able to conclusively determine either the type(s) of oligomers bound to the membrane or the conformation of the central pore-forming region of VacA in this lipid environment (Adrian et al., 2002; Czajkowsky et al., 1999; Geisse et al., 2004). Thus, very little is known about structural features of membrane-bound VacA.

The amino-terminus of VacA (within the p33 domain) is predicted to be highly hydrophobic (McClain et al., 2003; Vinion-Dubiel et al., 1999). A VacA mutant protein lacking a portion of this region (VacA Δ6-27) does not form pores in planar lipid bilayers and lacks cell-vacuolating activity, which indicates that sequences within the N-terminal hydrophobic region of the VacA p33 domain are required for the formation of membrane channels (McClain et al., 2001a; Vinion-Dubiel et al., 1999). The N-terminal portion of the p33 domain contains three GXXXG sequences, a motif often involved in facilitating oligomeric interactions

between transmembrane (TM) helices (Russ and Engelman, 2000; Teese and Langosch, 2015). A computationally generated structural model of the predicted VacA TM domain sequence suggests that the N-terminal GXXXG motifs pack together to form an anion-channel (Kim et al., 2004). Studies using genetically modified VacA show that the N-terminal 32 hydrophobic residues of p33, especially the proline residue at position 9 (P9) and the $G^{14}XXXG^{18}$ motif, are required for channel activity and cell-vacuolating activity (McClain et al., 2001a; McClain et al., 2003). These studies also showed that the GXXXG motifs facilitate dimerization in the context of membrane based on experiments using a TOXCAT system, a method developed to study TM helix-helix associations (McClain et al., 2001a; McClain et al., 2003; Russ and Engelman, 1999, 2000).

In solution, VacA forms hexamers, heptamers, dodecamers and tetradecamers, with the majority of soluble oligomers (>90%) organizing into double layered structures (dodecamers and tetradecamers) (Adrian et al., 2002; Chambers et al., 2013; Lanzavecchia et al., 1998; Lupetti et al., 1996). Although there is no atomic resolution structure of the 88 kDa VacA holotoxin, there is a 2.4 Å three-dimensional (3D) structure of the p55 domain, and 3D structures of "snowflake"-like soluble VacA oligomers have been determined using negative stain EM (Chambers et al., 2013; El-Bez et al., 2005; Gangwer et al., 2007; Sewald et al., 2008a). Our structural analysis showed that while soluble hexamers and heptamers form chiral structures with the "tips" of the snow-flakes all curving in the same direction, the dodecamers and tetradecamers are achiral (Chambers et al., 2013). VacA p55 domains have been localized to the peripheral arms of oligomers, and p33 is localized to the central region of the oligomers (Chambers et al., 2013; El-Bez et al., 2005; Gangwer et al., 2007).

In order to form a functional anion-specific channel, VacA must oligomerize and insert into the lipid bilayer (Adrian et al., 2002; Czajkowsky et al., 1999; Geisse et al., 2004; Tombola et al., 1999a). However, the mechanisms by which these steps occur are not fully understood. In the current study, we show that VacA oligomerizes on membranes under buffer conditions that do not support oligomerization in solution, and that membrane-bound VacA is also membrane-inserted. Studies of individual VacA domains show that while p55 can interact with membranes, p33 is required for insertion into the lipid bilayer. Importantly, we show that VacA organizes into single layered oligomers on membranes, and show that the p33 central region of VacA hexamers has a different structural organization when comparing membrane-associated hexamers to soluble hexamers. These are the first in-depth studies of VacA oligomer conformation in the context of membranes and provide important new insights into the process by which VacA inserts into membranes.

Materials and Methods

Purification of H. pylori VacA, p55 recombinant VacA, and Schizosaccharomyces pombe Cdc15 F-BAR. H. pylori strain 60190 expressing VacA s1/i1/m1 and mutant strains expressing VacA s2/i1/m1 or VacA Δ6-27 have been previously described (McClain et al., 2001b; Vinion-Dubiel et al., 1999). Strains were grown in Brucella broth supplemented with cholesterol and VacA was isolated as previously described (Cover et al., 1997; Jimenez-Soto et al., 2012; Vinion-Dubiel et al., 1999). To purify a non-oligomerizing form of VacA, an *H. pylori* strain expressing VacA Δ346-347 was modified so that it produced VacA containing an internal strep tag inserted at amino acid 312 (Willhite and Blanke, 2004; Ye et al., 1999). VacA Δ346-347-Str312 was then purified using Strep-Tactin

resin (IBA, Goettingen, Germany). The VacA p55 domain (residues 312-821) was expressed in *Escherichia coli* and purified as described (Gangwer et al., 2007). Recombinant *S. pombe* Cdc15 F-BAR-E30K/E152K was expressed and purified as described (McDonald et al., 2015). Recombinant proteins were visualized using SDS-PAGE and Coomassie staining.

Liposome co-pelleting assays. Large unilamellar vesicles (LUVs) were generated as described (Itoh et al., 2005), using the following lipid mixtures: 1,2-dioleoyl-*sn*-glycero-3-phosphocholine (DOPC); L-α-phosphatidylcholine from egg (ePC), 1,2-dioleoyl-*sn*-glycero-3-phospho-L-serine (DOPS), and ovine cholesterol (55/15/30 % of total moles (mol%)); DOPC, DOPS, and egg sphingomyelin (eSM) (45/20/35 mol%); DOPC, DOPS, eSM, and cholesterol (35/20/35/10 mol%). All lipids were purchased from Avanti Polar Lipids (Alabaster, AL). Briefly, lipids in chloroform ($CHCl_3$) were mixed at the desired ratios and evaporated under a nitrogen stream, further dried in a vacuum overnight, and rehydrated in 10 mM HEPES pH 7.2 and 100 mM potassium chloride (KCl) to a final concentration of 1 mg/mL lipid. Lipid mixtures were vortexed, exposed to three cycles of freeze thawing using a dry ice/ethanol bath and 37°C water bath, and then extruded using an Avanti extruder with an 800 nm filter. Before being mixed with the LUVs, VacA (s1/i1/m1, s2/i1/m1, and Δ6-27) was acid activated by lowering the pH to 3.0 resulting in disassembly of oligomers as previously described (Cover et al., 1997). VacA Δ346-347 was not acid activated since this mutant protein is defective in oligomerization and does not require acid-induced disassembly (Ivie et al., 2008). Acid activated VacA s1/i1/m1, s2/i1/m1, Δ6-27, Δ346-347, p55, and bovine serum albumin (BSA) were mixed at increasing concentrations (μM) with 100 μg LUVs and incubated for 15 minutes at 25°C. Samples were spun down using a Beckman Coulter (Pasadena, CA) TL-100 ultracentrifuge and TLA-100 rotor at 156,425 x g

for 45 minutes at 25°C. The supernatant (unbound sample) was removed and the liposome pellet (bound sample) suspended in 10 mM HEPES pH 7.2 and 100 mM KCl. Samples were run on 4-12% Bis-Tris SDS-PAGE gels (Invitrogen, Carlsbad CA) and stained with Coomassie. Gels were digitized using a CanonScan 8800F digital scanner and quantified using ImageJ (Schneider et al., 2012). Each liposome co-pelleting assay was repeated three times in independent experiments. The percent of VacA bound to membrane was determined by averaging intensity measurements of bands corresponding to membrane-bound and unbound VacA. Results represent the mean $\pm$ standard error of the mean (SEM) based on three independent experiments. Graphs and statistics were generated using GraphPad Prism (version 5.0a).

VacA insertion assay. VacA s1/i1/m1, s2/i1/m1, Δ6-27, Δ346-347, and p55 were incubated with ePC/DOPS/chol (55/15/30 mol%) at a lipid-to-protein ratio (LPR) of 50:1 (w/w) for 15 minutes at room temperature. Cdc15 F-BAR-E30K/E152K was mixed with DOPC/DOPS (80/20 mol%) LUVs at a LPR of 5:1 (w/w) and incubated for 15 minutes at room temperature. Buffer only controls were prepared for all protein-lipid samples. Protein-bound liposome samples were alkalinized with an equal volume of 0.2 M sodium carbonate (Na_2CO_3) for 30 minutes on ice to compete off peripherally bound protein. This treatment strips peripheral, but not integral, bound proteins from the membrane (Fossati et al., 2014). A final concentration of 1.2 M sucrose in 0.1 M Na_2CO_3 was then added. A discontinuous sucrose gradient was prepared with alkalinized protein-liposomes at the bottom, followed by layers of 1 M, 0.5 M, 0.25 M, 0.15 M, and 0 M sucrose in 0.1 M Na_2CO_3. The gradients were spun at 108,759 x g for 16 hours at 4°C to allow flotation of liposomes into lower density fractions (Beckman Coulter, Pasadena, CA). Fractions of 700 µL were collected and precipitated with TCA.

Samples were hydrated with 10 mM HEPES pH 7.2, 100 mM KCl and 2X SDS sample loading dye. Samples were run on a 10% Bis-Tris SDS-PAGE gel (Life Technologies) and Coomassie stained.

*Sample preparation for EM analysis***.** For negative stain single particle EM of membrane-bound VacA, LUVs composed of ePC/DOPS/chol (55/15/30 mol%) and heart lipid extract in 10 mM HEPES pH 7.2, 100 mM KCl were prepared as described above. VacA s1/i1/m1, s2/i1/m1, and Δ6-27 were acid activated by lowering the pH to 3.0, mixed with LUVs (either ePC/DOPS/chol or heart lipids), and incubated for 15 minutes at 37˚C. A LPR of 50:1 (w/w) was used for each VacA sample (Cover et al., 1997). For analyzing membrane-bound VacA Δ346-347, LUVs composed of ePC/DOPS/chol (55/15/30 mol%) or DOPC/DOPS/eSM/chol (35/20/35/10 mol%) in 10 mM HEPES pH 7.2, 100 mM KCl at LPRs of 100:1 (w/w) and 50:1 (w/w), were prepared as described above. VacA Δ346-347 was not acid activated prior to mixing with LUVs, since this mutant protein is defective in oligomerization and does not require acid-induced disassembly (Ivie et al., 2008). Grids containing soluble VacA s1/i1/m1, s2/i1/m1, Δ346-347, and Δ6-27 were made as described (Chambers et al., 2013). To visualize soluble monomeric VacA s1/i1/m1, the pH of the sample was lowered to 3.0 before making grids.

Electron Microscopy (EM). For negative stain EM grids, samples were adsorbed to a glow discharged 200-mesh copper grid covered with carbon-coated collodion film (EMS, Hatfield, PA). Grids were washed in two drops of water and stained with two drops of uranyl formate (0.75%) (EMS, Hatfield, PA) as described (Ohi et al., 2004). Samples were visualized on a Tecnai TF20 electron microscope (FEI, Hillsboro, OR) equipped with a field emission gun at an acceleration voltage of 200 kV under low-dose conditions. Images were taken at a magnification of

62,000x at a defocus value of -1.5 µm and recorded on a 4k x 4k CCD Ultrascan camera (Gatan, Pleasanton, CA). Images were converted to mixed raster content (mrc) format and binned by two, resulting in final images with a pixel size of 3.5 Å/pixel. Images of VacA ∆346-347-LUVs were taken on a FEI Morgagni (FEI, Hillsboro, OR) equipped with a tungsten filament at an acceleration voltage of 100kV and a magnification of 28,000x.

Classification and difference mapping. Particles were selected interactively using BOXER in the program EMAN and windowed into 120 x 120 pixel images (42 nm x 42 nm) (Ludtke, 2010). Boxed particles were rotationally and translationally aligned and subjected to ten rounds of reference free alignment using the program SPIDER (Shaikh et al., 2008). Datasets used include: 5,763 particles for soluble VacA s1/i1/m1; 2,207 particles for VacA s1/i1/m1-ePC/DOPS/chol LUVs; 3,800 particles for VacA s1/i1/m1-heart lipid LUVs; 2,142 particles for VacA s2/i1/m1-ePC/DOPS/chol LUVs; 2,919 particles for s2/i1/m1-heart lipid LUVs; 4,186 particles for VacA Δ6-27; 2,429 particles for VacA Δ6-27-ePC/DOPS/chol LUVs; and 2,111 particles for VacA Δ6-27-heart lipid LUVs. Four or five representative averages for each VacA variant were chosen and particles were subjected to reference based alignment. 2D averages of soluble and membrane-bound oligomers were compared by generating and then overlaying radial density distribution plots of normalized 2D averages as described (Dang et al., 2005b). Averages were normalized and values for the radial density distribution plots and difference maps were calculated using the program SPIDER (Shaikh et al., 2008).

Results

VacA s1/i1/m1 oligomerizes as chiral hexamers on membranes. As an initial step towards characterizing the structural organization of membrane-bound

VacA, we first confirmed VacA's ability to bind vesicles using lipid compositions previously used in planar lipid bilayer experiments that characterized VacA channel activity (Czajkowsky et al., 1999; Iwamoto et al., 1999; Tombola et al., 1999a; Vinion-Dubiel et al., 1999). For these assays, 0.8 μM of VacA s1/i1/m1 was acid activated to disassemble soluble oligomers into monomers and then mixed with liposomes composed of DOPC, ePC/DOPS/chol (55/15/30 mol%), DOPC/DOPS/eSM (45/20/35 mol%), or DOPC/DOPS/eSM/chol (35/20/35/10 mol%) before being pelleted by centrifugation (Cover et al., 1997; Molinari et al., 1998). BSA at 1.1 μM was used as a negative control to measure non-specific membrane binding. Each binding experiment was done in triplicate and samples were analyzed by Coomassie staining, quantifying VacA or BSA in the supernatant (unbound) and the vesicle pellet (bound) (Fig. 3-1). The results show that VacA s1/i1/m1 bound to all lipid compositions tested (Fig. 3-2A). Statistically significant differences in VacA binding to specific lipid compositions were detected, but the differences in magnitude were small and probably not biologically meaningful (Fig. 3-2A). The negative control BSA did not bind the liposomes (Fig. 3-2B).

AFM, deep-etch EM, and 2D crystallization techniques have been used to visualize VacA s1/i1/m1 associated with membranes (Adrian et al., 2002; Czajkowsky et al., 1999; Geisse et al., 2004; Vinion-Dubiel et al., 1999). However, the limited resolution of the images in these studies made it difficult to determine whether the membrane-bound oligomers were single or double layer oligomers and impossible to visualize the conformation of the central pore-forming region of

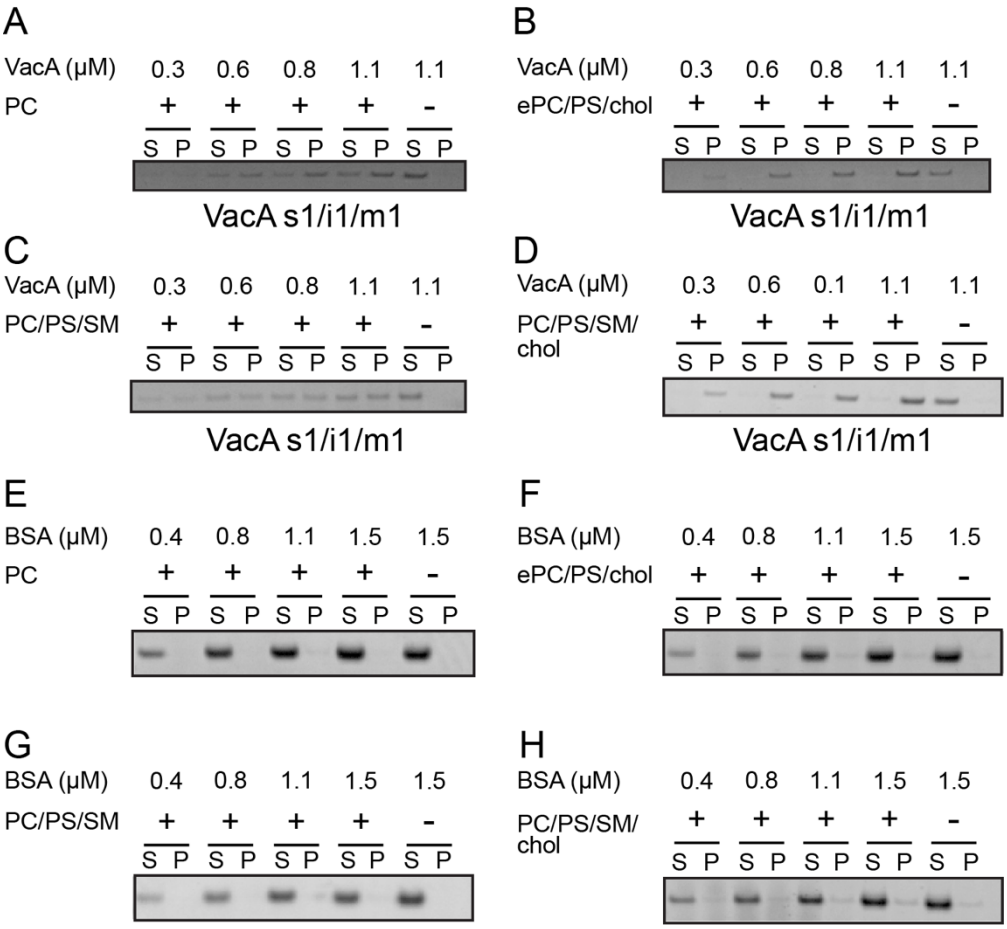

Figure 3-1: Liposome co-pelleting assays with VacA s1/i1/m1 and BSA. (A-D) VacA s1/i1/m1 binds liposomes composed of DOPC (PC) (A), eggPC/DOPS/cholesterol (ePC/PS/chol) (55/15/30 mol%) (B), DOPC/DOPS/eggSphingomyelin (PC/PS/SM) (45/20/35 mol%) (C), and DOPC/DOPS/eggSphingomyelin/cholesterol (PC/PS/SM/chol) (35/20/35/10 mol%) (D). Increasing concentrations of VacA s1/i1/m1 (μM) were added to a constant amount of LUVs. + = LUVs present; - = no LUV control. S = supernatant (unbound); P = pellet (bound). VacA visualized by Coomassie staining of SDS-PAGE gel. Gel shown is one of three independent co-pelleting experiments. (E-H) BSA does not bind robustly to liposomes composed of PC (E), ePC/PS/chol (55/15/30 mol%) (F), PC/PS/SM (45/20/35 mol%) (G), and PC/PS/SM/chol (35/20/35/10 mol%) (H). Increasing concentrations of BSA (μM) were added to a constant amount of LUVs. + = LUVs present; - = no LUV control. S = supernatant (unbound); P = pellet (bound). BSA visualized by Coomassie staining of SDS-PAGE gel. Gel shown is one of three independent co-pelleting experiments.

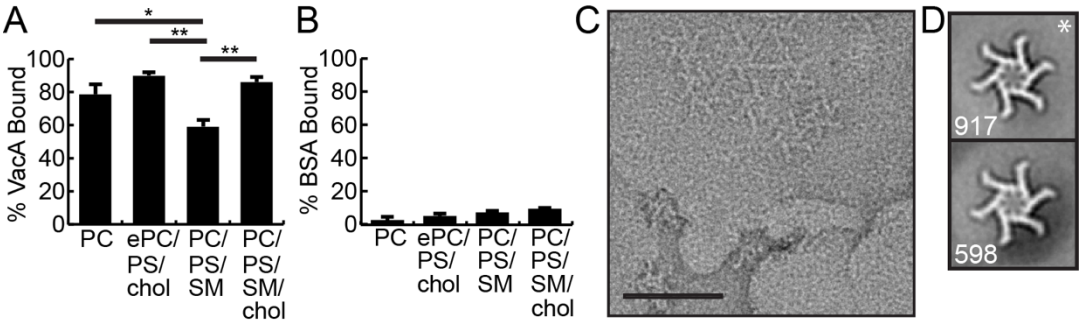

Figure 3-2: **VacA s1/i1/m1 organizes on membranes as hexamers.** (A-B) Large unilamellar vesicles (LUVs) with various lipid compositions were incubated with 0.8 μM VacA s1/i1/m1 or 1.1 μM BSA, and the proportion of protein bound to the vesicles was determined. $p < 0.05$, *; $p < 0.01$, **. Results represent the mean ± SEM based on three independent binding assays. PC: 1,2-dioleoyl-*sn*-glycero-3-phosphocholine (DOPC); ePC: L-α-phosphatidylcholine from egg; PS: 1,2-dioleoyl-*sn*-glycero-3-phospho-L-serine (DOPS); SM: sphingomyelin from egg; chol: cholesterol. (C) Representative negative stain image of VacA s1/i1/m1 bound to ePC/DOPS/chol (55/15/30 mol%) LUVs. Scale bar, 50 nm. (D) Representative class averages of membrane-bound VacA s1/i1/m1 hexamers. Number of particles in each average shown in bottom left. *, marks the average used for comparison between soluble and membrane bound VacA s1/i1/m1 hexamers in Figure 2. False colored average shows the location of the p55 (red) and p33 (blue) domains. Side length of panels, 42 nm

membrane-bound VacA. To define structural organization of VacA s1/i1/m1 associated with lipid bilayers, we used negative stain EM to image VacA bound to ePC/DOPS/chol (55/15/30 mol%) and heart lipid LUVs (Fig. 3-2C and data not shown), two lipid compositions that support formation of anion-selective VacA pores (Czajkowsky et al., 1999; Vinion-Dubiel et al., 1999). From this analysis, we found that VacA can oligomerize on membranes in an acidic buffer condition (*i.e.* pH of 3) that does not support oligomerization in solution, suggesting that monomeric VacA can bind to lipid and then oligomerize (Cover et al., 1997; Molinari et al., 1998). From our EM images, we collected datasets of greater than 2,000 particles for both ePC/DOPS/chol- and heart lipid-bound VacA s1/i1/m1. The datasets were classified into 2D class averages using multi-reference alignment (Figs. 3-3A-D). Analyses of the resulting classes showed that VacA s1/i1/m1 binds to membranes of either composition as an oligomer with six chiral "arms" (Figs. 3-2D and 3-3A-D). While a small number of oligomers with seven chiral arms were observed, there were not enough in the dataset to form a stable class average. Oligomers with achiral arms were not detected. Previous studies showed that oligomers with six or seven chiral arms correspond to hexamers or heptamers, whereas achiral oligomers correspond to dodecamers or tetradecamers (Adrian et al., 2002; Chambers et al., 2013; Cover et al., 1997; El-Bez et al., 2005). From these data we conclude that VacA s1/i1/m1 assembles on membranes predominantly as hexamers.

Membrane-bound VacA hexamers are structurally distinct from soluble oligomers and are inserted into the lipid bilayer. To determine whether there are structural differences between soluble and membrane-bound VacA hexamers, we compared 2D class averages of the two types of oligomers using radial density distribution plots, previously used to

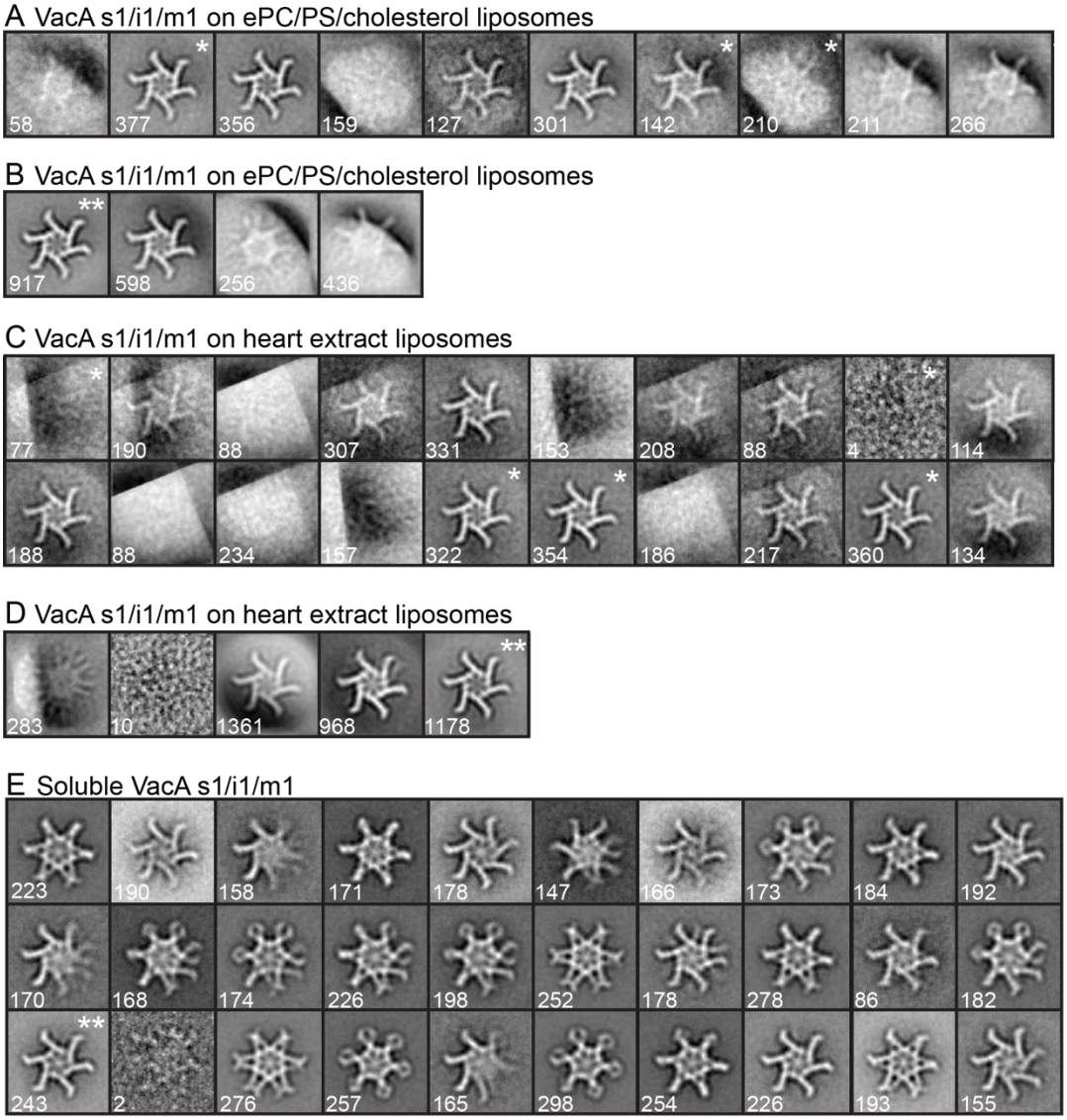

Figure 3-3: Negative stain averages of membrane-bound and soluble VacA s1/i1/m1. (A) Reference free alignment of 2,207 particles of VacA s1/i1/m1 bound to eggPC/DOPS/cholesterol (ePC/PS/chol) (55/15/30 mol%) into ten classes. Classes chosen as references marked with "*". (B) Reference based alignment of membrane-bound (ePC/PS/chol) VacA s1/i1/m1. "**" is class shown in Figure 1D. (C) Reference free alignment of 3,800 particles of VacA s1/i1/m1 bound to heart lipid into 20 classes. Classes chosen as references marked with "*". (D) Reference based alignment of membrane-bound (heart lipid) s1/i1/m1. "**" marks class shown in Figure S3B. (E) Reference free alignment of 5,763 particles of soluble VacA s1/i1/m1 into thirty classes. "**" marks the class shown in Figures 2A and S3A. Number of particles in each class shown in bottom left corner. Side length of all panels, 42 nm.

visualize differences between pre-pore and pore-formed Perfringolysin O, and difference maps (Dang et al., 2005b). Radial density distribution plots were generated from normalized 2D class averages of soluble and membrane-bound VacA s1/i1/m1 hexamers (Fig. 3-4A,B and 3-3). The plots were overlaid to compare the density across the radius of the soluble and membrane-bound hexamers (Fig. 3-4C). Additionally, a difference map was generated by subtracting the average of the membrane-bound VacA hexamer from the average of the soluble VacA hexamer (Fig. 3-5A-C). Both analyses showed that there is less density in the central, p33, region of membrane-bound s1/i1/m1 hexamers compared to soluble hexamers, suggesting that the p33 pore-forming domain undergoes a structural change when associated with membrane. To determine whether this difference is membrane composition-specific, we compared the radial density distribution plots and a difference map of soluble VacA s1/i1/m1 and VacA s1/i1/m1 bound to heart lipid membranes and obtained results similar to what was observed for VacA hexamers bound to ePC/DOPS/chol (Fig. 3-5D-G), indicating that the gross structural change observed in the central region of membrane-bound VacA s1/i1/m1 hexamers is not dependent on membrane composition.

One explanation for decreased central region density of membrane-bound oligomers could be that the p33 domains inserted into the lipid bilayer, where they would not be visible by negative stain EM analysis; however, it is also possible that binding to membrane causes a loss of structural organization in the p33 domain which would also lead to a loss of density in the 2D average. Since the negative stain 2D averages were not sufficient to definitively differentiate among these models, we used alkaline carbonate sucrose gradient centrifugation to test whether the membrane-bound VacA hexamers were also membrane-inserted (Fig. 3-4D). This treatment separates integral membrane proteins from peripheral

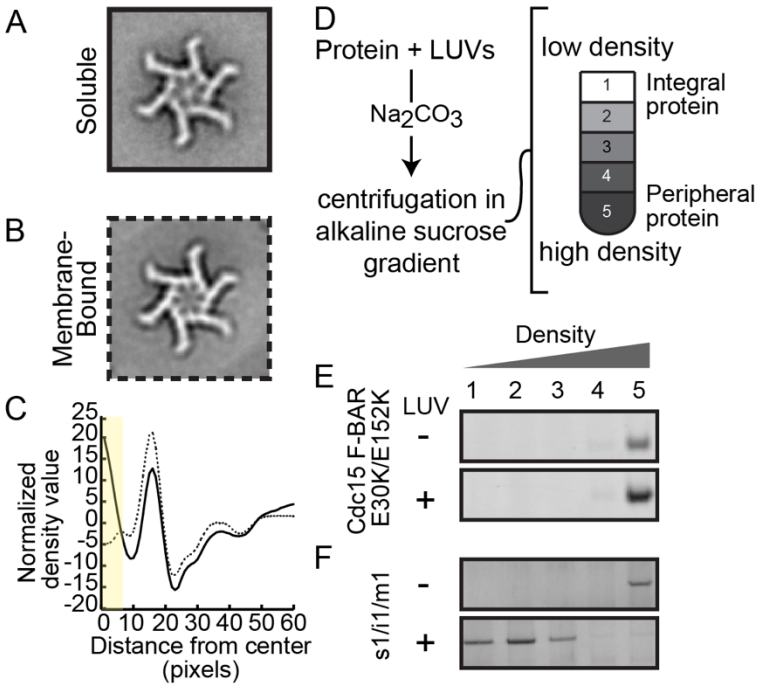

Figure 3-4: **The p33 domain of VacA s1/i1/m1 changes structure when bound to membranes.** (A-D) Comparison of soluble and membrane-bound VacA s1/i1/m1 hexamers. (A) Negative stain 2D average of soluble VacA s1/i1/m1 hexamers; 243 particles in class. (B) Negative stain 2D average of VacA s1/i1/m1 bound to ePC/DOPS/chol (55/15/30 mol%) LUVs; 917 particles in class. Same average shown in Figure 1D. Side length of averages, 42 nm. (C) Overlapping radial density distribution plots of normalized 2D averages of the soluble and membrane-bound s1/i1/m1 hexamers shown in panels A and B. Solid line = soluble hexamer; dotted line = membrane-bound hexamer. Yellow bar highlights the region of maximum difference. (D) Diagram showing the use of sodium carbonate stripped membranes to address whether membrane-bound proteins are peripheral or integral. Membranes treated with sodium carbonate are loaded at the bottom of an alkaline sucrose gradient (the highest density). After centrifugation, proteins peripherally associated with membranes remain in the highest density fraction, while membrane-inserted proteins float with the membranes into the lower density fractions. (E-F) Alkaline sucrose gradient analysis of Cdc15 F-BAR-E30K/E152K (E) and VacA s1/i1/m1 (F) without (-) or with (+) LUVs. Cdc15 F-BAR-E30K/E152K was bound to LUVs composed of DOPC/DOPS (80/20 mol%), and VacA s1/i1/m1 was bound to LUVs composed of ePC/DOPS/chol (55/15/30 mol%) before being treated with sodium carbonate and centrifuged in an alkaline sucrose gradient. Fractions were collected from top (low density) to bottom (high density) and analyzed by SDS-PAGE and Coomassie staining.

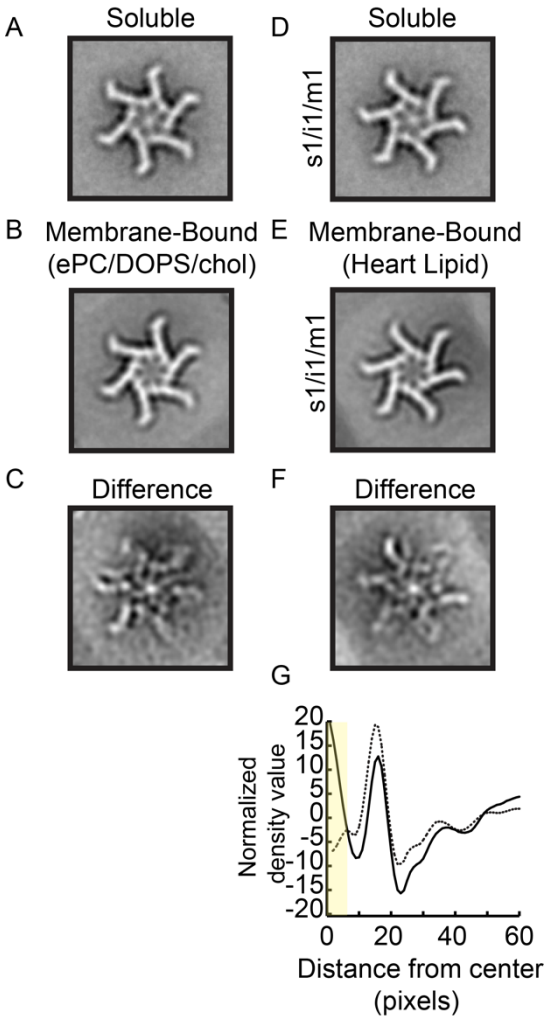

Figure 3-5: The p33 domain of VacA s1/i1/m1 changes structure when bound to membrane. (A) Negative stain 2D average of soluble VacA s1/i1/m1 hexamers; 243 particles in class. Same class averages as shown in Figure 2A. (B) Negative stain 2D average of VacA s1/i1/m1 bound to ePC/DOPS/chol (55/15/30 mol%) LUVs; 917 particles in class. Same average shown in Figure 1D. (C) Difference map subtracting the average of the membrane-bound VacA hexamer with the average of the soluble VacA hexamer. (D) Negative stain 2D average of soluble VacA s1/i1/m1 hexamers; 243 particles in class. Same class averages as shown in Figure 2A. (E) Negative stain 2D average of VacA s1/i1/m1 bound to heart lipid membranes; 1178 particles in class. (F) Difference map subtracting the average of VacA hexamer bound to heart lipids with the average of the soluble VacA hexamer. Side length of all averages, 42 nm. (G) Overlapping radial density distribution plots of normalized 2D averages of the soluble and membrane-bound s1/i1/m1 hexamers shown in panels A and B. Solid line = soluble hexamer; dotted line = membrane-bound hexamer. Yellow bar highlights the region of maximum difference.

membrane proteins (Fossati et al., 2014). In this assay, the VacA bound LUVs were generated as described above and then treated with sodium carbonate before being loaded at the bottom (highest density fraction) of an alkaline sucrose gradient. Peripheral membrane-associated proteins are stripped from the LUVs under alkaline conditions and pellet in the high density sucrose fractions during centrifugation, while membrane-inserted proteins remain bound to the membranes and float into the lower density sucrose fractions (Fig. 3-4D). To verify this assay's sensitivity for peripheral membrane binding proteins, we tested a mutant F-BAR domain from *Schizosaccharomyces pombe* Cdc15 (E30K/E152K), which binds but does not insert into membranes (McDonald et al., 2015). Cdc15 F-BAR-E30K/E152K was mixed with DOPC/DOPS (80/20 mol%) and acid activated VacA s1/i1/m1 was mixed with ePC/DOPS/chol (55/15/30 mol%) liposomes. Gradient fractions were collected from the top (low density) to the bottom (high density) and visualized by Coomassie staining on a SDS-PAGE gel. Cdc15 F-BAR-E30K/E152K sedimented in the highest density fraction, both in the absence and presence of liposomes (Fig. 3-4E), as expected for a peripheral membrane binding protein. VacA s1/i1/m1 remained in the highest density fraction when no liposomes were present, but floated into the lower density fractions in the presence of liposomes (Fig. 3-4F). The inability to strip VacA from membranes under alkaline conditions indicates that membrane-bound VacA s1/i1/m1 hexamers are membrane-inserted. Based on these results and combined with our analysis of the 2D averages of soluble and membrane-bound s1/i1/m1 hexamers (Fig. 3-4C and 3-5F,G), we conclude that the structural differences seen between soluble and membrane-bound VacA hexamers arise from insertion of the p33 domain into the membrane, a step required for pore formation.

Oligomerization is not required for insertion into the lipid bilayer. Next we investigated whether VacA Δ346-347, a mutant that cannot oligomerize in solution, could oligomerize and insert into the lipid bilayer when bound to membrane (Ivie et al., 2008). VacA ∆346-347 lacks two residues in the p55 domain (Fig. 3-6A), and consequently cannot form soluble oligomers even under neutral conditions, as determined by gel filtration and negative stain EM (Fig. 3-6B) (Ivie et al., 2008). Importantly, 2D averages of VacA s1/i1/m1 at pH 3 (a condition that causes soluble oligomers to disassemble into monomers) and VacA ∆346-347 at pH 7 were very similar, indicating that the two amino acid deletion in VacA ∆346-347 does not alter the overall structure of p88 monomers (Fig. 3-6C-E). Using liposome co-pelleting assays, we confirmed that VacA ∆346-347 binds to the same liposome compositions as those bound by VacA s1/i1/m1 (Fig. 3-6F and Fig. 3-7A-D); however, VacA ∆346-347 binds at reduced levels compared to wild-type VacA. We visualized VacA ∆346-347 bound to liposomes composed of ePC/DOPS/chol (55/15/30 mol%) using negative stain EM. Although VacA ∆346-347 bound to the LUVs (Fig. 3-6F), it remained monomeric (Fig. 3-6G). Thus, VacA residues 346 and 347 are essential for VacA oligomerization, both in solution and in the presence of membrane. In addition, the reduced binding of VacA ∆346-347 compared to wild-type VacA suggests that oligomerization may contribute to VacA-membrane interaction.

We next tested whether VacA ∆346-347 acts like a peripheral or integral membrane protein using the sodium carbonate extraction vesicle flotation assay. In the absence of liposomes, VacA ∆346-347 pelleted in the highest density gradient fractions. However, when combined with vesicles, VacA ∆346-347 floated into the low density gradient fractions (Fig. 3-6H), indicating the monomeric toxin

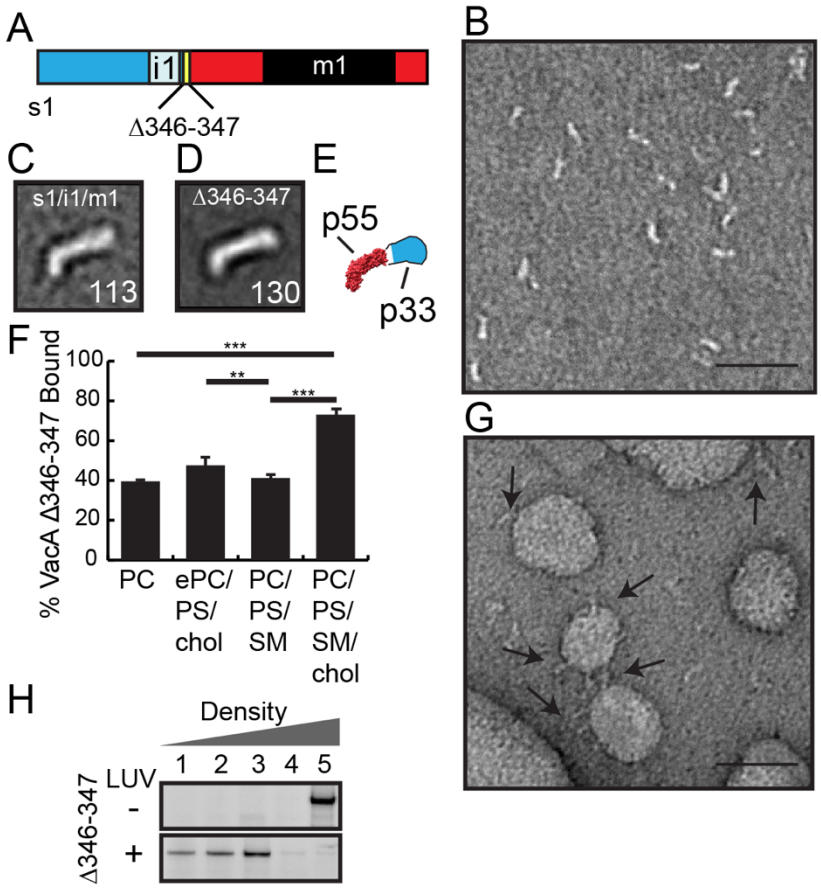

Figure 3-6: VacA Δ346-347, a non-oligomerizing mutant, can insert into the lipid bilayer. (A) Schematic of VacA Δ346-347 mutant. p33 = blue; p55 = red; i1 = light blue; m1= black, location of Δ346-347 = yellow. (B) Representative negative stain image of soluble VacA Δ346-347. Scale bar, 50 nm. (C-D) 2D average of negatively stained acidified VacA s1/i1/m1 monomers (C) and VacA Δ346-347 at neutral pH (D). Side length of panels, 22.4 nm. Number of particles in each average shown in bottom right corner. (E) Cartoon of p88 to scale with averages in C and D. p55 (PDB: 2QV3(Gangwer et al., 2007)) in red, p33 in blue. (F) LUVs with various lipid compositions were incubated with 0.8 μM VacA Δ346-347 and the proportion of VacA Δ346-347 bound to the vesicles was determined. p <0.01, **; p < 0.001, ***. Results represent the mean ± SEM based on three independent binding assays. PC: 1,2-dioleoyl-*sn*-glycero-3-phosphocholine (DOPC); ePC: L-α-phosphatidylcholine from egg; PS: 1,2-dioleoyl-*sn*-glycero-3-phospho-L-serine (DOPS); SM: sphingomyelin from egg; chol: cholesterol. (G) Representative negative stain image of VacA Δ346-347 bound to ePC/DOPS/chol (55/15/30 mol%) LUVs. Scale bar, 50 nm. (H) Alkaline sucrose gradient analysis of VacA Δ346-347 without (-) or with (+) LUVs. VacA Δ346-347 alone and bound to ePC/DOPS/chol (55/15/30 mol%) LUVs were treated with sodium carbonate and centrifuged in an alkaline sucrose gradient. Fractions were collected from top (low density) to bottom (high density) and analyzed by SDS-PAGE and Coomassie staining

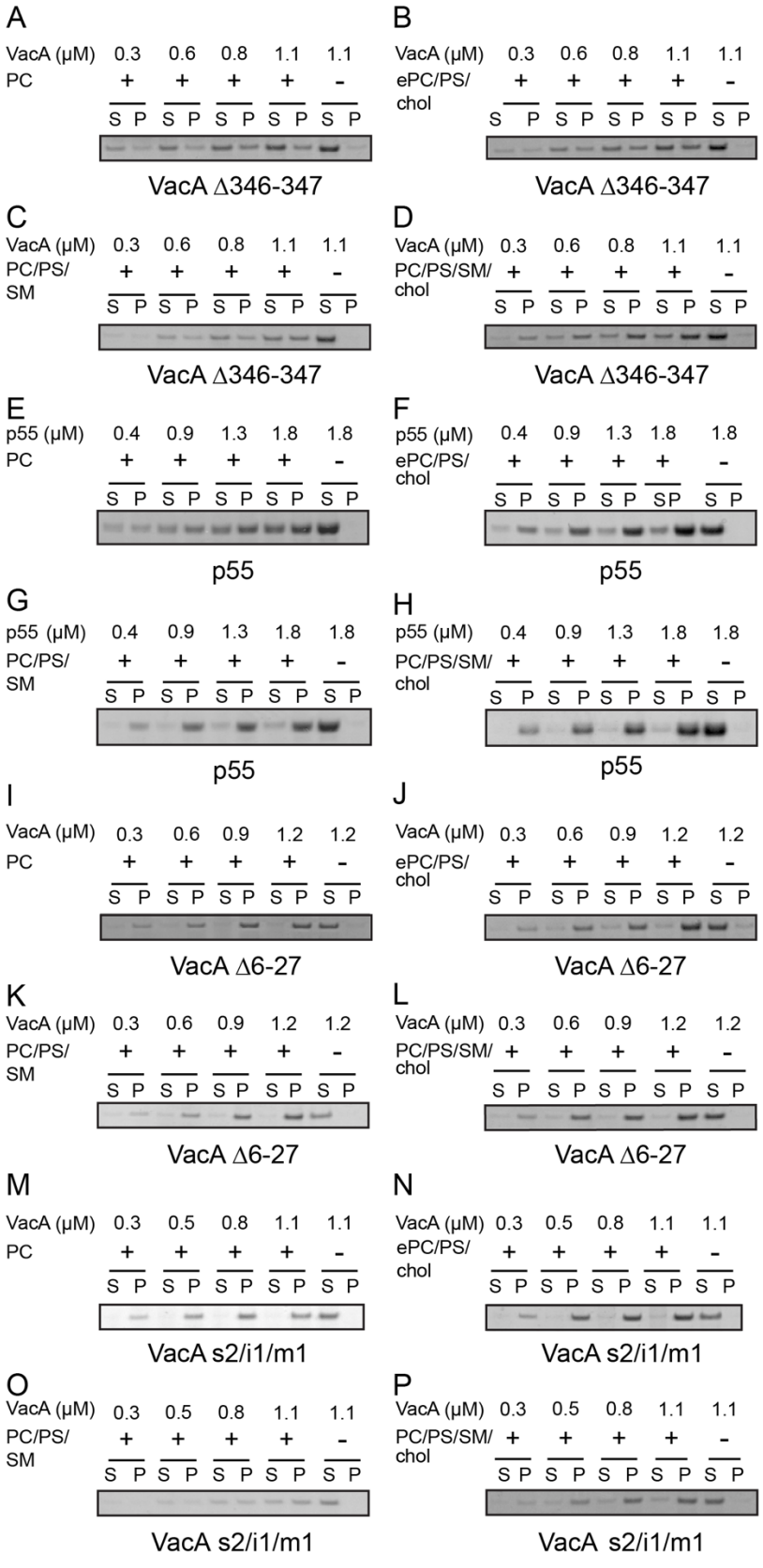
A
VacA (μM) 0.3 0.6 0.8 1.1 1.1
PC + + + + -
S P S P S P S P S P
VacA Δ346-347
B
VacA (μM) 0.3 0.6 0.8 1.1 1.1
ePC/PS/ chol + + + + -
S P S P S P S P S P
VacA Δ346-347
C
VacA (μM) 0.3 0.6 0.8 1.1 1.1
PC/PS/ SM + + + + -
S P S P S P S P S P
VacA Δ346-347
D
VacA (μM) 0.3 0.6 0.8 1.1 1.1
PC/PS/SM/ chol + + + + -
S P S P S P S P S P
VacA Δ346-347
E
p55 (μM) 0.4 0.9 1.3 1.8 1.8
PC + + + + -
S P S P S P S P S P
p55
F
p55 (μM) 0.4 0.9 1.3 1.8 1.8
ePC/PS/ chol + + + + -
S P S P S P SP S P
p55
G
p55 (μM) 0.4 0.9 1.3 1.8 1.8
PC/PS/ SM + + + + -
S P S P S P S P S P
p55
H
p55 (μM) 0.4 0.9 1.3 1.8 1.8
PC/PS/SM/ chol + + + + -
S P S P S P S P S P
p55
I
VacA (μM) 0.3 0.6 0.9 1.2 1.2
PC + + + + -
S P S P S P S P S P
VacA Δ6-27
J
VacA (μM) 0.3 0.6 0.9 1.2 1.2
ePC/PS/ chol + + + + -
S P S P S P S P S P
VacA Δ6-27
K
VacA (μM) 0.3 0.6 0.9 1.2 1.2
PC/PS/ SM + + + + -
S P S P S P S P S P
VacA Δ6-27
L
VacA (μM) 0.3 0.6 0.9 1.2 1.2
PC/PS/SM/ chol + + + + -
S P S P S P S P S P
VacA Δ6-27
M
VacA (μM) 0.3 0.5 0.8 1.1 1.1
PC + + + + -
S P S P S P S P S P
VacA s2/i1/m1
N
VacA (μM) 0.3 0.5 0.8 1.1 1.1
ePC/PS/ chol + + + + -
S P S P S P S P S P
VacA s2/i1/m1
O
VacA (μM) 0.3 0.5 0.8 1.1 1.1
PC/PS/ SM + + + + -
S P S P S P S P S P
VacA s2/i1/m1
P
VacA (μM) 0.3 0.5 0.8 1.1 1.1
PC/PS/SM/ chol + + + + -
S P S P S P S P S P
VacA s2/i1/m1

Figure 3-7: Liposome co-pelleting assays with VacA ∆346-347, p55, VacA ∆6-27, and VacA s2/i1/m1. (A-D) VacA ∆346-347 binds liposomes composed of DOPC (PC) (A), eggPC/DOPS/cholesterol (ePC/PS/chol) (55/15/30 mol%) (B), DOPC/DOPS/eggSphingomyelin (PC/PS/SM) (45/20/35 mol%) (C), and DOPC/DOPS/eggSphingomyelin/cholesterol (PC/PS/SM/chol) (35/20/35/10 mol%) (D). (E-H) p55 binds liposomes composed of DOPC (PC) (E), eggPC/DOPS/cholesterol (ePC/PS/chol) (55/15/30 mol%) (F), DOPC/DOPS/eggSphingomyelin (PC/PS/SM) (45/20/35 mol%) (G), and DOPC/DOPS/eggSphingomyelin/cholesterol (PC/PS/SM/chol) (35/20/35/10 mol%) (H). (I-L) VacA ∆6-27 binds liposomes composed of DOPC (PC) (I), eggPC/DOPS/cholesterol (ePC/PS/chol) (55/15/30 mol%) (J), DOPC/DOPS/eggSphingomyelin (PC/PS/SM) (45/20/35 mol%) (K), and DOPC/DOPS/eggSphingomyelin/cholesterol (PC/PS/SM/chol) (35/20/35/10 mol%) (L). (M-P) VacA s2/i1/m1 binds liposomes composed of DOPC (PC) (M), eggPC/DOPS/cholesterol (ePC/PS/chol) (55/15/30 mol%) (N), DOPC/DOPS/eggSphingomyelin (PC/PS/SM) (45/20/35 mol%) (O), and DOPC/DOPS/eggSphingomyelin/cholesterol (PC/PS/SM/chol) (35/20/35/10 mol%) (P). For all binding experiments an increasing concentration of protein (μM) was added to a constant amount of LUVs. + = LUVs present; - = no LUVs control. S = supernatant (unbound); P = pellet (bound). VacA visualized by Coomassie staining of SDS-PAGE gel. Gel shown is one of three independent co-pelleting experiments.

had inserted into the bilayer. This finding shows that oligomerization is not required for VacA to transition from a soluble protein to a membrane-inserted protein.

*Role of VacA p55 and p33 domains in membrane binding and insertion.*With the unexpected finding that VacA can insert into membranes without first oligomerizing, we next investigated whether specific VacA domain(s) are required for membrane binding and insertion. First we tested whether the p55 domain alone can bind to membrane. p55 (amino acids 312-821) was expressed and purified as described and used in liposome co-pelleting experiments (Gangwer et al., 2007). Similar to full length VacA s1/i1/m1, p55 bound to all the lipid compositions tested (Fig. 3-8A and 3-7E-H). Using negative stain EM analysis, the membrane-bound p55 was not visible (data not shown), consistent with the expected failure of membrane-bound p55 to form large oligomeric structures. To determine whether p55 binds as a peripheral membrane binding protein or inserts into the membrane, p55-bound vesicles were treated with sodium carbonate and subjected to centrifugation in an alkaline sucrose gradient. p55 sedimented in the highest density fraction, both in the absence and presence of liposomes (Fig. 3-8B) indicating that it is a peripheral membrane binding protein that does not insert into the membrane. These results provide direct biochemical evidence that while p55 binds membranes, the p33 domain is required for membrane insertion of VacA.

VacA's p33 domain contains three GXXXG motifs, is essential for anion-selective channel formation, and has an altered structure when bound to membrane as compared to soluble hexamers (Fig. 3-4A-C), suggesting that it binds and inserts into membrane (McClain et al., 2003). Since recombinantly expressed p33 is insoluble and only folds correctly in the presence of p55, it was not possible to use isolated p33 in our assays. Therefore, to test the contribution of

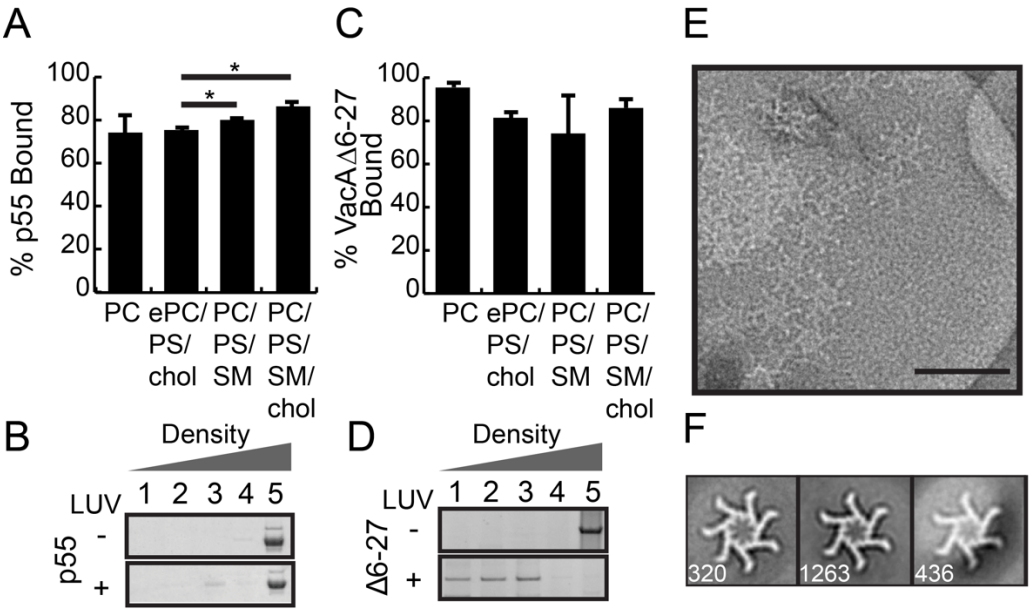

Figure 3-8: The roles of VacA domains in membrane insertion and binding. (A) LUVs with various lipid compositions were incubated with 1.3 μM p55 and the proportion of p55 bound to the vesicles was then determined. $p < 0.05$, *. Results represent the mean ± SEM based on three independent binding assays. PC: 1,2-dioleoyl-*sn*-glycero-3-phosphocholine (DOPC); ePC: L-α-phosphatidylcholine from egg; PS: 1,2-dioleoyl-*sn*-glycero-3-phospho-L-serine (DOPS); SM: sphingomyelin from egg; chol: cholesterol. (B) Alkaline sucrose gradient analysis of p55 without (-) or with (+) LUVs. p55 alone or p55 bound to ePC/DOPS/chol (55/15/30 mol%) LUVs were treated with sodium carbonate and centrifuged in an alkaline sucrose gradient. Fractions were collected from top (low density) to bottom (high density) and analyzed by SDS-PAGE and Coomassie staining. (C) LUVs with various lipid compositions were incubated with 0.9 μM VacA Δ6-27 and the proportion of VacA Δ6-27 bound to the vesicles was determined. Graph represents quantification of three independent binding assays. (D) Alkaline sucrose gradient of VacA Δ6-27 without (-) or with (+) LUVs. VacA Δ6-27 alone or bound to LUVs composed of ePC/DOPS/chol (55/15/30 mol%) were treated with sodium carbonate and centrifuged in an alkaline sucrose gradient. Fractions were collected from top (low density) to bottom (high density) and analyzed by SDS-PAGE and Coomassie staining. (E) Representative negative stain image of VacA Δ6-27 bound to ePC/DOPS/chol (55/15/30 mol%) LUVs. Scale bar, 50 nm. (F) Representative class averages of membrane-bound VacA Δ6-27 hexamers and heptamers. Number of particles in each average shown in bottom left. Side length of panels, 42 nm.

the N-terminus and the GXXXG repeats in membrane insertion, we examined the ability of VacA Δ6-27, a mutant lacking all three GXXXG repeats, to bind membrane, insert into the lipid bilayer, and oligomerize (Vinion-Dubiel et al., 1999). The GXXXG repeats are required for channel activity and have been computationally modeled to form an α-helix that traverses the membrane and participates in toxin oligomerization (Kim et al., 2004; McClain et al., 2003). The 3D structures of soluble VacA Δ6-27 oligomers lack an organized central density (Chambers et al., 2013). VacA Δ6-27 bound to all lipid compositions tested (Figs. 3-8C and 3-7I-L). To determine whether the three GXXXG motifs are required for membrane insertion, VacA Δ6-27 was mixed with liposomes and subjected to sodium carbonate extraction followed by centrifugation in an alkaline sucrose gradient. VacA Δ6-27 remained in the highest density fraction in the absence of liposomes, but surprisingly, this mutant floated with membranes into the low density fractions, indicating that it had inserted into the membrane (Fig. 3-8D). Therefore, while the GXXXG motifs are required for active pore formation, our analysis suggests that these repeats are not the only region of the p33 domain that inserts into the membrane (McClain et al., 2003). To explore whether the GXXXG repeats are required for VacA oligomerization when bound to membranes, we used negative stain EM to visualize membrane-bound VacA Δ6-27. Unlike membrane-bound VacA Δ346-347, which remains monomeric (Fig. 3-6G), membrane-bound VacA Δ6-27 oligomerized into chiral hexamers (87%) and heptamers (13%) (Figs. 3-8E,F and 3-9A-D). Thus, the putative transmembrane N-terminal GXXXG repeats are not required for either VacA membrane insertion or oligomerization.

Finally, we investigated the interactions of type s2 forms of VacA with membranes. In comparison to type s1 forms of VacA, type s2 VacA variants

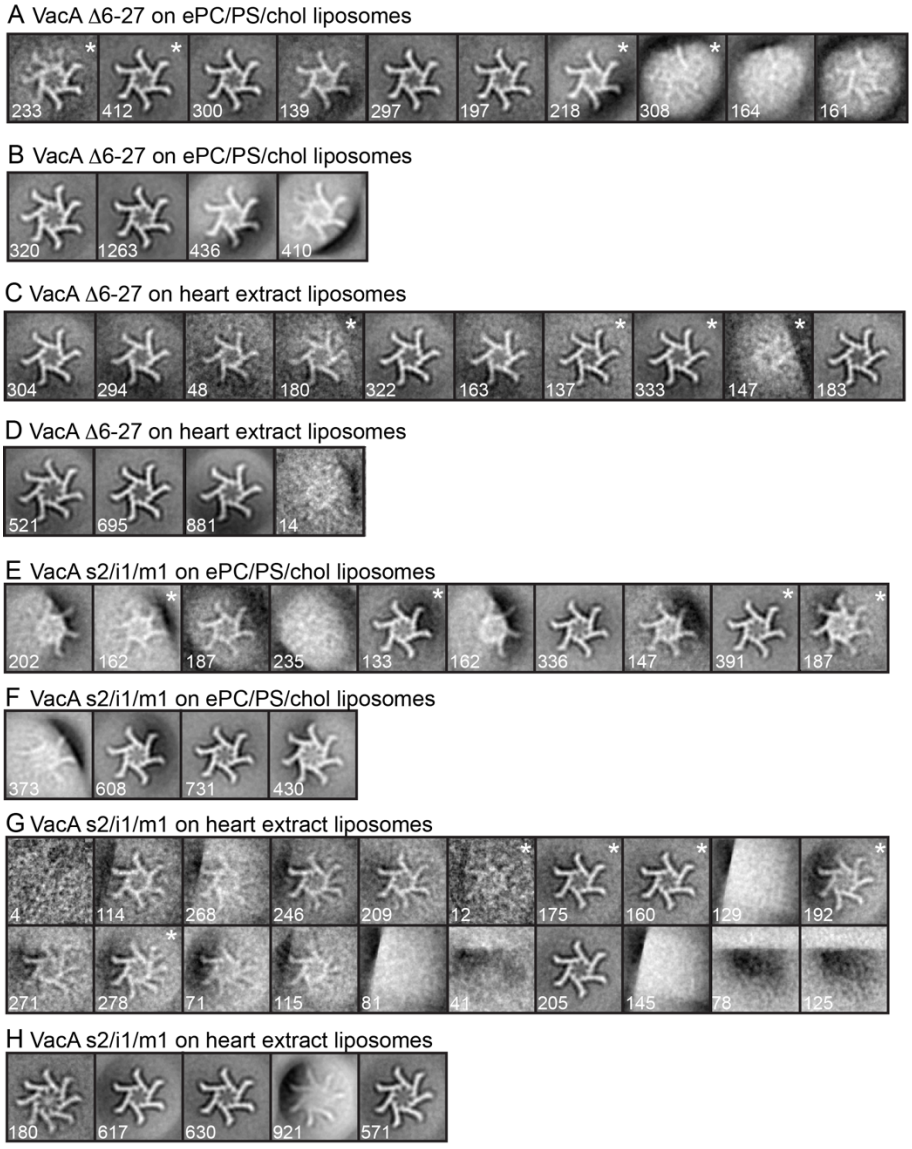

Figure 3-9: Negative stain averages of membrane-bound VacA Δ6-27 and VacA s2/i1/m1. (A) Reference free alignment of 2,429 particles of VacA Δ6-27 bound to eggPC/DOPS/cholesterol (ePC/PS/chol) (55/15/30 mol%) into ten classes. Classes chosen as references marked with "*". (B) Reference based alignment of membrane-bound VacA Δ6-27. (C) Reference free alignment of 2,111 particles of VacA Δ6-27 bound to heart lipid into 10 classes. Classes chosen as references marked with "*". (D) Reference based alignment of heart lipid membrane bound VacA Δ6-27. (E) Reference free alignment of 2,142 particles of VacA s2/i1/m1 bound to eggPC/DOPS/cholesterol (ePC/PS/chol) (55/15/30 mol%) into ten classes. Classes chosen for references marked with "*". (F) Reference based alignment of membrane-bound (ePC/PS/chol) VacA s2/i1/1m1. (G) Reference free alignment of 2,919 particles of VacA s2/i1/m1 bound to heart lipid into 20 classes. Classes chosen as references marked with "*". (H) Reference based alignment of membrane (heart lipid) bound s2/i1/m1. Number of particles in each class shown in bottom left corner. Side length of all panels, 42 nm.

contain a 12-residue hydrophilic N-terminal extension (Atherton et al., 1995). The s2 variants of VacA form ion channels less efficiently than s1 variants, and do not vacuolate cells (Atherton et al., 1995; Letley and Atherton, 2000; Letley et al., 2003; McClain et al., 2001b). The N-terminal extension could potentially ablate VacA function by disrupting toxin oligomerization on membranes, blocking insertion into the lipid bilayer, and/or altering pore conformation. While 3D structural analysis of soluble VacA s2/i1/m1 oligomers found no significant differences between soluble s1/i1/m1 and s2/i1/m1 dodecamers and tetradecamers, the effect of this extension on VacA interactions with membranes has not been tested (Chambers et al., 2013). To investigate this topic, we first confirmed that VacA s2/i1/m1 bound to all membrane compositions previously assayed (Fig. 3-10A and 3-7M-P). To determine whether the s2 VacA variant can insert into the lipid bilayer, VacA s2/i1/m1 bound vesicles were treated with sodium carbonate and centrifuged in an alkaline sucrose gradient. VacA s2/i1/m1 sedimented in the highest density fraction in the absence of liposomes, but when added to vesicles it floated with the membranes into the low density fractions (Fig. 3-10B). Therefore, the 12-amino acid extension does not inhibit membrane insertion. Visualizing VacA s2/i1/m1 bound to LUVs using single particle negative stain EM showed that the s2 variant oligomerizes into chiral hexamers (80%), heptamers (20%) (Fig. 3-10C,D and 3-9E-H), and under certain lipid compositions, even octamers (Fig. 3-9H). In contrast, heptamers and octamers were infrequently observed under these conditions in experiments with s1/i1/m1 VacA (Fig. 3-2 and 3-3). Thus, the addition or the deletion of residues at the N-terminus of VacA alters the types of membrane-bound oligomers that are able to form.

DISCUSSION

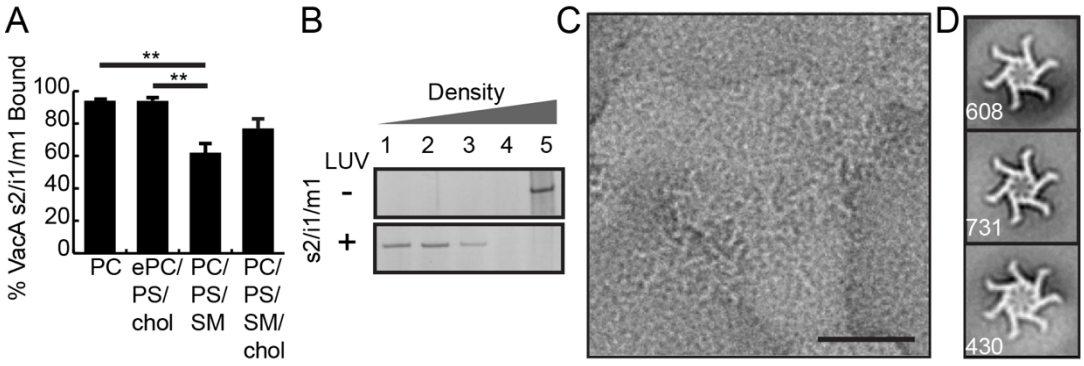

Figure 3-10: **The N-terminal extension on VacA s2/i1/m1 does not alter membrane binding or membrane insertion, but does influence the types of oligomers that form.** (A) LUVs with various lipid compositions were incubated with 0.8 μM VacA s2/i1/m1 and the proportion of VacA s2/i1/m1 bound to the vesicles was determined. p <0.01, **. Results represent the mean ± SEM based on three independent binding assays. PC: 1,2-dioleoyl-*sn*-glycero-3-phosphocholine (DOPC); ePC: L-α-phosphatidylcholine from egg; PS: 1,2-dioleoyl-*sn*-glycero-3-phospho-L-serine (DOPS); SM: sphingomyelin from egg; chol: cholesterol. (B) Alkaline sucrose gradient of VacA s2/i1/m1 without (-) or with (+) LUVs. VacA s2/i1/m1 alone or bound to LUVs composed of ePC/DOPS/chol (55/15/30 mol%) were treated with sodium carbonate and centrifuged in an alkaline sucrose gradient. Fractions were collected from top (low density) to bottom (high density) and analyzed by SDS-PAGE and Coomassie staining. (C) Representative negative stain image of VacA s2/i1/m1 bound to ePC/DOPS/chol (55/15/30 mol%) LUVs. Scale bar, 50 nm. (D) Representative class averages of membrane-bound VacA s2/i1/m1 hexamers and heptamers. Number of particles in each average shown in bottom left. Side length of panels, 42 nm.

Our studies provide the first detailed structural characterization of membrane-bound VacA and address the role(s) of specific regions of VacA in membrane binding, oligomerization, and membrane-insertion. We show that VacA oligomerizes into hexamers when bound to membrane and that this oligomerization occurs under pH conditions that do not support oligomerization of soluble VacA. Comparison of soluble and membrane-bound VacA hexamers reveals a prominent structural difference in the central region of the oligomers. Combined with our biochemical results indicating that membrane-bound VacA hexamers are also membrane-inserted, we conclude that this structural difference results from insertion of the p33 domains into the membrane to form a hexameric pore. Importantly, membrane insertion is not dependent on toxin oligomerization.

Under neutral buffer conditions in solution, we previously showed that VacA organizes into a heterogeneous combination of hexamers, heptamers, dodecamers, and tetradecamers, with ~90% of soluble VacA found as achiral, double layer dodecamers and tetradecamers (Chambers et al., 2013). In contrast, we find that membrane-bound VacA s1/i1/m1 organizes mainly into chiral hexamers, with no dodecamers or tetradecamers present. The oligomerization into membrane-bound VacA hexamers is not dependent on membrane composition, since hexamers formed on membranes composed of either DOPC or heart lipids. Additionally, membrane-bound VacA hexamers formed independent of whether lipid raft components, such as cholesterol and sphingomyelin, were present. Our negative stain EM analysis concurs with the results of single channel and computational modeling studies that predicted VacA pores would be hexamers composed of six subunits (Iwamoto et al., 1999; Kim et al., 2004). The double layer oligomers found in solution are presumed to result from hydrophobic

interactions between p88 molecules that would normally be made with membranes. Altogether, these data indicate that in the presence of membranes, VacA monomers organize into stable hexamers and these hexamers form membrane-inserted pores.

It has long been appreciated that maximum toxin activity *in vitro* requires acid activation of purified VacA before it is added to cells (Cover et al., 1997; de Bernard et al., 1995; McClain et al., 2000; Molinari et al., 1998; Yahiro et al., 1999). The need for acid activation has been attributed to changes in VacA structure, most notably the disassembly of VacA oligomers in an acidic environment, but it has also been proposed that low pH changes the conformation of p88 so that it can penetrate the lipid bilayer more efficiently (de Bernard et al., 1995; McClain et al., 2000; Molinari et al., 1998; Pagliaccia et al., 2000). While there are many precedents for toxins undergoing conformational changes upon exposure to low pH environments, our results for VacA show that exposure to low pH does not lead to a gross structural rearrangement (Boquet and Pappenheimer, 1976; Choe et al., 1992; Leka et al., 2014; O'Keefe et al., 1992; Pruitt et al., 2010). Indeed, 2D class averages of VacA s1/i1/m1 monomers at pH 3 and VacA ∆346-347 at pH 7 are indistinguishable. Additionally, VacA ∆346-347 still inserts into the lipid bilayer at a neutral pH, showing that acid activation is not required for membrane insertion. From these results we conclude that the main importance of acid activating VacA is to simply dissociate the dodecamers and tetradecamers that make up ~90% of the sample at a neutral pH. The released p88 monomers can then oligomerize on membranes (perhaps via hydrophobic regions that were inaccessible in the double layer oligomers), or alternatively, the monomers may bind specific cell surface receptors with increased affinity compared to that of oligomerized toxin (Yahiro et al., 1999). Once bound to the membrane, we predict

that regions of p33 undergo structural rearrangement(s) that allow VacA to insert into the bilayer and oligomerize.

Multiple lines of evidence suggest that the p33 domain forms the VacA anion-selective channel, and both the p33 and p55 domains are involved in VacA binding to host cells and oligomerization (Cover and Blanke, 2005; Domanska et al., 2010; Gonzalez-Rivera et al., 2010; McClain et al., 2003; Torres et al., 2005). Difficulties in purifying properly folded recombinant p33 have made it a challenge to examine the individual contributions of the p33 and p55 domains to membrane binding, membrane insertion, oligomerization, and pore formation. We found that while recombinant p55 binds membranes, it does not oligomerize on membranes or insert into the lipid bilayer. In previous studies using the TOXCAT system, a method developed to study TM helix-helix associations, the N-terminal hydrophobic region of VacA (amino acids 1-32) was found to insert into the membrane and drive dimerization (McClain et al., 2001a; McClain et al., 2003; Russ and Engelman, 1999, 2000). Conversely, in the current study we found that VacA ∆6-27, a mutant lacking all three N-terminal GXXXG repeats, was still able to insert into the lipid bilayer. This finding suggests that there are previously unrecognized regions of p33 that are important for facilitating the transition of VacA from a soluble toxin into an active ion channel; since these regions presumably insert into membranes, they could potentially be important structural components of the VacA ion channel.

It is currently not clear which regions in addition to the hydrophobic N-terminus can insert into the membrane. Analysis of the p33 domain hydrophobicity plot does not predict any obvious TM domains in addition to the previously recognized GXXXG motifs (McClain et al., 2003; Vinion-Dubiel et al., 1999). However, previous studies using VacA deletion mutants to map regions in p33 that

are required for oligomerization in solution provided evidence that multiple regions of p33 other than the N-terminus contribute to oligomerization (Genisset et al., 2006; Vinion-Dubiel et al., 1999). Additionally, one study, using a combination of proteolytic digestion and mass spectrometry analysis, reported that VacA residues 40-66, 111-169, 205-266, 548-574 and 723-767 were protected from proteolysis because of their interaction with the membrane (Wang et al., 2000). Two of these protected peptides (548-574 and 723-767) are in p55, a domain that we show does not insert into the membrane. The other three peptides (40-66, 111-169 and 205-266) are located in the p33 domain, making them possible candidates for membrane insertion. Membrane-protected peptides spanning residues 1-32 were not detected, leading the authors to suggest that the N-terminus of VacA regulates channel formation through an unknown mechanism that does not involve forming the actual channel (Wang et al., 2000). While this conclusion is consistent with their mass spectrometry results, it does not fit with other studies showing that the N-terminus of VacA is required for insertion of the protein into membranes and formation of an anion channel (Kim et al., 2004; McClain et al., 2001a; McClain et al., 2003; Vinion-Dubiel et al., 1999). High-resolution structural analysis of membrane-bound VacA will be needed to elucidate the membrane topology of VacA in the context of the lipid bilayer and conclusively define which regions of p33 are essential and sufficient for pore formation.

While the current results show that VacA Δ6-27 can still insert into membranes, several lines of evidence indicate that the first 32 amino acids of the p33 domain are essential for the formation of a functional ion channel. Deletion of amino acids Δ6-27 abrogates the capacity of VacA to form pores in planar lipid bilayers and its capacity to cause vacuolation of cells, and mutant proteins containing specific point mutations near or in the third $G^{14}XXXG^{18}$ motif lack

channel activity and do not cause cellular vacuolation (McClain et al., 2001b; McClain et al., 2003; Vinion-Dubiel et al., 1999). Additionally, VacA s2/i1/m1, a mutant that contains a 12-amino acid N-terminal extension, has reduced pore activity and does not vacuolate cells (McClain et al., 2001b). Collectively, these studies show that the p33 N-terminal region is required for pore formation and is sensitive to structural alterations. While the first 32 amino acids are not required for oligomerization in solution or on membrane, modifying the VacA N-terminus, either by adding or deleting amino acids, alters the ratio of hexamer and heptamer formation on membranes (Chambers et al., 2013; El-Bez et al., 2005; Vinion-Dubiel et al., 1999). Thus, the first 32 amino acids of VacA play at least an ancillary role in organizing oligomer formation of membrane-bound VacA. This conclusion is consistent with previous studies showing that point mutations made in the N-terminus of VacA reduce TM dimerization, as well as the prediction made by computational modeling that the GXXXG motifs make numerous intramolecular contacts required for the proper organization of a hexameric ion channel (Kim et al., 2004; McClain et al., 2001a; McClain et al., 2003).

In summary, we have shown that membrane-bound VacA assembles into hexameric structures, that there is a distinct structural difference in the central region of soluble hexamers compared to membrane-bound hexamers, and that insertion of VacA into the lipid membrane is not dependent on oligomerization. Our findings predict that VacA pore formation requires multiple regions of VacA in addition to the N-terminal GXXXG repeats. We propose a model where monomeric VacA binds to lipids and the p33 domain inserts into the lipid bilayer to oligomerize and form a pore (Fig. 3-11). The insertion of p33 into the membrane leads to a clear structural difference between soluble and membrane-bound VacA hexamers.

Since oligomerization is not required for p33 to insert into the membrane, we propose a model in which 1) VacA monomers bind to membrane, 2) the p33 domain inserts into the lipid-bilayer, and 3) the pore is formed (Fig. 3-11A). However, our data do not resolve questions about the temporal order of membrane-insertion, oligomerization, and pore formation. Thus, multiple models are possible, including one where VacA membrane insertion and pore formation occur concomitantly (Fig. 3-11B). Continuing biophysical and structural analyses of membrane-bound VacA s1/i1/m1 and VacA mutants will be essential for dissecting the interrelated steps of oligomerization, insertion, and pore formation, and elucidating the molecular organization of the VacA anion channel.

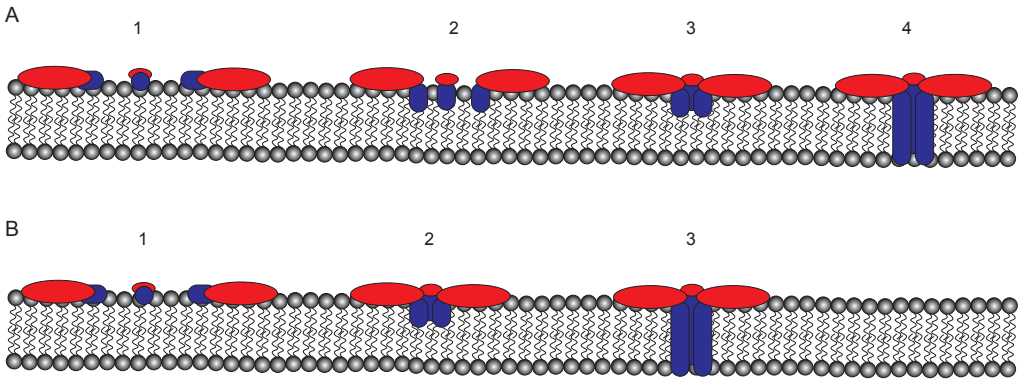

Figure 3-11: Models of VacA pore formation in membranes. Monomeric VacA binds to membrane where regions of p33 insert into the lipid bilayer, either before (A) or concomitant (B) with p88 oligomerization into a hexamer forming a functional pore. Further biophysical studies are needed to determine the temporal order of membrane insertion, oligomerization, and pore formation. p55 depicted in red, while p33 is shown in blue.

CHAPTER IV

HIGH RESOLUTION STRUCTURAL ANALYSIS OF A *HELICOBACTER PYLORI* VacA TOXIN OLIGOMER

Introduction

Helicobacter pylori is a gram-negative bacterium that infects and colonizes the human stomach (Atherton and Blaser, 2009; Cover and Blaser, 2009; Marshall et al., 1984). This bacterium infects over 50% of the world's population and its presence induces chronic gastritis and can lead to the development of peptic ulcers and in more severe cases, gastric lymphoma and adenocarcinoma (Amieva and El-Omar, 2008; Atherton, 2006; Suerbaum and Michetti, 2002). The role that *H. pylori* plays in the development of these cancers led the World Health Organization to classify it as a type I carcinogen (Anonymous, 1994).

One of the major virulence factors secreted by *H. pylori* is vacuolating cytotoxin A (VacA). VacA is named for its ability to induce larges vacuoles in cells when infected (Boquet and Ricci, 2012; Cover and Blanke, 2005; Fischer et al., 2004; Montecucco and de Bernard, 2003; Rassow and Meinecke, 2012). VacA is secreted as an 88 kDa monomer and is divided into two domains: an N-terminal p33 domain required for receptor binding and pore-formation and a C-terminal p55 domain reported to be required for receptor binding and specificity (Cover and Blanke, 2005; Domanska et al., 2010; El-Bez et al., 2005; Gonzalez-Rivera et al., 2010; McClain et al., 2003; Torres et al., 2005). A crystal structure of the p55 domain revealed that it is comprised of a beta helix with a C-terminal globular domain (Gangwer et al., 2007). Recently, a crystal structure determined of a mutant of p88, VacA Δ346-347, which contains a two amino acid deletion near the

junction of p33 and p55, showed that the beta helix extends into the p33 domain (Gonzalez-Rivera et al., 2016). Unfortunately, the N-terminus of the p33 domain was unable to be resolved with this analysis and therefore there is still a lack of high resolution structural information regarding this domain.

At neutral pH, VacA forms large water soluble oligomers, or “snowflake” like structures, including single-layer hexamers and heptamers and double-layer dodecamers and tetradecamers which have been visualized using various methods (Adrian et al., 2002; Chambers et al., 2013; Cover et al., 1997; Czajkowsky et al., 1999; El-Bez et al., 2005; Gonzalez-Rivera et al., 2010; Lanzavecchia et al., 1998; Lupetti et al., 1996; Reyrat et al., 1999). Cryo-negative EM structures were determined to ~19 Å and generated using computational modeling methods since random conical tilt (RCT) was not performed (El-Bez et al., 2005). Most recently, ~15 Å resolution VacA oligomer structures were determined using negative stain random conical tilt (RCT) electron microscopy (Chambers et al., 2013). Unfortunately, the cryo-negative stain and RCT structures were at too low of a resolution to discern any secondary structure detail. However, analysis of the p55 crystal structure together with the EM density maps indicated that the p55 domain is localized to the arms of the oligomers thus leaving the p33 domain to comprise the central region (Chambers et al., 2013; Gangwer et al., 2007; Ivie et al., 2008).

Previous studies have shown that VacA forms in anion channel in planar lipid bilayers (Adrian et al., 2002; Czajkowsky et al., 1999; Geisse et al., 2004; Iwamoto et al., 1999; Tombola et al., 1999a). Although VacA does not share any sequence similarity to any other chloride channel, the toxin does possess characteristics of a typical chloride channel (Iwamoto et al., 1999; Rassow and Meinecke, 2012). For example, VacA exhibits a moderate preference for anions

over cations and a known channel blocker has uneven blocking power at opposing ends of the channel (Iwamoto et al., 1999). VacA also contains 3 GXXXG motifs which are known transmembrane motifs and upon deletion of these motifs, channel activity is severly diminished (McClain et al., 2001a; McClain et al., 2003; Russ and Engelman, 2000; Teese and Langosch, 2015). While a high-resolution structure has yet to be determined of the VacA pore, computational modeling has been performed (Kim et al., 2004). The model showed similarities with the structure of a known chloride channel, mechanosensitive channel of small conductance, or MscS, which also contains the GXXXG membrane spanning motifs. Both channel structures were found to possess similar pore lining residues (Kim et al., 2004). The authors also proposed that the first positively charged residue of the channel, Lys-33, may be responsible for pore selectivity (Kim et al., 2004). Despite these efforts, high resolution structural analysis will be required to fully understand VacA pore formation.

Since VacA does not have any sequence similarity to any other protein toxin of known structure, it is essential that a high-resolution structure of both soluble and membrane inserted VacA be determined in order to begin to understand the mechanism by which VacA undergoes the transition in order to infect cells. Here we report the structure of a VacA dodecamer at 10 Å resolution, determined by single particle cryo-EM.

Materials and Methods

Expression and Purification of VacA. H. pylori strain 60190 expressing VacA s1/i1/m1 has been previously described (McClain et al., 2001b). The strain was grown in Brucella broth supplemented with cholesterol and VacA oligomers

were isolated as previously described (Cover et al., 1997; Jimenez-Soto et al., 2012).

Specimen Preparation for Cryo-EM Analysis. VacA s1/i1/m1 was prepared as described above and diluted to 75-85 μg/mL in 10 mM HEPES pH 7.2 and 100 mM potassium chloride (KCl). Cryo-EM grids were prepared using a Mark II/III Vitrobot (FEI) at 25°C and 60% humidity. Sample was applied (2-3 μL) to a glow discharged Quantifoil R2/1 400 mesh grid (EMS) and blotted for 2-3 seconds prior plunging in liquid ethane cooled by liquid nitrogen.

Image Acquisition. Images were taken on a Tecnai F30 Polara (FEI) operating at an acceleration voltage of 300kV and at magnification of 40,109x. Images were recorded using a Gatan K2 Summit Direct Electron Detector (DED) with a pixel size of 0.624. Images were acquired using super-resolution mode, and dose fractionated to 40 frames for a total of eight seconds, 0.25 seconds/frame, with a dose rate of 2.5 e^-/pix/sec or 5 e^-/pix/sec. Images were collected using a defocus range of -1.5 to -4.0 μm. Digital Micrograph (Gatan, Inc.) was used for data collection. VacA exhibited preferential orientations in ice, therefore, a subset of images (1,004) were taken at a tilt angle of 10° to increase particle views.

Data Processing. Motion correction was performed with Motioncor2 (Zheng, 2016). A total number of 5,780 images were taken and CTF estimations on whole micrographs were determined using Gctf to assess micrograph quality (Zhang, 2016). A total number of 210,641 particles were manually selected using RELION 1.4 followed by autopicking using Gautomatch (developed by Dr. Kai Zhang, Cambridge, UK) without a reference stack applied. After multiple rounds of 2D classification were performed (particles further binned by 4 at this stage), 126,239 particles were subjected to 3D classification without symmetry applied

followed by two rounds of classification with D6 symmetry applied. The major class was identified, with 21,655 particles, and subjected to refinement with a final resolution of ~10 Å according to the gold standard FSC (Fig. 4-1). Surface rendering of the reconstructions were performed using the program Chimera (Pettersen et al., 2004).

Results and Discussion

This work details the highest resolution structure of a VacA oligomer to date. Utilizing the advancements made in cryo-EM with the direct electron detector and improved data processing programs, the structure of a VacA dodecamer presented here has reached ~10 Å resolution.

Data analysis reveals that VacA is found in multiple orientations in vitrified ice (Fig. 4-2). The first round of 2D classification indicates that the sample is heterogeneous, as expected, with hexamers, heptamers, dodecamers, and tetradecamers. 'Junk' classes were removed and resulting particles were subjected to three more rounds of 2D classification. The final round of 2D classification exhibited misaligning of particles and also revealed a more limitednumber of views than expected (Fig. 4-3). 3D classification was then performed without symmetry applied and classes were not well resolved. Classes that appeared to be heptamers or tetradecamers were removed and symmetry was applied to the remaining rounds of classification. Once symmetry was applied, the resolution did improve; however, the structure did not reach below 10 Å

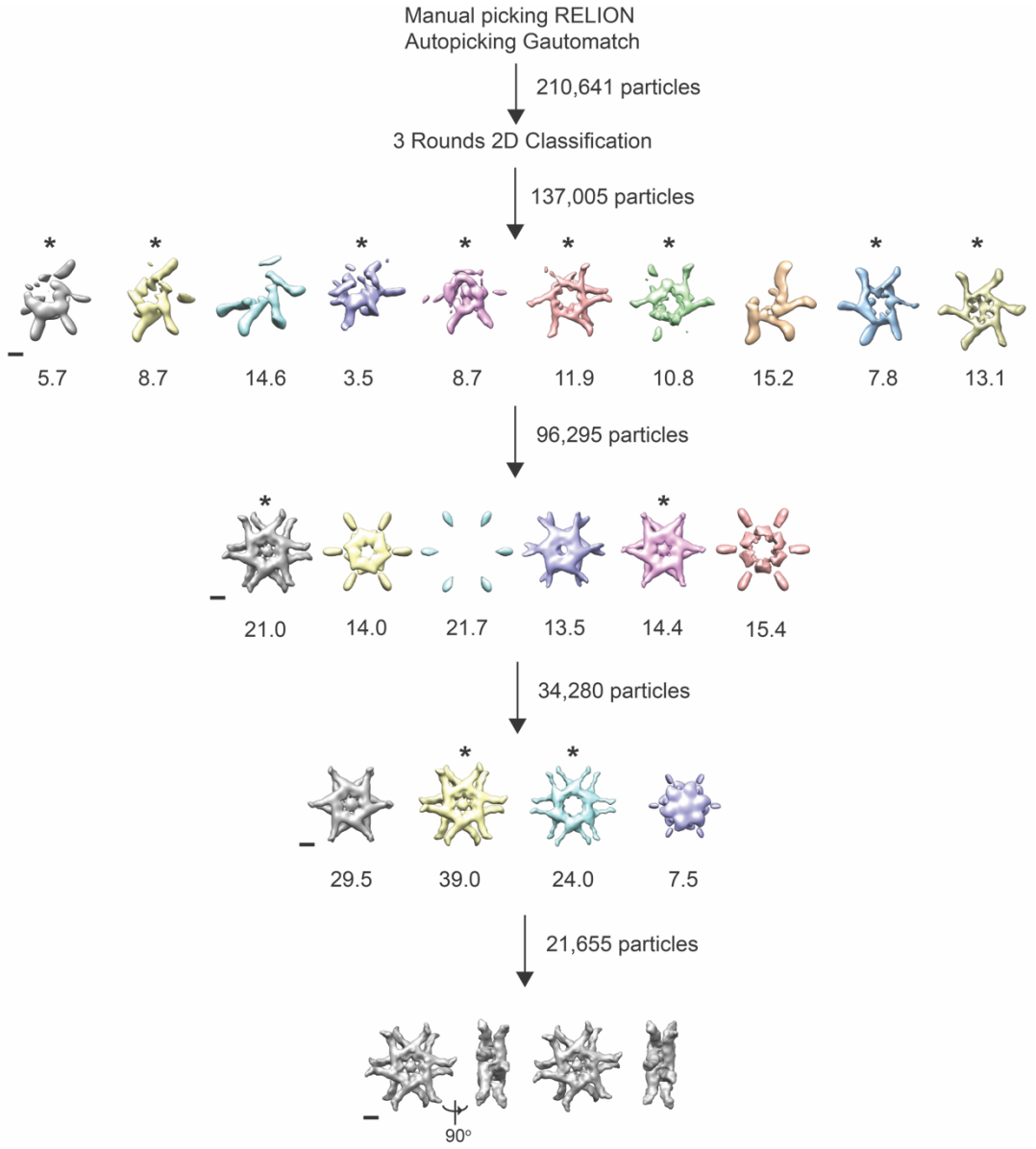

Figure 4-1: Data processing schematic. After 2D classification completed, the data were subjected to three rounds of 3D classification and then a final refinement step on a VacA s1/i1/m1 dodecamer with D6 symmetry applied. Numbers below structures represent percent of total number of particles.

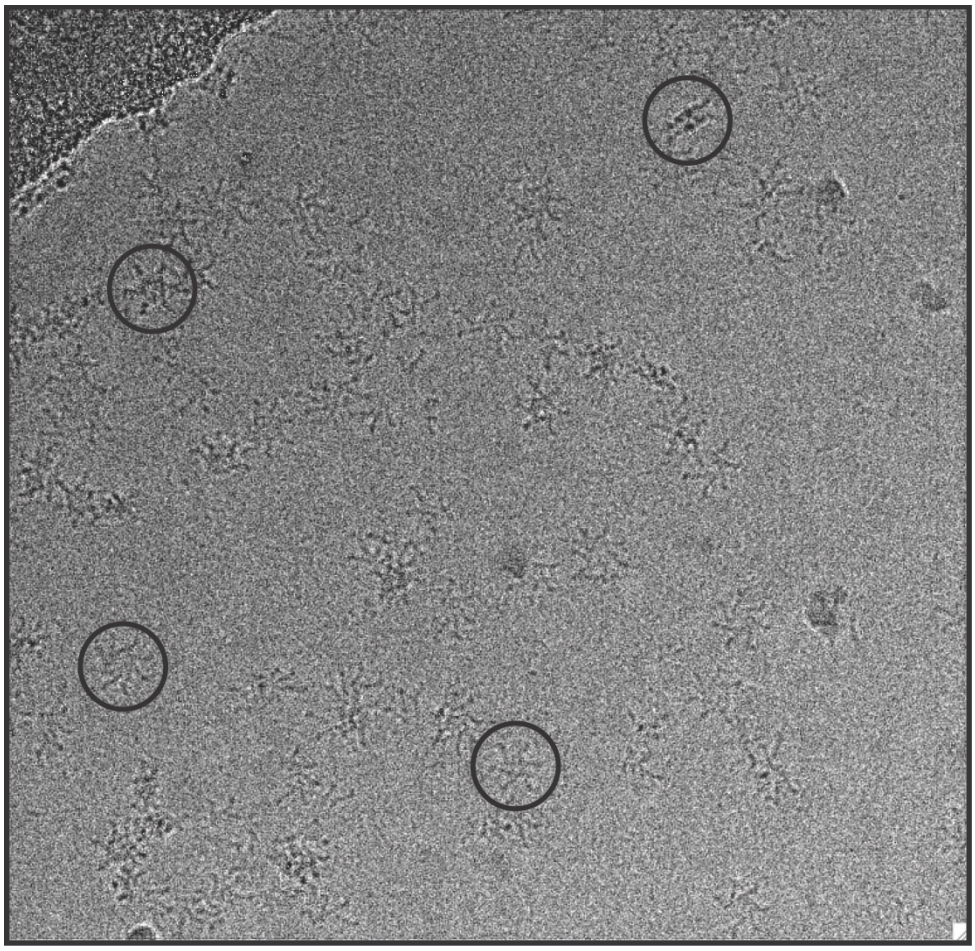

Figure 4-2: Representative vitrified ice image of VacA s1/i1/m1. Circled particles represent different oligomeric forms and views.

resolution (Fig. 4-1 and 4-4A). Despite taking a subset of micrographs at a 10° tilt angle to improve particle orientations, the angular distribution shows there is a strong preference for front face views of the particles (Fig. 4-4B). Resolution could be hindered due to the heterogeneity of the sample. Initial analysis should be performed without symmetry applied, but this could potentially require a much larger number of particles.

Further analysis and refinements need to be performed in order to improve the current resolution. Unfortunately, with VacA, a resolution of ~8 Å will be required to see the alpha helices postulated to comprise the p33 domain and in order to identify the beta helix within the p55 domain, a resolution of ~4 Å is necessary. Therefore, in order to understand how VacA oligomerizes and double-layer formation occurs a resolution of <4 Å needs to be achieved.

Improvements can be made in resolution for the VacA dodecamer. As mentioned, over 200,000 particles have been selected from 5,780 micrographs. After the first round of 3D classification, a D6 symmetry was applied to particles from the selected classes. There are two complications with this – 1) since the resolution was low for round one (~20 Å), there may have been seven sided oligomers and 2) there were particles present that are six-sided single-layer oligomers as well that do not possess D6 symmetry (Fig. 4-1, first round of 3D classification, last class). Applying symmetry at this stage could be hindering resolution. Therefore, future efforts should not apply symmetry until the 3D refinement step. Ideally, multiple rounds of 3D classification should separate different oligomeric forms, then the appropriate symmetry can be applied.

Once the above steps have been taken to improve the quality and resolution of the dataset, masking can be performed to refine the central region of

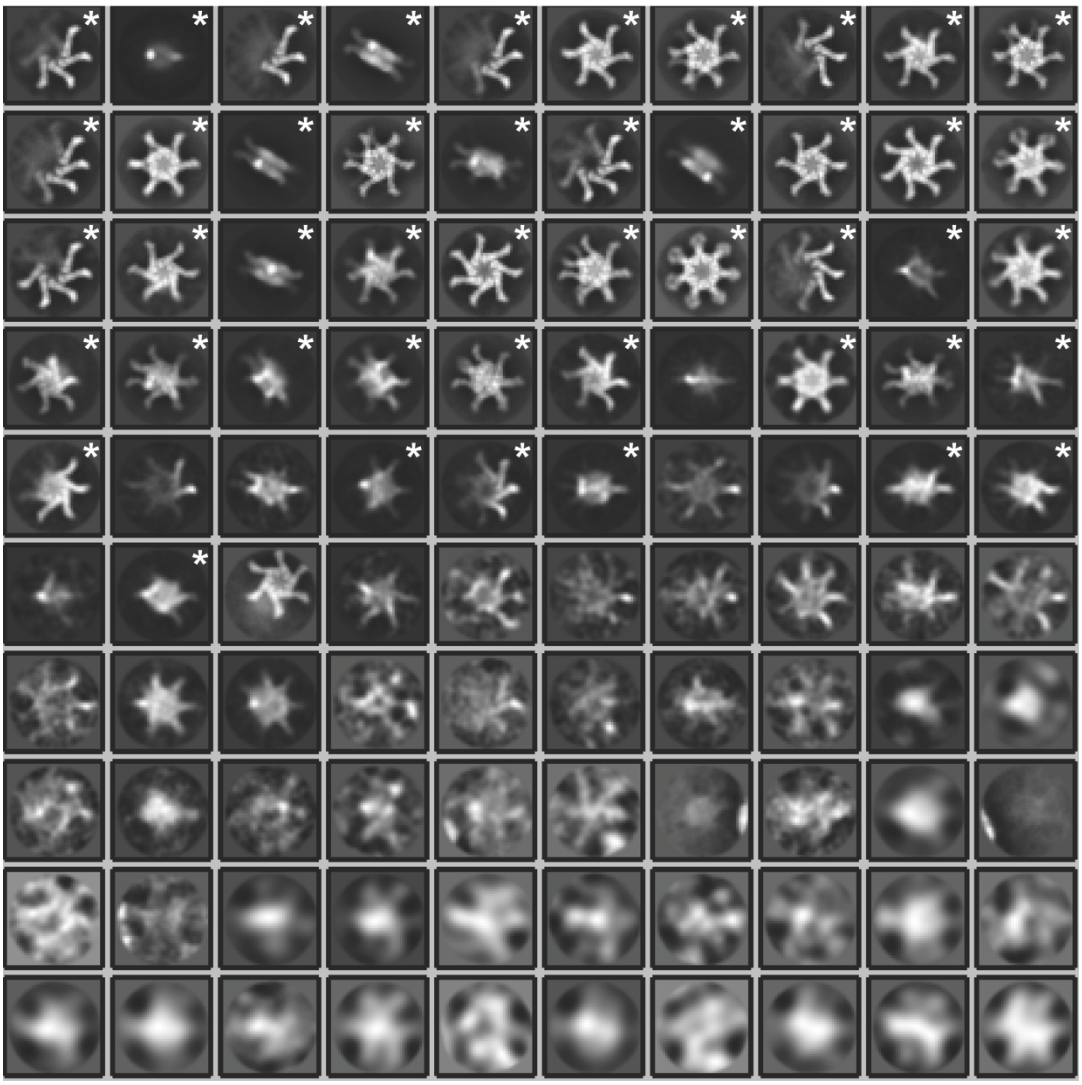

Figure 4-3: 2D classification performed in RELION. Classification shows the sample is heterogeneous. Classes are sorted based on distribution, with the first class containing the highest number of particles. Particles from * classes saved and subjected to 3D classification. Side length of panel, 39.9 nm.

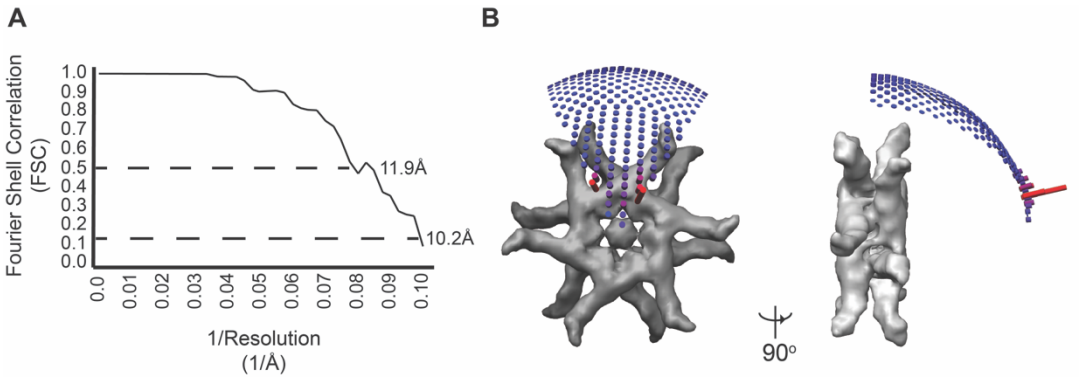

Figure 4-4: VacA s1i1/m1 resolution is ~10 Å. A) FSC curve showing resolution. At FSC of 0.5, the resolution is ~12 Å and at the gold standard FSC of 0.143 the resolution is ~10 Å. B) Angular distribution shows preference for front face views of particles.

the oligomer. Masking has been shown to optimize resolution by focusing on a region of interest and performing a classification solely on this region to obtain the most homogeneous population (for example - (Galej et al., 2016)). In the case of VacA, the arms of the oligomers should be masked so that only the central region is aligned.

There are other EM processing programs that may be better suited for this dataset. For example, FREALIGN and SPARX have both been utilized to determine high resolution structures by cryo-EM (Bartesaghi et al., 2014; von der Ecken et al., 2015). If after each of these steps has been performed and different programs utilized and the resolution has not significantly increased, a larger dataset will need to be collected. The sample may be more heterogeneous than expected. Also, even with the improvements to data processing, it appears to still be difficult to identify whether the side views of the oligomers are six-sided or seven-sided oligomers. A larger dataset consisting of ~500,000 particles should be collected and the methods described here should be performed.

CHAPTER V

DISCUSSION AND FUTURE DIRECTIONS

Discussion

This work details the structural analysis of the pore-forming toxin VacA of *H. pylori*. Chapter II focuses on structural characterization of VacA s1/i1/m1 along with three other mutants, s2/i1/m1, Δ6-27, and Δ301-328. Using RCT negative stain EM, the work detailed ~15 Å resolution structures of each oligomeric form. Chapter III describes the membrane bound and inserted form of VacA, making advancements toward optimal conditions for high resolution structural work of a VacA pore. Chapter IV details the highest resolution structure of a soluble VacA oligomer to date at ~10 Å due to the advancements of image acquisition and processing techniques.

A major question surrounding VacA structure has been whether each oligomeric form is responsible for pore formation and how pore formation occurs. To date, there are three major models for VacA oligomerization and pore formation (Fig. 5-1), which are similar to proposed models for other PFTs (Figs. 1-4 and 1-5). The first model posits that VacA binds to membrane as a monomer then inserts. Next, oligomerization occurs followed by pore formation (Fig. 5-1A). The second model posits that VacA first binds as a monomer and oligomerization and insertion occur concomitantly with a final step of pore formation (Fig. 5-1B). The final model proposes that VacA binds as a monomer then oligomerizes on the membrane. The next step is oligomer insertion and prior to pore formation (Fig. 5-1C). Multiple studies have investigated how VacA binds to membrane

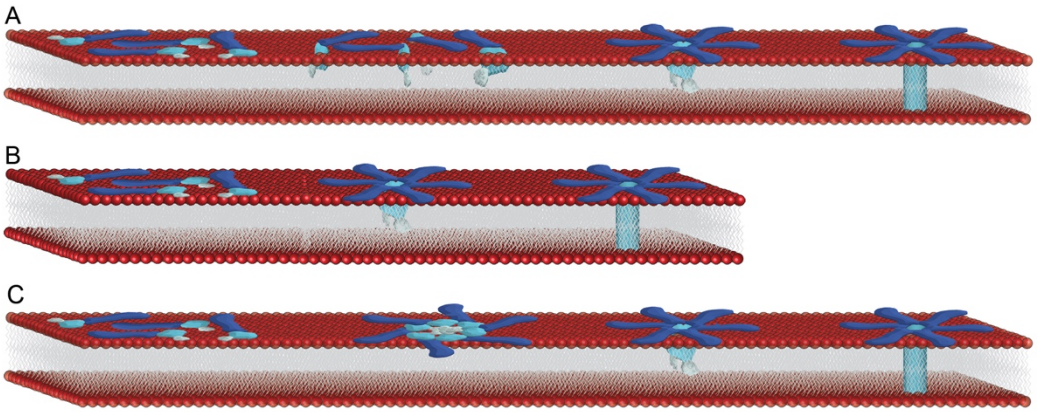

Figure 5-1: Models for VacA oligomerization and pore formation. A) Model one proposes monomer binding, insertion, oligomerization, then pore formation. B) Model two proposes that VacA binds as a monomer followed by concomitant oligomerization and membrane insertion and finally proe formation. C) Model three shows VacA monomer binding followed by oligomerization on the membrane. Next, the oligomer inserts into the membrane and the pore is formed.

(Atherton et al., 1995; Czajkowsky et al., 1999; Iwamoto et al., 1999; Pagliaccia et al., 1998; Pyburn et al., 2016; Rhead et al., 2007; Szabo et al., 1999; Tombola et al., 1999b). VacA applied to supported lipid bilayers combine with AFM strongly suggested that VacA bound to the bilayers as a single-layer hexamer (Czajkowsky et al., 1999). More recently, it was found that when applied to large unilamellar vesicles (LUVs), VacA bound to the LUVs as a single-layer hexamer and further analysis showed that it was inserted into the lipid bilayer (Pyburn et al., 2016). However, despite efforts to investigate the pore-forming domain of VacA, high resolution structural information is still unavailable.

Previous reports have indicated that the toxin has a strong preference for lipid raft lipids (Geisse et al., 2004; Gupta et al., 2008; Gupta et al., 2010; Kuo and Wang, 2003; Nakayama et al., 2006; Patel et al., 2002). Chapter III reports that VacA binds to multiple sets of lipid compositions which has been previously demonstrated using planar lipid bilayers experiments with atomic force microscopy (Geisse et al., 2004; Pyburn et al., 2016). The AFM study also showed that even when raft lipids sphingomyelin and cholesterol are present, VacA preferentially binds negatively charged phospholipids, namely phosphatidylserine (PS) (Geisse et al., 2004). In agreement with this data, Fig. 3-2A shows a significant difference in binding when PS is present. Interestingly, binding was also elevated in the presence of cholesterol despite previous reports suggesting VacA does not directly interact with cholesterol (Patel et al., 2002). Surprisingly, the presence of sphingomyelin alone in the absence of cholesterol, exhibited the least binding. One potential explanation for the differences in binding is the use of artificial membranes versus biological membranes. Biological membranes may have a lipid dispersion more suited to VacA targeting and binding lipid raft domains.

VacA s2/i1/m1 showed a similar binding profile to s1/i1/m1 to lipid compositions tested in Chapter III (Fig. 3-10A) and inserted into the membrane according to sodium carbonate extraction experiments (Fig. 3-10B). The data suggest that membrane binding and insertion may not result in the reduced virulence exhibited by this variant. It may be possible that the 12 amino acid extension causes an altered pore to be formed, leading to reduced channel activity. Another possibility is that the intermediate and middle regions play a larger role in membrane binding and insertion and therefore variants with the i1 and m2 should be investigated.

Data in Chapter III strongly suggests that VacA binds to membrane as a monomer, inserts into membrane and oligomerizes followed by pore formation (Fig. 5-1A). This mode of pore formation is similar to that of FraC and the proposed model for colicin A, both of which are α-PFTs. Both models suggest a hypothetical pre-pore intermediate where the oligomer is bound on the membrane surface but has not yet inserted. A high-resolution structure of VacA bound to and inserted into the liposomes could verify whether a pore has formed or if an intermediate structure where part of the toxin is inserted has been created.

Future Directions

Investigating VacA oligomerization. The efforts toward a high-resolution structure of a soluble VacA oligomer are ongoing. Currently, the structure of residues 355-811 have been showed to compose a beta helix with a globular domain at the C-terminus. However, the remainder of the p55 domain has not been mapped and a structure of the pore-forming p33 domain has not been determined (Gangwer et al., 2007; Gonzalez-Rivera et al., 2016). How oligomerization into single-layer oligomers occurs and how double-layer formation occurs remain unknown and high-resolution structural analysis can begin to

answer these questions. Currently, cryo-EM analysis is being performed. As mentioned in Chapter IV, 3D classification is currently being revisited without applying symmetry. Another step to be taken is processing the dataset using different programs that are available for cryo-EM. Currently, RELION 1.4 is being utilized to classify and refine the data. A good technique during structure determination is to compare outputs from multiple programs. Both FREALIGN and SPARX (part of the newly developed SPHIRE) are software packages that should be explored for structure determination as each software package uses different algorithms (Grigorieff, 2007, 2016; Hohn et al., 2007). Recently, a newer version of RELION, RELION 2.0, has also been released. These differences could be critical when attempting to determine the highest resolution structure.

Investigating the VacA pore. The work presented in Chapter III has set the stage for determining a high-resolution structure of membrane inserted VacA. Lipid conditions have been determined that not only promote VacA insertion into membrane but has been previously been shown to promote active channel formation (Fig. 5-1A-D) (Czajkowsky et al., 1999; Iwamoto et al., 1999). Unfortunately, VacA inserted into LUVs would make structure determination by cryo-EM difficult. Negative stain analysis shows that VacA particles on LUVs are frequently close together and may be difficult to identify for selection as particles for classification (Fig. 5-2A-D). Three main methods of determining high resolution structures of membrane proteins today via cryo-EM are detergent micelles, amphipols and nanodiscs (Bokori-Brown et al., 2016; Gatsogiannis et al., 2016; Huynh et al., 2014).

Nanodisc technology utilizes a membrane scaffold protein (MSP) to act as a ‘belt’ around a lipid bilayer (Schuler et al., 2013). These discs range in size from 13-17 nm in diameter, depending on the MSP truncation. Inconsistent disc sizes of

nanodiscs can occur which would negatively affect data processing, making it more difficult. Also, initial experiments suggest that the diameter is too small to fit a VacA hexamer which has a diameter of ~29 Å. Recently, larger nanodiscs have been created with diameters reaching 30 and 50 nm which are more consistent in size when prepared (Nasr et al., 2017). These nanodiscs should be prepared and tested for VacA binding. If VacA still does not bind to the nanodiscs well, the use of detergent micelles or amphipols should be explored to determine the structure of a VacA pore. First, VacA can be prepared as described using LUVs and then dialyzed against multiple detergents at different temperatures to determine optimal conditions. Similarly, different amphipols should be tested with VacA for optimal conditions (Fig. 5-2M-N).

It is possible that the two aforementioned methods do not work due to difficulties with acid activation of VacA in the presence of detergent. Also, when VacA is bound to LUVs there can be unbound double-layer oligomers as well as soluble hexamers present which can make particle selection and classification in cryo-EM difficult (Fig. 5-2A-D). Therefore, progress has been made using VacA bound to small unilamellar vesicles (SUVs) (Fig. 5-2G-H). It was found that using the same lipid conditions used with LUV experiments, only preparing vesicles with a diameter of ~50 nm, that one VacA hexamer bound per SUV. This may the most promising method and recently there have been great strides in computational methods to handle the difficulties that arise from membrane curvature (Jensen et al., 2016a; Jensen et al., 2016b; Wang and Sigworth, 2009, 2010). Great care will need to be taken, with any of these methods, to isolate membrane bound VacA from unbound VacA, such as size exclusion chromatography, or a large dataset will need to be taken by cryo-EM since it may be difficult to differentiate VacA

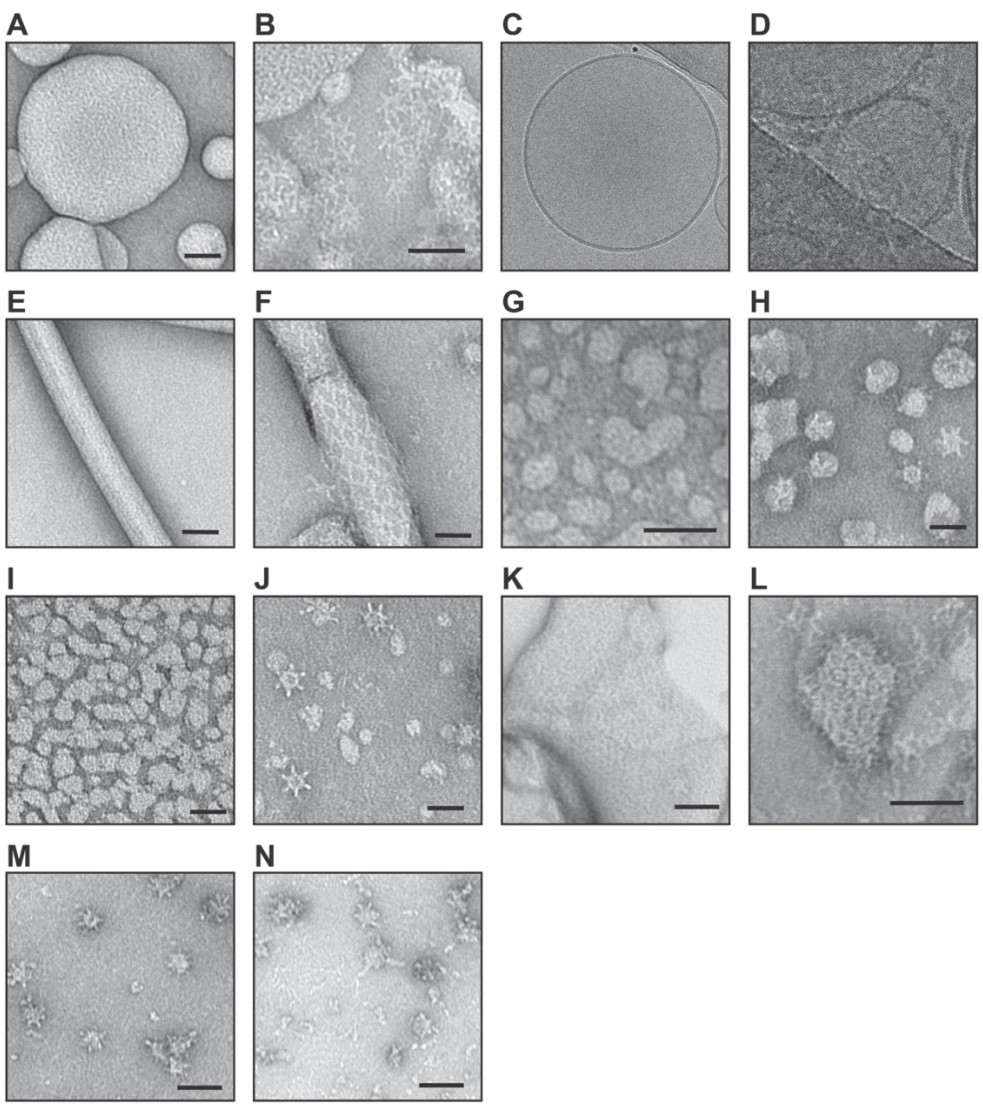

Figure 5-2. Efforts toward determining a high resolution structure of VacA bound to lipid. A) Negative stain image of LUVs comprised of ePC, DOPS, and cholesterol (55/15/30 mol%) in 10 mM HEPES pH 7.2 and 100 mM KCl. B) Negative stain image of VacA s1/i1/m1 bound to of ePC, DOPS, and cholesterol (55/15/30 mol%) LUVs at an LPR of 50:1. C) Image of ePC, DOPS, and cholesterol (55/15/30 mol%) LUVs in vitrified ice. D) Image of VacA s1/i1/m1 bound to ePC, DOPS, and cholesterol (55/15/30 mol%) LUVs in vitrified ice. E) Negative stain image of a lipid nanotube composed of ePC, DOPS, cholesterol, and GalCer (7.5/15/27.5/50 mol%). F) Negative stain image of VacA s1/i1/m1 bound to lipid nanotube. G) Negative stain image of ePC, DOPS, and cholesterol (55/15/30 mol%) SUVs. H) Negative stain image of Flag-tag VacA s1/i1/m1 bound to ePC, DOPS, and cholesterol (55/15/30 mol%) SUVs. I) Negative stain image of macrodiscs. J) Negative stain image of Flag-tag VacA s1/i1/m1 bound to macrodiscs. K) Negative stain image of 2D crystal of VacA s1/i1/m1. L) Negative stain image of 2D crystal of VacA s1/i1/m1. M) Negative stain image of neutral VacA s1/i1/m1 in A8-35. N) Negative stain image of acidified VacA s1/i1/m1 in A8-35.

bound liposomes (liposomes containing only a few VacA particles) from empty liposomes in vitrified ice. Also, if in the presence of detergent micelles or amphipols, it may be difficult to differentiate between soluble hexamers and hexamers in a pore formed state.

It is already known that VacA forms an anion channel, with a preference for choride ions (Adrian et al., 2002; Czajkowsky et al., 2005; Geisse et al., 2004; Tombola et al., 1999a). It has been demonstrated that when applied to LUVs, VacA s1/i1/m1, s2/i1/m1, and ∆6-27 are inserted into the membrane (Pyburn et al., 2016). Unfortunately, while the assay shows VacA was inserted, the technique limited the ability to determine if an active pore had formed. Therefore, a biochemical assay using a fluorescent chloride ion indicator, such as calcein, in conjunction with the LUV composition utilized in Chapter III could be applied to determine if each VacA mutant/variant has created a functional pore under these conditions. High resolution structural analysis would greatly complement these studies.

Computational modeling of the VacA pore suggested that Lys-33 was responsible for the anionic selectivity. In order to determine if this residue is responsible, mutating the residue to an alanine and performing planar lipid bilayer experiments could determine if the selectivity has been diminished. If anion selectivity has been altered with the mutation, this mutant should be applied to cells and tested for changes in cellular effects. The mutant should also be visualized by negative stain to assess if there are any differences in overall oligomer structure.

Understanding s2/i2/m2 virulence. In order to better understand why VacA s2/i1/m1 vacuolates cells less efficiently and why the s2/i2/m2 containing strain is less virulent than s1/i1/m1, high resolution structure determination of both soluble

and pore formed state of VacA s2/i1/m1 will be crucial to understand the differences. Potential explanations for the differences are 1) does s2/i1/m1 form incomplete pores due to the 12 amino acid hydrophilic extension at the N-terminus? 2) is s2/i2/m2 trafficked differently leading to the slow progression of vacuolation? 3) are there fewer receptors found on gastric epithelial cells that will bind to s2/i2/m2? It would be interesting to test lipid binding and insertion using the i2 and m2 forms of VacA to see if there are differences when compared to their i1 and m1 counterparts. Results of the aforementioned biochemical analysis could support the hypothesis that the s2/i1/m1 variant vacuolates less efficiently due to the formation of an altered pore. There are current studies investigating VacA trafficking using both VacA s1/i1/m1 and s2/i1/m1. Since the intermediate region has been proposed to be a major determinant of VacA virulence and the middle region is involved in receptor specificity, chimeras should be created to identify differences in intoxication and trafficking (Gonzalez-Rivera et al., 2012; Pagliaccia et al., 1998; Rhead et al., 2007). Results would aid in better understanding of VacA virulence.

VacA as a drug target. Lastly, since VacA is present in all strains of *H. pylori,* it would be beneficial to target this toxin to prevent its cellular effects. Pore-forming toxins have recently become targets to develop therapeutics. For example, oroxylin A inhibits hemolytic acitivity of haemolysin A (Dong et al., 2013). DNA aptamers have been utilized in order to inhibit the action of α-toxin, and thus used to treat *S. aureus* infection (Vivekananda et al., 2014). Inhibitors of glycosylphosphatidylinositols (GPIs) have been suggested as targets to inhibit pore-formation by aerolysins (Wu and Guo, 2010). Chloride channels have also been targeted for drug development. For example, a well known chloride channel, the cystic fibrosis transmembrane conductance regulator (CFTR), was subjected

to small molecule screening which revealed two types of potential inhibitors (Verkman and Galietta, 2009). One inhibitor blocks channel function by interactions with a key residue at one end of the pore (Taddei et al., 2004). Potentially, this idea could be applied to Lys-33 of VacA. If mutational analysis of this residue reveals altered channel activity, small molecule screening could be performed to identify potential channel blockers.

Once high resolution structures have been determined, potential inhibitors of pore-formation or oligomerization can begin to be investigated for therapeutics. Due to the increasing antibiotic resistance, developing a drug that would target this pore-forming toxin specifically would be essential in eradicating the infection.

LIST OF PUBLICATIONS

1. Takizawa, Y., Binshtein, E., Erwin, A.L., **Pyburn, T.M.**, Mittendorf, K.F., and Ohi, M.D. (2016). While the revolution will not be crystallized, biochemistry reigns supreme. *Protein Sci.* Sep 27. doi: 10.1002/pro.3054. Review.
2. Gonzalez-Rivera, C., Campbell, A., Rutherford, S.A., **Pyburn, T.M.,** Foegeding, N.J., Spiller, B., McClain, M.S., Ohi, M.D., Lacy, D.B., and Cover, T.L. (2016). A non-oligomerizing mutant form of *Helicobacter pylori* VacA allows structural analysis of the p33 domain. *Infection and Immunity*. 84(9):2662-70. doi: 10.1128/IAI.00254-16.
3. **Pyburn, T.M.,** Foegeding, N.J., Gonzalez-Rivera, C., McDonald, N.A., Gould, K.L., Cover, T.L., and Ohi, M.D. (2016) Structural organization of membrane-inserted hexamers formed by *Helicobacter pylori* VacA toxin. *MBio*. 7(1):e02001-15. doi: 10.1128/mBio.02001-15.

   ***Article featured on the cover of the journal**
4. Frick-Cheng, A.E., **Pyburn, T.M.**, Voss, B.J., McDonald, W.H., Ohi, M.D., and Cover, T.L. (2016). Molecular and Structural Analysis of the *Helicobacter pylori cag* Type IV Secretion System Core Complex. *mBio*. doi:10.1128/mBio.02001-15.

   ***Featured in F1000 Prime as a recommended article to read**
5. Chambers, M.G.*, **Pyburn, T.M**.*, Gonzalez-Rivera, C., Collier, S.E., Eli, I., Yip, C.K., Takizawa, Y., Lacy, D.B., Cover, T.L., and Ohi, M.D. (2013). Structural analysis of the oligomeric states of *Helicobacter pylori* VacA toxin. *Journal of Molecular Biology*. *425*, 524-535. doi: 10.1016/j.jmb.2012.11.020. ***authors contributed equally to this work.**

BIBLIOGRAPHY

Abeyrathne, P.D., Chami, M., Pantelic, R.S., Goldie, K.N., and Stahlberg, H. (2010). Preparation of 2D crystals of membrane proteins for high-resolution electron crystallography data collection. Methods Enzymol *481*, 25-43.

Adrian, M., Cover, T.L., Dubochet, J., and Heuser, J.E. (2002). Multiple oligomeric states of the Helicobacter pylori vacuolating toxin demonstrated by cryo-electron microscopy. Journal of molecular biology *318*, 121-133.

Akopyants, N.S., Clifton, S.W., Kersulyte, D., Crabtree, J.E., Youree, B.E., Reece, C.A., Bukanov, N.O., Drazek, E.S., Roe, B.A., and Berg, D.E. (1998). Analyses of the cag pathogenicity island of Helicobacter pylori. Molecular microbiology *28*, 37-53.

Aloush, V., Navon-Venezia, S., Seigman-Igra, Y., Cabili, S., and Carmeli, Y. (2006). Multidrug-resistant Pseudomonas aeruginosa: risk factors and clinical impact. Antimicrobial agents and chemotherapy *50*, 43-48.

Aly, K.A., and Baron, C. (2007). The VirB5 protein localizes to the T-pilus tips in Agrobacterium tumefaciens. Microbiology *153*, 3766-3775.

Amieva, M.R., and El-Omar, E.M. (2008). Host-bacterial interactions in Helicobacter pylori infection. Gastroenterology *134*, 306-323.

Amieva, M.R., Vogelmann, R., Covacci, A., Tompkins, L.S., Nelson, W.J., and Falkow, S. (2003). Disruption of the epithelial apical-junctional complex by Helicobacter pylori CagA. Science *300*, 1430-1434.

Anonymous (1994). Schistosomes, liver flukes and Helicobacter pylori. IARC Working Group on the Evaluation of Carcinogenic Risks to Humans. Lyon, 7-14 June 1994. IARC monographs on the evaluation of carcinogenic risks to humans *61*, 1-241.

Atherton, J.C. (2006). The pathogenesis of Helicobacter pylori-induced gastro-duodenal diseases. Annu Rev Pathol *1*, 63-96.

Atherton, J.C., and Blaser, M.J. (2009). Coadaptation of Helicobacter pylori and humans: ancient history, modern implications. The Journal of clinical investigation *119*, 2475-2487.

Atherton, J.C., Cao, P., Peek, R.M., Jr., Tummuru, M.K., Blaser, M.J., and Cover, T.L. (1995). Mosaicism in vacuolating cytotoxin alleles of Helicobacter pylori. Association of specific vacA types with cytotoxin production and peptic ulceration. The Journal of biological chemistry *270*, 17771-17777.

Bagnoli, F., Buti, L., Tompkins, L., Covacci, A., and Amieva, M.R. (2005). Helicobacter pylori CagA induces a transition from polarized to invasive phenotypes in MDCK cells. Proceedings of the National Academy of Sciences of the United States of America *102*, 16339-16344.

Bartesaghi, A., Matthies, D., Banerjee, S., Merk, A., and Subramaniam, S. (2014). Structure of beta-galactosidase at 3.2-A resolution obtained by cryo-electron microscopy. Proceedings of the National Academy of Sciences of the United States of America *111*, 11709-11714.

Bass, R.B., Strop, P., Barclay, M., and Rees, D.C. (2002). Crystal structure of Escherichia coli MscS, a voltage-modulated and mechanosensitive channel. Science *298*, 1582-1587.

Bernard, S.C., Simpson, N., Join-Lambert, O., Federici, C., Laran-Chich, M.P., Maissa, N., Bouzinba-Segard, H., Morand, P.C., Chretien, F., Taouji, S*., et al.* (2014). Pathogenic Neisseria meningitidis utilizes CD147 for vascular colonization. Nat Med *20*, 725-731.

Berry, J.L., and Pelicic, V. (2015). Exceptionally widespread nanomachines composed of type IV pilins: the prokaryotic Swiss Army knives. FEMS Microbiol Rev *39*, 134-154.

Blaser, M.J., Perez-Perez, G.I., Kleanthous, H., Cover, T.L., Peek, R.M., Chyou, P.H., Stemmermann, G.N., and Nomura, A. (1995). Infection with Helicobacter pylori strains possessing cagA is associated with an increased risk of developing adenocarcinoma of the stomach. Cancer research *55*, 2111-2115.

Bokori-Brown, M., Martin, T.G., Naylor, C.E., Basak, A.K., Titball, R.W., and Savva, C.G. (2016). Cryo-EM structure of lysenin pore elucidates membrane insertion by an aerolysin family protein. Nat Commun *7*, 11293.

Boncristiano, M., Paccani, S.R., Barone, S., Ulivieri, C., Patrussi, L., Ilver, D., Amedei, A., D'Elios, M.M., Telford, J.L., and Baldari, C.T. (2003). The Helicobacter pylori vacuolating toxin inhibits T cell activation by two independent mechanisms. The Journal of experimental medicine *198*, 1887-1897.

Boquet, P., and Pappenheimer, A.M., Jr. (1976). Interaction of diphtheria toxin with mammalian cell membranes. The Journal of biological chemistry *251*, 5770-5778.

Boquet, P., and Ricci, V. (2012). Intoxication strategy of Helicobacter pylori VacA toxin. Trends in microbiology *20*, 165-174.

Brandt, S., Kwok, T., Hartig, R., Konig, W., and Backert, S. (2005). NF-kappaB activation and potentiation of proinflammatory responses by the Helicobacter pylori CagA protein. Proceedings of the National Academy of Sciences of the United States of America *102*, 9300-9305.

Brandt, S., Shafikhani, S., Balachandran, P., Jin, S., Hartig, R., Konig, W., Engel, J., and Backert, S. (2007). Use of a novel coinfection system reveals a role for Rac1, H-Ras, and CrkII phosphorylation in Helicobacter pylori-induced host cell actin cytoskeletal rearrangements. FEMS immunology and medical microbiology *50*, 190-205.

Brown, L.M. (2000). Helicobacter pylori: epidemiology and routes of transmission. Epidemiol Rev *22*, 283-297.

Bui, D., Brown, H.E., Harris, R.B., and Oren, E. (2016). Serologic Evidence for Fecal-Oral Transmission of Helicobacter pylori. Am J Trop Med Hyg *94*, 82-88.

Burroni, D., Lupetti, P., Pagliaccia, C., Reyrat, J.M., Dallai, R., Rappuoli, R., and Telford, J.L. (1998). Deletion of the major proteolytic site of the Helicobacter pylori cytotoxin does not influence toxin activity but favors assembly of the toxin into hexameric structures. Infection and immunity *66*, 5547-5550.

Calore, F., Genisset, C., Casellato, A., Rossato, M., Codolo, G., Esposti, M.D., Scorrano, L., and de Bernard, M. (2010a). Endosome-mitochondria juxtaposition during apoptosis induced by H. pylori VacA. Cell Death Differ *17*, 1707-1716.

Calore, F., Genisset, C., Casellato, A., Rossato, M., Codolo, G., Esposti, M.D., Scorrano, L., and de Bernard, M. (2010b). Endosome-mitochondria juxtaposition during apoptosis induced by H. pylori VacA. Cell Death Differ *17*, 1707-1716.

Campello, S., Tombola, F., Cabrini, G., and Zoratti, M. (2002). The vacuolating toxin of Helicobacter pylori mimicks the CFTR-mediated chloride conductance. FEBS letters *532*, 237-240.

Capitani, G., Eidam, O., Glockshuber, R., and Grutter, M.G. (2006). Structural and functional insights into the assembly of type 1 pili from Escherichia coli. Microbes Infect *8*, 2284-2290.

Censini, S., Lange, C., Xiang, Z., Crabtree, J.E., Ghiara, P., Borodovsky, M., Rappuoli, R., and Covacci, A. (1996). cag, a pathogenicity island of Helicobacter pylori, encodes type I-specific and disease-associated virulence factors. Proceedings of the National Academy of Sciences of the United States of America *93*, 14648-14653.

Chambers, M.G., Pyburn, T.M., Gonzalez-Rivera, C., Collier, S.E., Eli, I., Yip, C.K., Takizawa, Y., Lacy, D.B., Cover, T.L., and Ohi, M.D. (2013). Structural analysis of the oligomeric states of Helicobacter pylori VacA toxin. Journal of molecular biology *425*, 524-535.

Chang, Y.J., Wu, M.S., Lin, J.T., Pestell, R.G., Blaser, M.J., and Chen, C.C. (2006). Mechanisms for Helicobacter pylori CagA-induced cyclin D1 expression that affect cell cycle. Cell Microbiol *8*, 1740-1752.

Cheng, Y., Wolf, E., Larvie, M., Zak, O., Aisen, P., Grigorieff, N., Harrison, S.C., and Walz, T. (2006). Single particle reconstructions of the transferrin-transferrin receptor complex obtained with different specimen preparation techniques. Journal of molecular biology *355*, 1048-1065.

Choe, S., Bennett, M.J., Fujii, G., Curmi, P.M., Kantardjieff, K.A., Collier, R.J., and Eisenberg, D. (1992). The crystal structure of diphtheria toxin. Nature *357*, 216-222.

Connell, I., Agace, W., Klemm, P., Schembri, M., Marild, S., and Svanborg, C. (1996). Type 1 fimbrial expression enhances Escherichia coli virulence for the urinary tract. Proceedings of the National Academy of Sciences of the United States of America *93*, 9827-9832.

Covacci, A., Censini, S., Bugnoli, M., Petracca, R., Burroni, D., Macchia, G., Massone, A., Papini, E., Xiang, Z., Figura, N.*, et al.* (1993). Molecular characterization of the 128-kDa immunodominant antigen of Helicobacter pylori associated with cytotoxicity and duodenal ulcer. Proceedings of the National Academy of Sciences of the United States of America *90*, 5791-5795.

Cover, T.L. (2016). Helicobacter pylori Diversity and Gastric Cancer Risk. mBio *7*, e01869-01815.

Cover, T.L., and Blanke, S.R. (2005). Helicobacter pylori VacA, a paradigm for toxin multifunctionality. Nature reviews Microbiology *3*, 320-332.

Cover, T.L., and Blaser, M.J. (2009). Helicobacter pylori in health and disease. Gastroenterology *136*, 1863-1873.

Cover, T.L., Hanson, P.I., and Heuser, J.E. (1997). Acid-induced dissociation of VacA, the Helicobacter pylori vacuolating cytotoxin, reveals its pattern of assembly. The Journal of cell biology *138*, 759-769.

Cover, T.L., Tummuru, M.K., Cao, P., Thompson, S.A., and Blaser, M.J. (1994). Divergence of genetic sequences for the vacuolating cytotoxin among Helicobacter pylori strains. The Journal of biological chemistry *269*, 10566-10573.

Crabtree, J.E., Taylor, J.D., Wyatt, J.I., Heatley, R.V., Shallcross, T.M., Tompkins, D.S., and Rathbone, B.J. (1991). Mucosal IgA recognition of Helicobacter pylori 120 kDa protein, peptic ulceration, and gastric pathology. Lancet *338*, 332-335.

Czajkowsky, D.M., Iwamoto, H., Cover, T.L., and Shao, Z. (1999). The vacuolating toxin from Helicobacter pylori forms hexameric pores in lipid bilayers at low pH. Proceedings of the National Academy of Sciences of the United States of America *96*, 2001-2006.

Czajkowsky, D.M., Iwamoto, H., Szabo, G., Cover, T.L., and Shao, Z. (2005). Mimicry of a host anion channel by a Helicobacter pylori pore-forming toxin. Biophysical journal *89*, 3093-3101.

Dal Peraro, M., and van der Goot, F.G. (2016). Pore-forming toxins: ancient, but never really out of fashion. Nature reviews Microbiology *14*, 77-92.

Dang, T.X., Farah, S.J., Gast, A., Robertson, C., Carragher, B., Egelman, E., and Wilson-Kubalek, E.M. (2005a). Helical crystallization on lipid nanotubes: streptavidin as a model protein. Journal of structural biology *150*, 90-99.

Dang, T.X., Milligan, R.A., Tweten, R.K., and Wilson-Kubalek, E.M. (2005b). Helical crystallization on nickel-lipid nanotubes: perfringolysin O as a model protein. Journal of structural biology *152*, 129-139.

de Bernard, M., Burroni, D., Papini, E., Rappuoli, R., Telford, J., and Montecucco, C. (1998). Identification of the Helicobacter pylori VacA toxin domain active in the cell cytosol. Infection and immunity *66*, 6014-6016.

de Bernard, M., Papini, E., de Filippis, V., Gottardi, E., Telford, J., Manetti, R., Fontana, A., Rappuoli, R., and Montecucco, C. (1995). Low pH activates the vacuolating toxin of Helicobacter pylori, which becomes acid and pepsin resistant. The Journal of biological chemistry *270*, 23937-23940.

de Martel, C., Ferlay, J., Franceschi, S., Vignat, J., Bray, F., Forman, D., and Plummer, M. (2012). Global burden of cancers attributable to infections in 2008: a review and synthetic analysis. Lancet Oncol *13*, 607-615.

De, S., and Olson, R. (2011). Crystal structure of the Vibrio cholerae cytolysin heptamer reveals common features among disparate pore-forming toxins. Proceedings of the National Academy of Sciences of the United States of America *108*, 7385-7390.

Debellis, L., Papini, E., Caroppo, R., Montecucco, C., and Curci, S. (2001). Helicobacter pylori cytotoxin VacA increases alkaline secretion in gastric epithelial cells. American journal of physiology Gastrointestinal and liver physiology *281*, G1440-1448.

Degiacomi, M.T., Iacovache, I., Pernot, L., Chami, M., Kudryashev, M., Stahlberg, H., van der Goot, F.G., and Dal Peraro, M. (2013). Molecular assembly of the aerolysin pore reveals a swirling membrane-insertion mechanism. Nat Chem Biol *9*, 623-629.

Desvaux, M., Parham, N.J., and Henderson, I.R. (2004). The autotransporter secretion system. Research in microbiology *155*, 53-60.

Domanska, G., Motz, C., Meinecke, M., Harsman, A., Papatheodorou, P., Reljic, B., Dian-Lothrop, E.A., Galmiche, A., Kepp, O., Becker, L.*, et al.* (2010). Helicobacter pylori VacA toxin/subunit p34: targeting of an anion channel to the inner mitochondrial membrane. PLoS pathogens *6*, e1000878.

Dong, J., Qiu, J., Zhang, Y., Lu, C., Dai, X., Wang, J., Li, H., Wang, X., Tan, W., Luo, M.*, et al.* (2013). Oroxylin A inhibits hemolysis via hindering the self-assembly of alpha-hemolysin heptameric transmembrane pore. PLoS Comput Biol *9*, e1002869.

Driscoll, J.A., Brody, S.L., and Kollef, M.H. (2007). The epidemiology, pathogenesis and treatment of Pseudomonas aeruginosa infections. Drugs *67*, 351-368.

El-Bez, C., Adrian, M., Dubochet, J., and Cover, T.L. (2005). High resolution structural analysis of Helicobacter pylori VacA toxin oligomers by cryo-negative staining electron microscopy. Journal of structural biology *151*, 215-228.

Eurosurveillance editorial, t. (2015). ECDC publishes 2014 surveillance data on antimicrobial resistance and antimicrobial consumption in Europe. Euro Surveill *20*.

Feil, S.C., Ascher, D.B., Kuiper, M.J., Tweten, R.K., and Parker, M.W. (2014). Structural studies of Streptococcus pyogenes streptolysin O provide insights into the early steps of membrane penetration. Journal of molecular biology *426*, 785-792.

Figueiredo, C., Machado, J.C., Pharoah, P., Seruca, R., Sousa, S., Carvalho, R., Capelinha, A.F., Quint, W., Caldas, C., van Doorn, L.J.*, et al.* (2002). Helicobacter pylori and interleukin 1 genotyping: an opportunity to identify high-risk individuals for gastric carcinoma. Journal of the National Cancer Institute *94*, 1680-1687.

Fischer, W., Gebert, B., and Haas, R. (2004). Novel activities of the Helicobacter pylori vacuolating cytotoxin: from epithelial cells towards the immune system. Int J Med Microbiol *293*, 539-547.

Foegeding, N.J., Caston, R.R., McClain, M.S., Ohi, M.D., and Cover, T.L. (2016). An Overview of Helicobacter pylori VacA Toxin Biology. Toxins *8*.

Fossati, M., Goud, B., Borgese, N., and Manneville, J.B. (2014). An investigation of the effect of membrane curvature on transmembrane-domain dependent protein sorting in lipid bilayers. Cell Logist *4*, e29087.

Franco, A.T., Israel, D.A., Washington, M.K., Krishna, U., Fox, J.G., Rogers, A.B., Neish, A.S., Collier-Hyams, L., Perez-Perez, G.I., Hatakeyama, M.*, et al.* (2005). Activation of beta-catenin by carcinogenic Helicobacter pylori. Proceedings of the National Academy of Sciences of the United States of America *102*, 10646-10651.

Frank, J., Radermacher, M., Penczek, P., Zhu, J., Li, Y., Ladjadj, M., and Leith, A. (1996). SPIDER and WEB: processing and visualization of images in 3D electron microscopy and related fields. Journal of structural biology *116*, 190-199.

Frick-Cheng, A.E., Pyburn, T.M., Voss, B.J., McDonald, W.H., Ohi, M.D., and Cover, T.L. (2016). Molecular and Structural Analysis of the Helicobacter pylori cag Type IV Secretion System Core Complex. mBio *7*, e02001-02015.

Fuchs, C.S., and Mayer, R.J. (1995). Gastric carcinoma. The New England journal of medicine *333*, 32-41.

Furthmayr, H., and Marchesi, V.T. (1976). Subunit structure of human erythrocyte glycophorin A. Biochemistry *15*, 1137-1144.

Galej, W.P., Wilkinson, M.E., Fica, S.M., Oubridge, C., Newman, A.J., and Nagai, K. (2016). Cryo-EM structure of the spliceosome immediately after branching. Nature *537*, 197-201.

Galmiche, A., Rassow, J., Doye, A., Cagnol, S., Chambard, J.C., Contamin, S., de Thillot, V., Just, I., Ricci, V., Solcia, E.*, et al.* (2000). The N-terminal 34 kDa fragment of Helicobacter pylori vacuolating cytotoxin targets mitochondria and induces cytochrome c release. The EMBO journal *19*, 6361-6370.

Gangwer, K.A., Mushrush, D.J., Stauff, D.L., Spiller, B., McClain, M.S., Cover, T.L., and Lacy, D.B. (2007). Crystal structure of the Helicobacter pylori vacuolating toxin p55 domain. Proceedings of the National Academy of Sciences of the United States of America *104*, 16293-16298.

Gangwer, K.A., Shaffer, C.L., Suerbaum, S., Lacy, D.B., Cover, T.L., and Bordenstein, S.R. (2010). Molecular evolution of the Helicobacter pylori vacuolating toxin gene vacA. Journal of bacteriology *192*, 6126-6135.

Gatsogiannis, C., Merino, F., Prumbaum, D., Roderer, D., Leidreiter, F., Meusch, D., and Raunser, S. (2016). Membrane insertion of a Tc toxin in near-atomic detail. Nature structural & molecular biology *23*, 884-890.

Gauthier, N.C., Monzo, P., Gonzalez, T., Doye, A., Oldani, A., Gounon, P., Ricci, V., Cormont, M., and Boquet, P. (2007). Early endosomes associated with dynamic F-actin structures are required for late trafficking of H. pylori VacA toxin. The Journal of cell biology *177*, 343-354.

Gauthier, N.C., Monzo, P., Kaddai, V., Doye, A., Ricci, V., and Boquet, P. (2005). Helicobacter pylori VacA cytotoxin: a probe for a clathrin-independent and Cdc42-dependent pinocytic pathway routed to late endosomes. Molecular biology of the cell *16*, 4852-4866.

Gauthier, N.C., Ricci, V., Gounon, P., Doye, A., Tauc, M., Poujeol, P., and Boquet, P. (2004). Glycosylphosphatidylinositol-anchored proteins and actin cytoskeleton modulate chloride transport by channels formed by the Helicobacter pylori vacuolating cytotoxin VacA in HeLa cells. The Journal of biological chemistry *279*, 9481-9489.

Gebert, B., Fischer, W., Weiss, E., Hoffmann, R., and Haas, R. (2003). Helicobacter pylori vacuolating cytotoxin inhibits T lymphocyte activation. Science *301*, 1099-1102.

Geisse, N.A., Cover, T.L., Henderson, R.M., and Edwardson, J.M. (2004). Targeting of Helicobacter pylori vacuolating toxin to lipid raft membrane domains analysed by atomic force microscopy. The Biochemical journal *381*, 911-917.

Genisset, C., Galeotti, C.L., Lupetti, P., Mercati, D., Skibinski, D.A., Barone, S., Battistutta, R., de Bernard, M., and Telford, J.L. (2006). A Helicobacter pylori vacuolating toxin mutant that fails to oligomerize has a dominant negative phenotype. Infection and immunity *74*, 1786-1794.

Genisset, C., Puhar, A., Calore, F., de Bernard, M., Dell'Antone, P., and Montecucco, C. (2007). The concerted action of the Helicobacter pylori cytotoxin VacA and of the v-ATPase proton pump induces swelling of isolated endosomes. Cell Microbiol *9*, 1481-1490.

Ghosh, P., Mel, S.F., and Stroud, R.M. (1994). The domain structure of the ion channel-forming protein colicin Ia. Nat Struct Biol *1*, 597-604.

Giltner, C.L., Nguyen, Y., and Burrows, L.L. (2012). Type IV pilin proteins: versatile molecular modules. Microbiol Mol Biol Rev *76*, 740-772.

Gonzalez-Rivera, C., Algood, H.M., Radin, J.N., McClain, M.S., and Cover, T.L. (2012). The intermediate region of Helicobacter pylori VacA is a determinant of toxin potency in a Jurkat T cell assay. Infection and immunity *80*, 2578-2588.

Gonzalez-Rivera, C., Campbell, A.M., Rutherford, S.A., Pyburn, T.M., Foegeding, N.J., Barke, T.L., Spiller, B.W., McClain, M.S., Ohi, M.D., Lacy, D.B.*, et al.* (2016). A Nonoligomerizing Mutant Form of Helicobacter pylori VacA Allows Structural Analysis of the p33 Domain. Infection and immunity *84*, 2662-2670.

Gonzalez-Rivera, C., Gangwer, K.A., McClain, M.S., Eli, I.M., Chambers, M.G., Ohi, M.D., Lacy, D.B., and Cover, T.L. (2010). Reconstitution of Helicobacter pylori VacA toxin from purified components. Biochemistry *49*, 5743-5752.

Greenfield, L.K., and Jones, N.L. (2013). Modulation of autophagy by Helicobacter pylori and its role in gastric carcinogenesis. Trends in microbiology *21*, 602-612.

Grigorieff, N. (2007). FREALIGN: high-resolution refinement of single particle structures. Journal of structural biology *157*, 117-125.

Grigorieff, N. (2016). Frealign: An Exploratory Tool for Single-Particle Cryo-EM. Methods Enzymol *579*, 191-226.

Gupta, V.R., Patel, H.K., Kostolansky, S.S., Ballivian, R.A., Eichberg, J., and Blanke, S.R. (2008). Sphingomyelin functions as a novel receptor for Helicobacter pylori VacA. PLoS pathogens *4*, e1000073.

Gupta, V.R., Wilson, B.A., and Blanke, S.R. (2010). Sphingomyelin is important for the cellular entry and intracellular localization of Helicobacter pylori VacA. Cell Microbiol *12*, 1517-1533.

Gwack, J., Shin, A., Kim, C.S., Ko, K.P., Kim, Y., Jun, J.K., Bae, J., Park, S.K., Hong, Y.C., Kang, D.*, et al.* (2006). CagA-producing Helicobacter pylori and increased risk of gastric cancer: a nested case-control study in Korea. Br J Cancer *95*, 639-641.

Hage, N., Howard, T., Phillips, C., Brassington, C., Overman, R., Debreczeni, J., Gellert, P., Stolnik, S., Winkler, G.S., and Falcone, F.H. (2015). Structural basis of Lewis(b) antigen binding by the Helicobacter pylori adhesin BabA. Sci Adv *1*, e1500315.

Hasler, L., Heymann, J.B., Engel, A., Kistler, J., and Walz, T. (1998). 2D crystallization of membrane proteins: rationales and examples. Journal of structural biology *121*, 162-171.

Havelaar, A.H., Kirk, M.D., Torgerson, P.R., Gibb, H.J., Hald, T., Lake, R.J., Praet, N., Bellinger, D.C., de Silva, N.R., Gargouri, N.*, et al.* (2015). World Health Organization Global Estimates and Regional Comparisons of the Burden of Foodborne Disease in 2010. PLoS Med *12*, e1001923.

Higashi, H., Tsutsumi, R., Fujita, A., Yamazaki, S., Asaka, M., Azuma, T., and Hatakeyama, M. (2002). Biological activity of the Helicobacter pylori virulence factor CagA is determined by variation in the tyrosine phosphorylation sites. Proceedings of the National Academy of Sciences of the United States of America *99*, 14428-14433.

Hohn, M., Tang, G., Goodyear, G., Baldwin, P.R., Huang, Z., Penczek, P.A., Yang, C., Glaeser, R.M., Adams, P.D., and Ludtke, S.J. (2007). SPARX, a new environment for Cryo-EM image processing. Journal of structural biology *157*, 47-55.

Huyet, J., Naylor, C.E., Savva, C.G., Gibert, M., Popoff, M.R., and Basak, A.K. (2013). Structural Insights into Clostridium perfringens Delta Toxin Pore Formation. PloS one *8*, e66673.

Huynh, K.W., Cohen, M.R., and Moiseenkova-Bell, V.Y. (2014). Application of amphipols for structure-functional analysis of TRP channels. J Membr Biol *247*, 843-851.

Iacovache, I., De Carlo, S., Cirauqui, N., Dal Peraro, M., van der Goot, F.G., and Zuber, B. (2016). Cryo-EM structure of aerolysin variants reveals a novel protein fold and the pore-formation process. Nat Commun *7*, 12062.

Inglesby, T.V., O'Toole, T., Henderson, D.A., Bartlett, J.G., Ascher, M.S., Eitzen, E., Friedlander, A.M., Gerberding, J., Hauer, J., Hughes, J.*, et al.* (2002). Anthrax as a biological weapon, 2002: updated recommendations for management. Jama *287*, 2236-2252.

Itoh, T., Erdmann, K.S., Roux, A., Habermann, B., Werner, H., and De Camilli, P. (2005). Dynamin and the actin cytoskeleton cooperatively regulate plasma membrane invagination by BAR and F-BAR proteins. Dev Cell *9*, 791-804.

Ivie, S.E., McClain, M.S., Algood, H.M., Lacy, D.B., and Cover, T.L. (2010). Analysis of a beta-helical region in the p55 domain of Helicobacter pylori vacuolating toxin. BMC microbiology *10*, 60.

Ivie, S.E., McClain, M.S., Torres, V.J., Algood, H.M., Lacy, D.B., Yang, R., Blanke, S.R., and Cover, T.L. (2008). Helicobacter pylori VacA subdomain required for intracellular toxin activity and assembly of functional oligomeric complexes. Infection and immunity *76*, 2843-2851.

Iwamoto, H., Czajkowsky, D.M., Cover, T.L., Szabo, G., and Shao, Z. (1999). VacA from Helicobacter pylori: a hexameric chloride channel. FEBS letters *450*, 101-104.

Jain, P., Luo, Z.Q., and Blanke, S.R. (2011). Helicobacter pylori vacuolating cytotoxin A (VacA) engages the mitochondrial fission machinery to induce host cell death. Proceedings of the National Academy of Sciences of the United States of America *108*, 16032-16037.

Jensen, K.H., Brandt, S.S., Shigematsu, H., and Sigworth, F.J. (2016a). Statistical modeling and removal of lipid membrane projections for cryo-EM structure determination of reconstituted membrane proteins. Journal of structural biology *194*, 49-60.

Jensen, K.H., Sigworth, F.J., and Brandt, S.S. (2016b). Removal of Vesicle Structures From Transmission Electron Microscope Images. IEEE Trans Image Process *25*, 540-552.

Ji, X., Fernandez, T., Burroni, D., Pagliaccia, C., Atherton, J.C., Reyrat, J.M., Rappuoli, R., and Telford, J.L. (2000). Cell specificity of Helicobacter pylori cytotoxin is determined by a short region in the polymorphic midregion. Infection and immunity *68*, 3754-3757.

Jimenez-Soto, L.F., Rohrer, S., Jain, U., Ertl, C., Sewald, X., and Haas, R. (2012). Effects of cholesterol on Helicobacter pylori growth and virulence properties in vitro. Helicobacter *17*, 133-139.

Kim, S., Chamberlain, A.K., and Bowie, J.U. (2004). Membrane channel structure of Helicobacter pylori vacuolating toxin: role of multiple GXXXG motifs in cylindrical channels. Proceedings of the National Academy of Sciences of the United States of America *101*, 5988-5991.

Koster, S., van Pee, K., Hudel, M., Leustik, M., Rhinow, D., Kuhlbrandt, W., Chakraborty, T., and Yildiz, O. (2014). Crystal structure of listeriolysin O reveals molecular details of oligomerization and pore formation. Nat Commun *5*, 3690.

Kuo, C.H., and Wang, W.C. (2003). Binding and internalization of Helicobacter pylori VacA via cellular lipid rafts in epithelial cells. Biochemical and biophysical research communications *303*, 640-644.

Lakey, J.H., Massotte, D., Heitz, F., Dasseux, J.L., Faucon, J.F., Parker, M.W., and Pattus, F. (1991). Membrane insertion of the pore-forming domain of colicin A. A spectroscopic study. Eur J Biochem *196*, 599-607.

Lakey, J.H., van der Goot, F.G., and Pattus, F. (1994). All in the family: the toxic activity of pore-forming colicins. Toxicology *87*, 85-108.

Lanzavecchia, S., Bellon, P.L., Lupetti, P., Dallai, R., Rappuoli, R., and Telford, J.L. (1998). Three-dimensional reconstruction of metal replicas of the Helicobacter pylori vacuolating cytotoxin. Journal of structural biology *121*, 9-18.

Lawrence, S.L., Feil, S.C., Morton, C.J., Farrand, A.J., Mulhern, T.D., Gorman, M.A., Wade, K.R., Tweten, R.K., and Parker, M.W. (2015). Crystal structure of Streptococcus pneumoniae pneumolysin provides key insights into early steps of pore formation. Sci Rep *5*, 14352.

Lee, I.O., Kim, J.H., Choi, Y.J., Pillinger, M.H., Kim, S.Y., Blaser, M.J., and Lee, Y.C. (2010). Helicobacter pylori CagA phosphorylation status determines the gp130-activated SHP2/ERK and JAK/STAT signal transduction pathways in gastric epithelial cells. The Journal of biological chemistry *285*, 16042-16050.

Leja, M., Axon, A., and Brenner, H. (2016). Epidemiology of Helicobacter pylori infection. Helicobacter *21 Suppl 1*, 3-7.

Leka, O., Vallese, F., Pirazzini, M., Berto, P., Montecucco, C., and Zanotti, G. (2014). Diphtheria toxin conformational switching at acidic pH. FEBS J *281*, 2115-2122.

Lemmon, M.A., Flanagan, J.M., Hunt, J.F., Adair, B.D., Bormann, B.J., Dempsey, C.E., and Engelman, D.M. (1992). Glycophorin A dimerization is driven by specific interactions between transmembrane alpha-helices. The Journal of biological chemistry *267*, 7683-7689.

Letley, D.P., and Atherton, J.C. (2000). Natural diversity in the N terminus of the mature vacuolating cytotoxin of Helicobacter pylori determines cytotoxin activity. Journal of bacteriology *182*, 3278-3280.

Letley, D.P., Rhead, J.L., Twells, R.J., Dove, B., and Atherton, J.C. (2003). Determinants of non-toxicity in the gastric pathogen Helicobacter pylori. The Journal of biological chemistry *278*, 26734-26741.

Ludtke, S.J. (2010). 3-D structures of macromolecules using single-particle analysis in EMAN. Methods in molecular biology *673*, 157-173.

Lupetti, P., Heuser, J.E., Manetti, R., Massari, P., Lanzavecchia, S., Bellon, P.L., Dallai, R., Rappuoli, R., and Telford, J.L. (1996). Oligomeric and subunit structure of the Helicobacter pylori vacuolating cytotoxin. The Journal of cell biology *133*, 801-807.

Mandlik, A., Swierczynski, A., Das, A., and Ton-That, H. (2008). Pili in Gram-positive bacteria: assembly, involvement in colonization and biofilm development. Trends in microbiology *16*, 33-40.

Marsh, P.D. (2004). Dental plaque as a microbial biofilm. Caries Res *38*, 204-211.

Marshall, B.J., McGechie, D.B., Francis, G.J., and Utley, P.J. (1984). Pyloric campylobacter serology. Lancet *2*, 281.

Marshall, J.E., Faraj, B.H., Gingras, A.R., Lonnen, R., Sheikh, M.A., El-Mezgueldi, M., Moody, P.C., Andrew, P.W., and Wallis, R. (2015). The Crystal Structure of Pneumolysin at 2.0 A Resolution Reveals the Molecular Packing of the Pre-pore Complex. Sci Rep *5*, 13293.

McClain, M.S., Cao, P., and Cover, T.L. (2001a). Amino-terminal hydrophobic region of Helicobacter pylori vacuolating cytotoxin (VacA) mediates transmembrane protein dimerization. Infection and immunity *69*, 1181-1184.

McClain, M.S., Cao, P., Iwamoto, H., Vinion-Dubiel, A.D., Szabo, G., Shao, Z., and Cover, T.L. (2001b). A 12-amino-acid segment, present in type s2 but not type s1 Helicobacter pylori VacA proteins, abolishes cytotoxin activity and alters membrane channel formation. Journal of bacteriology *183*, 6499-6508.

McClain, M.S., Iwamoto, H., Cao, P., Vinion-Dubiel, A.D., Li, Y., Szabo, G., Shao, Z., and Cover, T.L. (2003). Essential role of a GXXXG motif for membrane channel formation by Helicobacter pylori vacuolating toxin. The Journal of biological chemistry *278*, 12101-12108.

McClain, M.S., Schraw, W., Ricci, V., Boquet, P., and Cover, T.L. (2000). Acid activation of Helicobacter pylori vacuolating cytotoxin (VacA) results in toxin internalization by eukaryotic cells. Molecular microbiology *37*, 433-442.

McDonald, N.A., Vander Kooi, C.W., Ohi, M.D., and Gould, K.L. (2015). Oligomerization but Not Membrane Bending Underlies the Function of Certain F-BAR Proteins in Cell Motility and Cytokinesis. Dev Cell *35*, 725-736.

Mechaly, A.E., Bellomio, A., Gil-Carton, D., Morante, K., Valle, M., Gonzalez-Manas, J.M., and Guerin, D.M. (2011). Structural insights into the oligomerization and architecture of eukaryotic membrane pore-forming toxins. Structure *19*, 181-191.

Memon, A.A., Hussein, N.R., Miendje Deyi, V.Y., Burette, A., and Atherton, J.C. (2014). Vacuolating cytotoxin genotypes are strong markers of gastric cancer and duodenal ulcer-associated Helicobacter pylori strains: a matched case-control study. Journal of clinical microbiology *52*, 2984-2989.

Miller, B.A., Chen, L.F., Sexton, D.J., and Anderson, D.J. (2011). Comparison of the burdens of hospital-onset, healthcare facility-associated Clostridium difficile Infection and of healthcare-associated infection due to methicillin-resistant Staphylococcus aureus in community hospitals. Infect Control Hosp Epidemiol *32*, 387-390.

Mimuro, H., Suzuki, T., Tanaka, J., Asahi, M., Haas, R., and Sasakawa, C. (2002). Grb2 is a key mediator of helicobacter pylori CagA protein activities. Mol Cell *10*, 745-755.

Mobley, H.L. (1996). The role of Helicobacter pylori urease in the pathogenesis of gastritis and peptic ulceration. Alimentary pharmacology & therapeutics *10 Suppl 1*, 57-64.

Molinari, M., Galli, C., de Bernard, M., Norais, N., Ruysschaert, J.M., Rappuoli, R., and Montecucco, C. (1998). The acid activation of Helicobacter pylori toxin VacA: structural and membrane binding studies. Biochemical and biophysical research communications *248*, 334-340.

Montecucco, C., and de Bernard, M. (2003). Molecular and cellular mechanisms of action of the vacuolating cytotoxin (VacA) and neutrophil-activating protein (HP-NAP) virulence factors of Helicobacter pylori. Microbes Infect *5*, 715-721.

Montecucco, C., and Rappuoli, R. (2001). Living dangerously: how Helicobacter pylori survives in the human stomach. Nat Rev Mol Cell Biol *2*, 457-466.

Morante, K., Bellomio, A., Gil-Carton, D., Redondo-Morata, L., Sot, J., Scheuring, S., Valle, M., Gonzalez-Manas, J.M., Tsumoto, K., and Caaveiro, J.M. (2016). Identification of a Membrane-bound Prepore Species Clarifies the Lytic Mechanism of Actinoporins. The Journal of biological chemistry *291*, 19210-19219.

Morbiato, L., Tombola, F., Campello, S., Del Giudice, G., Rappuoli, R., Zoratti, M., and Papini, E. (2001). Vacuolation induced by VacA toxin of Helicobacter pylori requires the intracellular accumulation of membrane permeant bases, Cl(-) and water. FEBS letters *508*, 479-483.

Mueller, M., Grauschopf, U., Maier, T., Glockshuber, R., and Ban, N. (2009). The structure of a cytolytic alpha-helical toxin pore reveals its assembly mechanism. Nature *459*, 726-730.

Murata-Kamiya, N., Kurashima, Y., Teishikata, Y., Yamahashi, Y., Saito, Y., Higashi, H., Aburatani, H., Akiyama, T., Peek, R.M., Jr., Azuma, T.*, et al.* (2007). Helicobacter pylori CagA interacts with E-cadherin and deregulates the beta-catenin signal that promotes intestinal transdifferentiation in gastric epithelial cells. Oncogene *26*, 4617-4626.

Nakayama, M., Hisatsune, J., Yamasaki, E., Nishi, Y., Wada, A., Kurazono, H., Sap, J., Yahiro, K., Moss, J., and Hirayama, T. (2006). Clustering of Helicobacter pylori VacA in lipid rafts, mediated by its receptor, receptor-like protein tyrosine

phosphatase beta, is required for intoxication in AZ-521 Cells. Infection and immunity *74*, 6571-6580.

Nakayama, M., Kimura, M., Wada, A., Yahiro, K., Ogushi, K., Niidome, T., Fujikawa, A., Shirasaka, D., Aoyama, N., Kurazono, H.*, et al.* (2004). Helicobacter pylori VacA activates the p38/activating transcription factor 2-mediated signal pathway in AZ-521 cells. The Journal of biological chemistry *279*, 7024-7028.

Nasr, M.L., Baptista, D., Strauss, M., Sun, Z.J., Grigoriu, S., Huser, S., Pluckthun, A., Hagn, F., Walz, T., Hogle, J.M.*, et al.* (2017). Covalently circularized nanodiscs for studying membrane proteins and viral entry. Nature methods *14*, 49-52.

Nguyen, V.Q., Caprioli, R.M., and Cover, T.L. (2001). Carboxy-terminal proteolytic processing of Helicobacter pylori vacuolating toxin. Infection and immunity *69*, 543-546.

Nomura, A., Stemmermann, G.N., Chyou, P.H., Kato, I., Perez-Perez, G.I., and Blaser, M.J. (1991). Helicobacter pylori infection and gastric carcinoma among Japanese Americans in Hawaii. The New England journal of medicine *325*, 1132-1136.

O'Keefe, D.O., Cabiaux, V., Choe, S., Eisenberg, D., and Collier, R.J. (1992). pH-dependent insertion of proteins into membranes: B-chain mutation of diphtheria toxin that inhibits membrane translocation, Glu-349----Lys. Proceedings of the National Academy of Sciences of the United States of America *89*, 6202-6206.

O'Toole, G.A., and Kolter, R. (1998). Flagellar and twitching motility are necessary for Pseudomonas aeruginosa biofilm development. Molecular microbiology *30*, 295-304.

Ohi, M., Li, Y., Cheng, Y., and Walz, T. (2004). Negative Staining and Image Classification - Powerful Tools in Modern Electron Microscopy. Biol Proced Online *6*, 23-34.

Oliveira, M.J., Costa, A.M., Costa, A.C., Ferreira, R.M., Sampaio, P., Machado, J.C., Seruca, R., Mareel, M., and Figueiredo, C. (2009). CagA associates with c-Met, E-cadherin, and p120-catenin in a multiproteic complex that suppresses Helicobacter pylori-induced cell-invasive phenotype. The Journal of infectious diseases *200*, 745-755.

Olson, R., and Gouaux, E. (2005). Crystal structure of the Vibrio cholerae cytolysin (VCC) pro-toxin and its assembly into a heptameric transmembrane pore. Journal of molecular biology *350*, 997-1016.

Olson, R., Nariya, H., Yokota, K., Kamio, Y., and Gouaux, E. (1999). Crystal structure of staphylococcal LukF delineates conformational changes accompanying formation of a transmembrane channel. Nat Struct Biol *6*, 134-140.

Pagliaccia, C., de Bernard, M., Lupetti, P., Ji, X., Burroni, D., Cover, T.L., Papini, E., Rappuoli, R., Telford, J.L., and Reyrat, J.M. (1998). The m2 form of the Helicobacter pylori cytotoxin has cell type-specific vacuolating activity. Proceedings of the National Academy of Sciences of the United States of America *95*, 10212-10217.

Pagliaccia, C., Wang, X.M., Tardy, F., Telford, J.L., Ruysschaert, J.M., and Cabiaux, V. (2000). Structure and interaction of VacA of Helicobacter pylori with a lipid membrane. Eur J Biochem *267*, 104-109.

Palframan, S.L., Kwok, T., and Gabriel, K. (2012). Vacuolating cytotoxin A (VacA), a key toxin for Helicobacter pylori pathogenesis. Frontiers in cellular and infection microbiology *2*, 92.

Papini, E., Satin, B., de Bernard, M., Molinari, M., Arico, B., Galli, C., Telford, J.R., Rappuoli, R., and Montecucco, C. (1998a). Action site and cellular effects of cytotoxin VacA produced by Helicobacter pylori. Folia Microbiol (Praha) *43*, 279-284.

Papini, E., Satin, B., Norais, N., de Bernard, M., Telford, J.L., Rappuoli, R., and Montecucco, C. (1998b). Selective increase of the permeability of polarized epithelial cell monolayers by Helicobacter pylori vacuolating toxin. The Journal of clinical investigation *102*, 813-820.

Park, S.H., Berkamp, S., Cook, G.A., Chan, M.K., Viadiu, H., and Opella, S.J. (2011). Nanodiscs versus macrodiscs for NMR of membrane proteins. Biochemistry *50*, 8983-8985.

Parker, M.W., Buckley, J.T., Postma, J.P., Tucker, A.D., Leonard, K., Pattus, F., and Tsernoglou, D. (1994). Structure of the Aeromonas toxin proaerolysin in its water-soluble and membrane-channel states. Nature *367*, 292-295.

Parker, M.W., Postma, J.P., Pattus, F., Tucker, A.D., and Tsernoglou, D. (1992). Refined structure of the pore-forming domain of colicin A at 2.4 A resolution. Journal of molecular biology *224*, 639-657.

Parker, M.W., Tucker, A.D., Tsernoglou, D., and Pattus, F. (1990). Insights into membrane insertion based on studies of colicins. Trends Biochem Sci *15*, 126-129.

Parks, T., Barrett, L., and Jones, N. (2015). Invasive streptococcal disease: a review for clinicians. Br Med Bull *115*, 77-89.

Parsonnet, J., Friedman, G.D., Vandersteen, D.P., Chang, Y., Vogelman, J.H., Orentreich, N., and Sibley, R.K. (1991a). Helicobacter pylori infection and the risk of gastric carcinoma. The New England journal of medicine *325*, 1127-1131.

Parsonnet, J., Vandersteen, D., Goates, J., Sibley, R.K., Pritikin, J., and Chang, Y. (1991b). Helicobacter pylori infection in intestinal- and diffuse-type gastric adenocarcinomas. Journal of the National Cancer Institute *83*, 640-643.

Patel, H.K., Willhite, D.C., Patel, R.M., Ye, D., Williams, C.L., Torres, E.M., Marty, K.B., MacDonald, R.A., and Blanke, S.R. (2002). Plasma membrane cholesterol modulates cellular vacuolation induced by the Helicobacter pylori vacuolating cytotoxin. Infection and immunity *70*, 4112-4123.

Pathan, N., Faust, S.N., and Levin, M. (2003). Pathophysiology of meningococcal meningitis and septicaemia. Archives of disease in childhood *88*, 601-607.

Pelicic, V., Reyrat, J.M., Sartori, L., Pagliaccia, C., Rappuoli, R., Telford, J.L., Montecucco, C., and Papini, E. (1999). Helicobacter pylori VacA cytotoxin associated with the bacteria increases epithelial permeability independently of its vacuolating activity. Microbiology *145 (Pt 8)*, 2043-2050.

Pettersen, E.F., Goddard, T.D., Huang, C.C., Couch, G.S., Greenblatt, D.M., Meng, E.C., and Ferrin, T.E. (2004). UCSF Chimera--a visualization system for exploratory research and analysis. J Comput Chem *25*, 1605-1612.

Proft, T., and Baker, E.N. (2009). Pili in Gram-negative and Gram-positive bacteria - structure, assembly and their role in disease. Cell Mol Life Sci *66*, 613-635.

Pruitt, R.N., Chambers, M.G., Ng, K.K., Ohi, M.D., and Lacy, D.B. (2010). Structural organization of the functional domains of Clostridium difficile toxins A and B. Proceedings of the National Academy of Sciences of the United States of America *107*, 13467-13472.

Pyburn, T.M., Foegeding, N.J., Gonzalez-Rivera, C., McDonald, N.A., Gould, K.L., Cover, T.L., and Ohi, M.D. (2016). Structural organization of membrane-inserted hexamers formed by Helicobacter pylori VacA toxin. Molecular microbiology *102*, 22-36.

Radermacher, M. (1994). Three-dimensional reconstruction from random projections: orientational alignment via Radon transforms. Ultramicroscopy *53*, 121-136.

Radermacher, M., Wagenknecht, T., Verschoor, A., and Frank, J. (1987). Three-dimensional reconstruction from a single-exposure, random conical tilt series applied to the 50S ribosomal subunit of Escherichia coli. J Microsc *146*, 113-136.

Radin, J.N., Gonzalez-Rivera, C., Ivie, S.E., McClain, M.S., and Cover, T.L. (2011). Helicobacter pylori VacA induces programmed necrosis in gastric epithelial cells. Infection and immunity *79*, 2535-2543.

Raju, D., Hussey, S., Ang, M., Terebiznik, M.R., Sibony, M., Galindo-Mata, E., Gupta, V., Blanke, S.R., Delgado, A., Romero-Gallo, J.*, et al.* (2012). Vacuolating cytotoxin and variants in Atg16L1 that disrupt autophagy promote Helicobacter pylori infection in humans. Gastroenterology *142*, 1160-1171.

Rassow, J., and Meinecke, M. (2012). Helicobacter pylori VacA: a new perspective on an invasive chloride channel. Microbes Infect *14*, 1026-1033.

Reyrat, J.M., Lanzavecchia, S., Lupetti, P., de Bernard, M., Pagliaccia, C., Pelicic, V., Charrel, M., Ulivieri, C., Norais, N., Ji, X.*, et al.* (1999). 3D imaging of the 58 kDa cell binding subunit of the Helicobacter pylori cytotoxin. Journal of molecular biology *290*, 459-470.

Rhead, J.L., Letley, D.P., Mohammadi, M., Hussein, N., Mohagheghi, M.A., Eshagh Hosseini, M., and Atherton, J.C. (2007). A new Helicobacter pylori vacuolating cytotoxin determinant, the intermediate region, is associated with gastric cancer. Gastroenterology *133*, 926-936.

Ricci, V., Galmiche, A., Doye, A., Necchi, V., Solcia, E., and Boquet, P. (2000). High cell sensitivity to Helicobacter pylori VacA toxin depends on a GPI-anchored protein and is not blocked by inhibition of the clathrin-mediated pathway of endocytosis. Molecular biology of the cell *11*, 3897-3909.

Ridley, H., Johnson, C.L., and Lakey, J.H. (2010). Interfacial interactions of pore-forming colicins. Adv Exp Med Biol *677*, 81-90.

Rossjohn, J., Feil, S.C., McKinstry, W.J., Tweten, R.K., and Parker, M.W. (1997). Structure of a cholesterol-binding, thiol-activated cytolysin and a model of its membrane form. Cell *89*, 685-692.

Russ, W.P., and Engelman, D.M. (1999). TOXCAT: a measure of transmembrane helix association in a biological membrane. Proceedings of the National Academy of Sciences of the United States of America *96*, 863-868.

Russ, W.P., and Engelman, D.M. (2000). The GxxxG motif: a framework for transmembrane helix-helix association. Journal of molecular biology *296*, 911-919.

Salama, N.R., Hartung, M.L., and Muller, A. (2013). Life in the human stomach: persistence strategies of the bacterial pathogen Helicobacter pylori. Nature reviews Microbiology *11*, 385-399.

Sauer, F.G., Remaut, H., Hultgren, S.J., and Waksman, G. (2004). Fiber assembly by the chaperone-usher pathway. Biochim Biophys Acta *1694*, 259-267.

Sauer, M.M., Jakob, R.P., Eras, J., Baday, S., Eris, D., Navarra, G., Berneche, S., Ernst, B., Maier, T., and Glockshuber, R. (2016). Catch-bond mechanism of the bacterial adhesin FimH. Nat Commun *7*, 10738.

Savva, C.G., Fernandes da Costa, S.P., Bokori-Brown, M., Naylor, C.E., Cole, A.R., Moss, D.S., Titball, R.W., and Basak, A.K. (2013). Molecular architecture and functional analysis of NetB, a pore-forming toxin from Clostridium perfringens. The Journal of biological chemistry *288*, 3512-3522.

Schneider, C.A., Rasband, W.S., and Eliceiri, K.W. (2012). NIH Image to ImageJ: 25 years of image analysis. Nature methods *9*, 671-675.

Schraw, W., Li, Y., McClain, M.S., van der Goot, F.G., and Cover, T.L. (2002). Association of Helicobacter pylori vacuolating toxin (VacA) with lipid rafts. The Journal of biological chemistry *277*, 34642-34650.

Schuler, M.A., Denisov, I.G., and Sligar, S.G. (2013). Nanodiscs as a new tool to examine lipid-protein interactions. Methods in molecular biology *974*, 415-433.

Schwartz, M. (2009). Dr. Jekyll and Mr. Hyde: a short history of anthrax. Mol Aspects Med *30*, 347-355.

Seto, K., Hayashi-Kuwabara, Y., Yoneta, T., Suda, H., and Tamaki, H. (1998). Vacuolation induced by cytotoxin from Helicobacter pylori is mediated by the EGF receptor in HeLa cells. FEBS letters *431*, 347-350.

Sewald, X., Fischer, W., and Haas, R. (2008a). Sticky socks: Helicobacter pylori VacA takes shape. Trends in microbiology *16*, 89-92.

Sewald, X., Gebert-Vogl, B., Prassl, S., Barwig, I., Weiss, E., Fabbri, M., Osicka, R., Schiemann, M., Busch, D.H., Semmrich, M.*, et al.* (2008b). Integrin subunit CD18 Is the T-lymphocyte receptor for the Helicobacter pylori vacuolating cytotoxin. Cell Host Microbe *3*, 20-29.

Sewald, X., Jimenez-Soto, L., and Haas, R. (2011). PKC-dependent endocytosis of the Helicobacter pylori vacuolating cytotoxin in primary T lymphocytes. Cell Microbiol *13*, 482-496.

Shaikh, T.R., Gao, H., Baxter, W.T., Asturias, F.J., Boisset, N., Leith, A., and Frank, J. (2008). SPIDER image processing for single-particle reconstruction of biological macromolecules from electron micrographs. Nat Protoc *3*, 1941-1974.

Song, L., Hobaugh, M.R., Shustak, C., Cheley, S., Bayley, H., and Gouaux, J.E. (1996). Structure of staphylococcal alpha-hemolysin, a heptameric transmembrane pore. Science *274*, 1859-1866.

Soto, G.E., and Hultgren, S.J. (1999). Bacterial adhesins: common themes and variations in architecture and assembly. Journal of bacteriology *181*, 1059-1071.

Stryjewski, M.E., and Patel, K. (2003). Selective decontamination of digestive tract in intensive care. Lancet *362*, 2118; author reply 2119-2120.

Suerbaum, S., and Michetti, P. (2002). Helicobacter pylori infection. The New England journal of medicine *347*, 1175-1186.

Sundrud, M.S., Torres, V.J., Unutmaz, D., and Cover, T.L. (2004). Inhibition of primary human T cell proliferation by Helicobacter pylori vacuolating toxin (VacA) is independent of VacA effects on IL-2 secretion. Proceedings of the National Academy of Sciences of the United States of America *101*, 7727-7732.

Suzuki, M., Mimuro, H., Suzuki, T., Park, M., Yamamoto, T., and Sasakawa, C. (2005). Interaction of CagA with Crk plays an important role in Helicobacter pylori-induced loss of gastric epithelial cell adhesion. The Journal of experimental medicine *202*, 1235-1247.

Szabo, I., Brutsche, S., Tombola, F., Moschioni, M., Satin, B., Telford, J.L., Rappuoli, R., Montecucco, C., Papini, E., and Zoratti, M. (1999). Formation of anion-selective channels in the cell plasma membrane by the toxin VacA of

Helicobacter pylori is required for its biological activity. The EMBO journal *18*, 5517-5527.

Taddei, A., Folli, C., Zegarra-Moran, O., Fanen, P., Verkman, A.S., and Galietta, L.J. (2004). Altered channel gating mechanism for CFTR inhibition by a high-affinity thiazolidinone blocker. FEBS letters *558*, 52-56.

Tammer, I., Brandt, S., Hartig, R., Konig, W., and Backert, S. (2007). Activation of Abl by Helicobacter pylori: a novel kinase for CagA and crucial mediator of host cell scattering. Gastroenterology *132*, 1309-1319.

Tanaka, K., Caaveiro, J.M., Morante, K., Gonzalez-Manas, J.M., and Tsumoto, K. (2015). Structural basis for self-assembly of a cytolytic pore lined by protein and lipid. Nat Commun *6*, 6337.

Teese, M.G., and Langosch, D. (2015). Role of GxxxG Motifs in Transmembrane Domain Interactions. Biochemistry *54*, 5125-5135.

Terebiznik, M.R., Raju, D., Vazquez, C.L., Torbricki, K., Kulkarni, R., Blanke, S.R., Yoshimori, T., Colombo, M.I., and Jones, N.L. (2009). Effect of Helicobacter pylori's vacuolating cytotoxin on the autophagy pathway in gastric epithelial cells. Autophagy *5*, 370-379.

Thomas, W.E., Trintchina, E., Forero, M., Vogel, V., and Sokurenko, E.V. (2002). Bacterial adhesion to target cells enhanced by shear force. Cell *109*, 913-923.

Tilley, S.J., Orlova, E.V., Gilbert, R.J., Andrew, P.W., and Saibil, H.R. (2005). Structural basis of pore formation by the bacterial toxin pneumolysin. Cell *121*, 247-256.

Tombola, F., Carlesso, C., Szabo, I., de Bernard, M., Reyrat, J.M., Telford, J.L., Rappuoli, R., Montecucco, C., Papini, E., and Zoratti, M. (1999a). Helicobacter pylori vacuolating toxin forms anion-selective channels in planar lipid bilayers: possible implications for the mechanism of cellular vacuolation. Biophysical journal *76*, 1401-1409.

Tombola, F., Oregna, F., Brutsche, S., Szabo, I., Del Giudice, G., Rappuoli, R., Montecucco, C., Papini, E., and Zoratti, M. (1999b). Inhibition of the vacuolating and anion channel activities of the VacA toxin of Helicobacter pylori. FEBS letters *460*, 221-225.

Tombola, F., Pagliaccia, C., Campello, S., Telford, J.L., Montecucco, C., Papini, E., and Zoratti, M. (2001). How the loop and middle regions influence the properties of Helicobacter pylori VacA channels. Biophysical journal *81*, 3204-3215.

Ton-That, H., and Schneewind, O. (2004). Assembly of pili in Gram-positive bacteria. Trends in microbiology *12*, 228-234.

Torres, V.J., Ivie, S.E., McClain, M.S., and Cover, T.L. (2005). Functional properties of the p33 and p55 domains of the Helicobacter pylori vacuolating cytotoxin. The Journal of biological chemistry *280*, 21107-21114.

Torres, V.J., McClain, M.S., and Cover, T.L. (2004). Interactions between p-33 and p-55 domains of the Helicobacter pylori vacuolating cytotoxin (VacA). The Journal of biological chemistry *279*, 2324-2331.

Torres, V.J., McClain, M.S., and Cover, T.L. (2006). Mapping of a domain required for protein-protein interactions and inhibitory activity of a Helicobacter pylori dominant-negative VacA mutant protein. Infection and immunity *74*, 2093-2101.

Tweten, R.K. (2005). Cholesterol-dependent cytolysins, a family of versatile pore-forming toxins. Infection and immunity *73*, 6199-6209.

Uemura, N., Okamoto, S., Yamamoto, S., Matsumura, N., Yamaguchi, S., Yamakido, M., Taniyama, K., Sasaki, N., and Schlemper, R.J. (2001). Helicobacter pylori infection and the development of gastric cancer. The New England journal of medicine *345*, 784-789.

Urgesi, R., Cianci, R., and Riccioni, M.E. (2012). Update on triple therapy for eradication of Helicobacter pylori: current status of the art. Clin Exp Gastroenterol *5*, 151-157.

Utt, M., Danielsson, B., and Wadstrom, T. (2001). Helicobacter pylori vacuolating cytotoxin binding to a putative cell surface receptor, heparan sulfate, studied by surface plasmon resonance. FEMS immunology and medical microbiology *30*, 109-113.

Verkman, A.S., and Galietta, L.J. (2009). Chloride channels as drug targets. Nat Rev Drug Discov *8*, 153-171.

Vinion-Dubiel, A.D., McClain, M.S., Czajkowsky, D.M., Iwamoto, H., Ye, D., Cao, P., Schraw, W., Szabo, G., Blanke, S.R., Shao, Z.*, et al.* (1999). A dominant

negative mutant of Helicobacter pylori vacuolating toxin (VacA) inhibits VacA-induced cell vacuolation. The Journal of biological chemistry *274*, 37736-37742.

Vivekananda, J., Salgado, C., and Millenbaugh, N.J. (2014). DNA aptamers as a novel approach to neutralize Staphylococcus aureus alpha-toxin. Biochemical and biophysical research communications *444*, 433-438.

von der Ecken, J., Muller, M., Lehman, W., Manstein, D.J., Penczek, P.A., and Raunser, S. (2015). Structure of the F-actin-tropomyosin complex. Nature *519*, 114-117.

Wallace, A.J., Stillman, T.J., Atkins, A., Jamieson, S.J., Bullough, P.A., Green, J., and Artymiuk, P.J. (2000). E. coli hemolysin E (HlyE, ClyA, SheA): X-ray crystal structure of the toxin and observation of membrane pores by electron microscopy. Cell *100*, 265-276.

Wang, L., and Sigworth, F.J. (2009). Structure of the BK potassium channel in a lipid membrane from electron cryomicroscopy. Nature *461*, 292-295.

Wang, L., and Sigworth, F.J. (2010). Liposomes on a streptavidin crystal: a system to study membrane proteins by cryo-EM. Methods Enzymol *481*, 147-164.

Wang, W.C., Wang, H.J., and Kuo, C.H. (2001). Two distinctive cell binding patterns by vacuolating toxin fused with glutathione S-transferase: one high-affinity m1-specific binding and the other lower-affinity binding for variant m forms. Biochemistry *40*, 11887-11896.

Wang, X., Wattiez, R., Paggliacia, C., Telford, J.L., Ruysschaert, J., and Cabiaux, V. (2000). Membrane topology of VacA cytotoxin from H. pylori. FEBS letters *481*, 96-100.

Wiener, M., Freymann, D., Ghosh, P., and Stroud, R.M. (1997). Crystal structure of colicin Ia. Nature *385*, 461-464.

Wiles, T.J., Kulesus, R.R., and Mulvey, M.A. (2008). Origins and virulence mechanisms of uropathogenic Escherichia coli. Exp Mol Pathol *85*, 11-19.

Willhite, D.C., and Blanke, S.R. (2004). Helicobacter pylori vacuolating cytotoxin enters cells, localizes to the mitochondria, and induces mitochondrial membrane permeability changes correlated to toxin channel activity. Cellular Microbiology *6*, 143-154.

Willhite, D.C., Cover, T.L., and Blanke, S.R. (2003). Cellular vacuolation and mitochondrial cytochrome c release are independent outcomes of Helicobacter pylori vacuolating cytotoxin activity that are each dependent on membrane channel formation. The Journal of biological chemistry *278*, 48204-48209.

Wilmsen, H.U., Leonard, K.R., Tichelaar, W., Buckley, J.T., and Pattus, F. (1992). The aerolysin membrane channel is formed by heptamerization of the monomer. The EMBO journal *11*, 2457-2463.

Wilson-Kubalek, E.M. (2000). Preparation of functionalized lipid tubules for electron crystallography of macromolecules. Methods Enzymol *312*, 515-519.

Wilson-Kubalek, E.M., Brown, R.E., Celia, H., and Milligan, R.A. (1998). Lipid nanotubes as substrates for helical crystallization of macromolecules. Proceedings of the National Academy of Sciences of the United States of America *95*, 8040-8045.

Wu, Q., and Guo, Z. (2010). Glycosylphosphatidylinositols are potential targets for the development of novel inhibitors for aerolysin-type of pore-forming bacterial toxins. Med Res Rev *30*, 258-269.

Yahiro, K., Niidome, T., Kimura, M., Hatakeyama, T., Aoyagi, H., Kurazono, H., Imagawa, K., Wada, A., Moss, J., and Hirayama, T. (1999). Activation of Helicobacter pylori VacA toxin by alkaline or acid conditions increases its binding to a 250-kDa receptor protein-tyrosine phosphatase beta. The Journal of biological chemistry *274*, 36693-36699.

Yahiro, K., Satoh, M., Nakano, M., Hisatsune, J., Isomoto, H., Sap, J., Suzuki, H., Nomura, F., Noda, M., Moss, J.*, et al.* (2012). Low-density lipoprotein receptor-related protein-1 (LRP1) mediates autophagy and apoptosis caused by Helicobacter pylori VacA. The Journal of biological chemistry *287*, 31104-31115.

Yahiro, K., Wada, A., Nakayama, M., Kimura, T., Ogushi, K., Niidome, T., Aoyagi, H., Yoshino, K., Yonezawa, K., Moss, J.*, et al.* (2003). Protein-tyrosine phosphatase alpha, RPTP alpha, is a Helicobacter pylori VacA receptor. The Journal of biological chemistry *278*, 19183-19189.

Yamasaki, E., Wada, A., Kumatori, A., Nakagawa, I., Funao, J., Nakayama, M., Hisatsune, J., Kimura, M., Moss, J., and Hirayama, T. (2006). Helicobacter pylori vacuolating cytotoxin induces activation of the proapoptotic proteins Bax and Bak, leading to cytochrome c release and cell death, independent of vacuolation. The Journal of biological chemistry *281*, 11250-11259.

Yamashita, D., Sugawara, T., Takeshita, M., Kaneko, J., Kamio, Y., Tanaka, I., Tanaka, Y., and Yao, M. (2014). Molecular basis of transmembrane beta-barrel formation of staphylococcal pore-forming toxins. Nat Commun *5*, 4897.

Yamashita, K., Kawai, Y., Tanaka, Y., Hirano, N., Kaneko, J., Tomita, N., Ohta, M., Kamio, Y., Yao, M., and Tanaka, I. (2011). Crystal structure of the octameric pore of staphylococcal gamma-hemolysin reveals the beta-barrel pore formation mechanism by two components. Proceedings of the National Academy of Sciences of the United States of America *108*, 17314-17319.

Ye, D., Willhite, D.C., and Blanke, S.R. (1999). Identification of the minimal intracellular vacuolating domain of the Helicobacter pylori vacuolating toxin. The Journal of biological chemistry *274*, 9277-9282.

Zhang, K. (2016). Gctf: Real-time CTF determination and correction. Journal of structural biology *193*, 1-12.

Zheng, S.Q.P., Eugene; Armache, Jean-Paul; Cheng, Yifan; Agard, David A. (2016). Anisotropic Correction of Beam-induced Motion for Improved Single-particle Electron Cryo-microscopy. Nature methods *submitted*.

Zhou, G., Mo, W.J., Sebbel, P., Min, G., Neubert, T.A., Glockshuber, R., Wu, X.R., Sun, T.T., and Kong, X.P. (2001). Uroplakin Ia is the urothelial receptor for uropathogenic Escherichia coli: evidence from in vitro FimH binding. J Cell Sci *114*, 4095-4103.

APPENDIX

Materials and Methods

Preparation of nanotubes. The protocol for preparation of lipid nanotubes was modified from Wilson-Kubalek, *et.al.* 1998, 2000 (Dang et al., 2005a; Dang et al., 2005b; Wilson-Kubalek, 2000; Wilson-Kubalek et al., 1998). D-galactosyl-ß-1,1' N-nervonoyl-D-*erythro*-sphingosine (GalCer; Avanti Polar Lipids, Alabaster, AL) was rehydrated to a concentration of 5 mg/mL. Three lipid compositions were tested: DOPS/GalCer (50/50, 40/60, 30/70, 20/80, and 10/90 mol%), DOPS/GalCer/chol (30/55/15 and 20/70/10 mol%), and ePC/DOPS/chol/GalCer (27.5/7.5/15/50 mol%). Lipids were rehydrated in 10 mM HEPES pH 7.2, 100 mM KCl for one hour at RT. The lipid mixture was then sonicated for 3 to 6 minutes in a water bath. Nanotube formation was assessed by negative stain EM. Once nanotube formation was verified, acid activated VacA s1/i1/m1 was added to nanotubes (LPR range from 10:1 to 100:1) at RT and incubated for fifteen minutes and binding visualized by negative stain EM (Fig. 5-2E-F).

Small Unilamellar Vesicles. Protocol adapted from the Morrisey lab protocol for preparation of SUVs. Lipid compositions used were 1,2-dioleoyl-*sn*-glycero-3-phosphocholine (DOPC) and 1,2-dioleoyl-*sn*-glycero-3-phospho-L-serine (DOPS) (DOPC:DOPS 20/80 % of total moles (mol%)) and L-α-phosphatidylcholine from egg (ePC), DOPS, and ovine cholesterol (55/15/30 mol%). All lipids were purchased from Avanti Polar Lipids (Alabaster, AL). Briefly, lipids in chloroform ($CHCl_3$) were mixed at the desired ratios and evaporated under a nitrogen stream, further dried in a vacuum for one hour, and rehydrated for one hour at room temperature (RT) in 10 mM HEPES pH 7.2 and 100 mM potassium

chloride (KCl) to a final concentration of 1 mg/mL lipid. The lipids were vigorously vortexed for one minute, then sonicated between 25-50 minutes in a water bath.

To first assess binding of VacA s1/i1/m1, VacA was acid activated to induce oligomer dissociation into monomers. Once acid activated, VacA and the SUVs were mixed at 37°C for fifteen minutes and then negative stain grids were prepared as described. Lipid-to-protein ratios (LPRs; weight to weight) used ranged from 25:1 to 50:1, LUVs to protein.

Once it was determined that VacA binds to SUVs, Flag tag VacA s1/i1/m1 was utilized to separate unbound from bound SUVs. Once VacA bound SUVs were prepared, sample was added to 250 μL Anti-Flag M2 Affinity Gel (Sigma-Aldrich) and nutated for one hour at RT. After washing with 12 column volumes (CVs) of HEPES Buffered Saline (HBS), 18 μL of 3x Flag peptide (Sigma-Aldrich) was added. The mixture was nutated for 30 minutes at RT and purified sample eluted (Fig. 5-2G-H).

Preparation of macrodiscs. The protocol for the preparation of macrodiscs was modified from Park, *et.al.* (Park et al., 2011). The peptide used for macrosdisc formation, Ac-DYLKAFYDKLKEAF-NH_2, was purchased from BioSynthesis and rehydrated in 10mM HEPES pH 7.2 and 100 mM KCl. Lipids (DMPC and ePC/DOPS/cholesterol 55/15/30 mol%) were dried under a nitrogen stream and further dried in a vacuum for 18 hours. Lipids were rehydrated in buffer containing the peptide at a 13.3 mol ratio (lipid:peptide) and vortexed. Next, the lipid/peptide mixture was warmed and cooled for six cycles using an ice bath and 37°C water bath. Macrodisc formation was assessed using negative stain EM. Acidified Flag-tag VacA s1/i1/m1 was added to macrodiscs at neutral pH to assess binding.

Separation of empty macrodiscs and macrodiscs with bound VacA was performed as previously described for SUVs (Fig. 5-2I-J).

Preparation of 2D crystals. This protocol was adapted from several sources. (Abeyrathne et al., 2010; Hasler et al., 1998). Total heart extract lipids (Avanti Polar Lipids) were dried under a nitrogen gas stream and further dried in a vacuum. Lipids were then solubilized in detergent (3-[(3-Cholamidopropyl)dimethylammonio]-1-propanesulfonate hydrate, CHAPS; n-Octyl-β-D-Glucopyranoside, OG; n-Decyl-α-D-Maltopyranoside, DM). Acid activated VacA was added to the detergent solubilized lipids (LPRs ranging from 1:1 to 1:20) to a final volume of 60 μL and then placed in 50 μL dialysis buttons (Hampton Research) and 20,000 MWCO dialysis tubing (Spectrum Labs) placed over it. The buttons were then placed in dialysis buffers (listed below) and placed at either RT or 4°C and mixed for 3 to 5 days. Buttons were then removed and negative stain grids prepared of samples (Fig. 5-2K-L).

Dialysis buffers:

10 mM glycine pH 3.5, 100 mM KCl, 2 mM MgCl2

10 mM sodium citrate pH 5, 100 mM KCl

10 mM HEPES pH 7.2, 100 mM KCl

30 mM HEPES pH 7.2, 70 mM KCl

Amphipol preparation. Prepared 10% A8-35 amphipol in 10 mM HEPES pH 7.2 and 100 mM KCl. Mixed A8-35 with neutral and acidified VacA s1/i1/m1 and VacA Δ346-347 at three different ratios, 1:1, 1:2, 1:3, and 1:4 (amphipol:protein w/w). Samples were visualized with negative stain EM (Fig. 5-2M-N).